AD-A053 830 NAVAL AIR DEVELOPMENT CENTER WARMINSTER PA SYSTEMS D--ETC F/G 5/9
INVESTIGATION OF MOTION BASE DRIVE TECHNIQUES,(U)
MAR 78 M E BITNER
UNCLASSIFIED NADC-77306-20 NL

1 OF 2
AD A053830

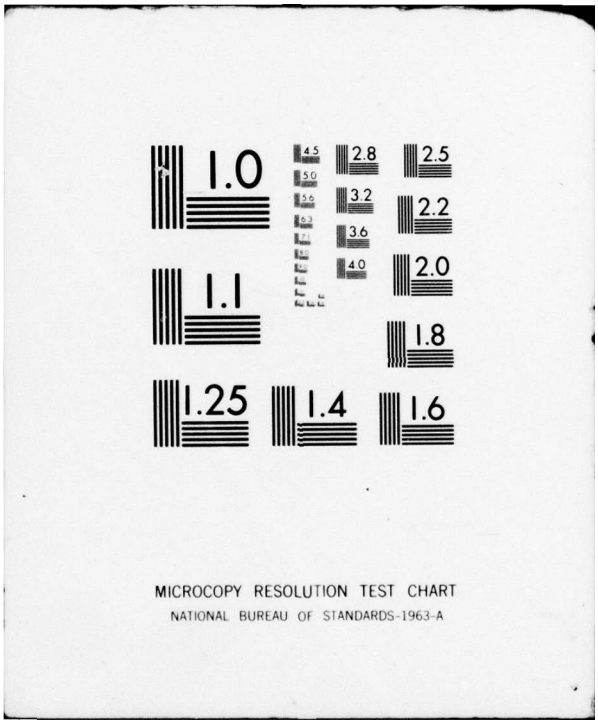
1.0
1.1
1.25
1.4
1.6
1.8
2.0
2.2
2.5
2.8
3.2
3.6
4.0
4.5
5.0
5.6
6.3
7.1
MICROCOPY RESOLUTION TEST CHART
NATIONAL BUREAU OF STANDARDS-1963-A

REPORT NO. NADC-77306-20

12

INVESTIGATION OF MOTION BASE DRIVE TECHNIQUES

M. E. Bitner
Systems Directorate
NAVAL AIR DEVELOPMENT CENTER
Warminster, PA 18974

3 MARCH 1978

TASK NO. ZRO 1403
IR WORK UNIT NO. GC165

Approved for Public Release; Distribution Unlimited

Prepared for
Dr. R. K. Lobb - Technical Director
NAVAL AIR DEVELOPMENT CENTER
Warminster, PA 18974

NOTICES

REPORT NUMBERING SYSTEM - The numbering of technical project reports issued by the Naval Air Development Center is arranged for specific identification purposes. Each number consists of the Center acronym, the calendar year in which the number was assigned, the sequence number of the report within the specific calendar year, and the official 2-digit correspondence code of the Command Office or the Functional Directorate responsible for the report. For example: Report No. NADC-78015-20 indicates the fifteenth Center report for the year 1978, and prepared by the Systems Directorate. The numerical codes are as follows:

CODE	OFFICE OR DIRECTORATE
00	Commander, Naval Air Development Center
01	Technical Director, Naval Air Development Center
02	Comptroller
10	Directorate Command Projects
20	Systems Directorate
30	Sensors & Avionics Technology Directorate
40	Communication & Navigation Technology Directorate
50	Software Computer Directorate
60	Aircraft & Crew Systems Technology Directorate
70	Planning Assessment Resources
80	Engineering Support Group

PRODUCT ENDORSEMENT - The discussion or instructions concerning commercial products herein do not constitute an endorsement by the Government nor do they convey or imply the license or right to use such products.

APPROVED BY: R. M. Baker DATE: 3/3/78

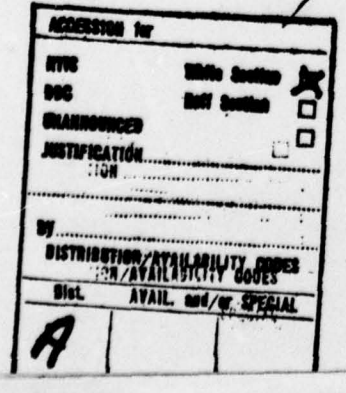

UNCLASSIFIED

SECURITY CLASSIFICATION OF THIS PAGE (When Data Entered)

REPORT DOCUMENTATION PAGE		READ INSTRUCTIONS BEFORE COMPLETING FORM
1. REPORT NUMBER (14) NADC-77306-20	2. GOVT ACCESSION NO.	3. RECIPIENT'S CATALOG NUMBER
4. TITLE (and Subtitle) (6) Investigation of Motion Base Drive Techniques (9)		5. TYPE OF REPORT & PERIOD COVERED
		6. PERFORMING ORG. REPORT NUMBER
7. AUTHOR(s) (10) M. E./Bitner		8. CONTRACT OR GRANT NUMBER(s)
9. PERFORMING ORGANIZATION NAME AND ADDRESS Systems Directorate Naval Air Development Center Warminster, PA 18974		10. PROGRAM ELEMENT, PROJECT, TASK AREA & WORK UNIT NUMBERS Task No. ZRO1403 IR Work Unit No. GC165
11. CONTROLLING OFFICE NAME AND ADDRESS Dr. R. K. Lobb - Technical Director Naval Air Development Center Warminster, PA 18974		12. REPORT DATE (11) 3 MARCH 1978 13. NUMBER OF PAGES 146 (12) 153 p.
14. MONITORING AGENCY NAME & ADDRESS(if different from Controlling Office)		15. SECURITY CLASS. (of this report) UNCLASSIFIED 15a. DECLASSIFICATION/DOWNGRADING SCHEDULE

16. DISTRIBUTION STATEMENT (of this Report)

APPROVED FOR PUBLIC RELEASE; DISTRIBUTION UNLIMITED

17. DISTRIBUTION STATEMENT (of the abstract entered in Block 20, if different from Report)

(17) ZRO1403

18. SUPPLEMENTARY NOTES

19. KEY WORDS (Continue on reverse side if necessary and identify by block number)

Motion Simulation
Moving Base Simulator
Drive Functions
Piloted Flight Simulation

20. ABSTRACT (Continue on reverse side if necessary and identify by block number)

Motion base drive functions required for simulating helicopter and V/STOL aircraft were investigated, developed and evaluated on the NAVAIRDEVCEN three degree of freedom motion base.

DD FORM 1 JAN 73 1473 EDITION OF 1 NOV 65 IS OBSOLETE

UNCLASSIFIED

SECURITY CLASSIFICATION OF THIS PAGE (When Data Entered)

393 539

TABLE OF CONTENTS

LIST OF FIGURES

LIST OF FIGURES (Continued)

LIST OF FIGURES (Continued)

LIST OF TABLES

SUMMARY

Motion base driving functions required for simulating helicopter and Vertical/Short Take-Off Landing (V/STOL) aircraft were investigated, developed and evaluated on the NAVAIRDEVCEN three degree-of-freedom motion base.

The motion base drive investigation was carried out in three steps. The first step entailed a survey of both the civilian and military branches of the flight simulation community for the purpose of determining the state-of-the-art moving base drive techniques. The second step was the simulation design where these drive techniques were adapted to the NAVAIRDEVCEN simulation facilities and Research and Development (R&D) mission. Finally, the motion base drive functions were implemented in the simulation laboratory and experienced pilots were used to evaluate and optimize the drive techniques.

Results of the survey indicated that all drive techniques have the same underlying assumption: pilots are capable of sensing two kinds of motion - rotational acceleration and specific force (the apparent force at the pilot's station). Because of severe motion base acceleration, velocity and position constraints, the aircraft motion cannot be simulated exactly. Washout filters must be employed in order to limit the travel of the motion base hardware. Traditionally, therefore, motion base drive functions have consisted of washout circuits of one type or another.

In recent years, attempts to improve motion base drive functions have been in three areas: 1) the type of washout filter used, 2) the axis system in which washout filters are applied, and 3) the use of a technique known as "tilt" to simulate low frequency specific forces.

A hybrid simulation was designed to investigate these three areas. In particular, four washout filter types (first order, third order, high order with tilt and nonlinear adaptive) were applied to the aircraft rotational degrees of freedom and specific force vector in body axes, inertial axes and in conjunction with a linearized transformation from body axes to inertial axes.

An experiment was devised where washout filter parameter settings were chosen and the relative merit of each motion base drive algorithm was evaluated.

The results of the experiment show that the axis system of application for washout has no effect on the accuracy with which pilots fly the aircraft. Indeed, the axis system transformations may be linearized by applying the small angle approximation without jeopardizing the quality of the motion.

High order washout filters, with or without tilt, produced anomalous cues which led to pilot induced oscillations. These anomalous cues could not be compensated for in the motion drive algorithms because no lateral or longitudinal linear drive mechanism exists for a three degree-of-freedom motion base.

Pilots flew the aircraft with greater accuracy when first order washout filters were used then they did for any other washout type. Nonlinear adaptive washout filters were preferred by the pilots and, indeed, they did produce the most accurate recovery of aircraft motion. The poorer performance of the pilots when using nonlinear adaptive may have been due to a turbulence model used in the experiment. Flight in turbulent air produces motion which actually hinders the pilot when flying the aircraft. The nonlinear adaptive filter was more effective than the other washout filter types in reproducing the turbulent motion and may have suffered for it.

DISCUSSION

BACKGROUND

Piloted flight simulators are used extensively for both research and pilot training purposes. Escalating costs of operation and aircraft procurement can be cited as primary reasons.

It has been clearly established that an important aspect of piloted flight simulation is associated with the generation of realistic motion cues, especially in simulations of aircraft with stability and control problems such as the V/STOL.

Today's state-of-the-art motion systems are classified as either moving base systems or sustained force systems. A motion platform or motion base is an example of the former, while a G-seat or manned centrifuge is classified the latter. This research project was concerned with investigating the drive functions for a moving base system.

Motion simulation via moving base simulators is made possible because the human nervous system is highly adaptable. Specifically, certain types of stimuli can evoke the same sensations and responses even when the stimulus magnitude varies. As a result moving base simulators, which contain activators and drive linkages with severe position, velocity and acceleration limitations, are not called on to produce one-to-one motion simulation of the actual aircraft. The best motion is a compromise which attempts to provide the simulator test pilot with those flight sensations and motion cues that he needs while staying within the constraints of the motion drive system. However, adaptability of the nervous system is limited and care must be taken to "tune" the motion stimuli lest disorientation and resulting nausea reactions occur.

The functions which transform aircraft motion to motion base actuator commands are commonly referred to as "motion cue drive function/logic." These functions embody the knowledge of aircraft dynamics, control theory, and human sensory systems.

OBJECTIVES

The objectives for this exploratory development program were to investigate motion base driving functions and to expand and enhance expertise at NAVAIRDEVCEN in the area of simulating motion sensations of manned aircraft. Specifically, this project was directed toward the investigation, development and evaluation of motion base driving functions required for simulating helicopter and V/STOL aircraft.

APPROACH

It was first planned to survey both the civilian and military branches of the flight simulation community for the state-of-the-art moving base techniques.

The second step was the simulation design where these drive techniques were adapted to the NAVAIRDEVCEN simulation facilities and R&D mission. Included in the second step of the project was the refurbishment and dynamic optimization of the NAVAIRDEVCEN motion base hardware. After the motion base drive functions were implemented in the simulation laboratory, experienced pilots were used to evaluate and optimize the drive techniques.

MOTION BASE DRIVE INVESTIGATION

GENERAL DISCUSSION

A bibliography of research articles dealing with the physics and physiology of motion simulation via motion base hardware was compiled and is included at the end of this report. Highlighting the survey were visits to NASA Ames Research Center, Moffett Field, California, and the Naval Training Equipment Center (NTEC), Orlando, Florida.

It is apparent from the survey that a variety of techniques exist for simulating aircraft motion on a motion base platform. However, all of the various drive functions have the same underlying assumption. Pilots are capable of sensing two kinds of motion:

1. Rotational Acceleration

2. Specific Force

The first is self explanatory. Specific force is the apparent force at the pilot's station. It is the quantity we can feel by virtue of surface pressures on our bodies. Therefore, specific force is that which can be sensed through a relative deformation of different parts of the body. Specifically, it is the sum of the external forces divided by the vehicle mass less the gravitational components, i.e., it is the lift, drag, thrust, and Coriolis accelerations at the pilot's station.

Simulation of rotational acceleration and specific force on a motion base requires the use of washout circuits. Commonly, these washout circuits receive as an input the computed aircraft motion and provide a motion onset cue to the pilot in the simulator. Low frequency accelerations are washed out to prevent the motion base platform from exceeding its position constraints.

In the early days of motion simulation, the drive functions accepted aircraft accelerations resolved in a body axis coordinate system and passed them through linear first order washout filters. The washed-out accelerations were then transformed to an inertial axis system where they were doubly integrated and converted to motion base position commands (see figure 1). The frequency breakpoints of the washout filters were adjusted such that the washout rate was less than the sensory threshold of the pilot. As a result, the pilot ideally felt the onset of the motion and then the platform was gradually slowed to a halt at a rate imperceptable to him. Gains were adjusted to insure that the simulator did not exceed its position constraints.

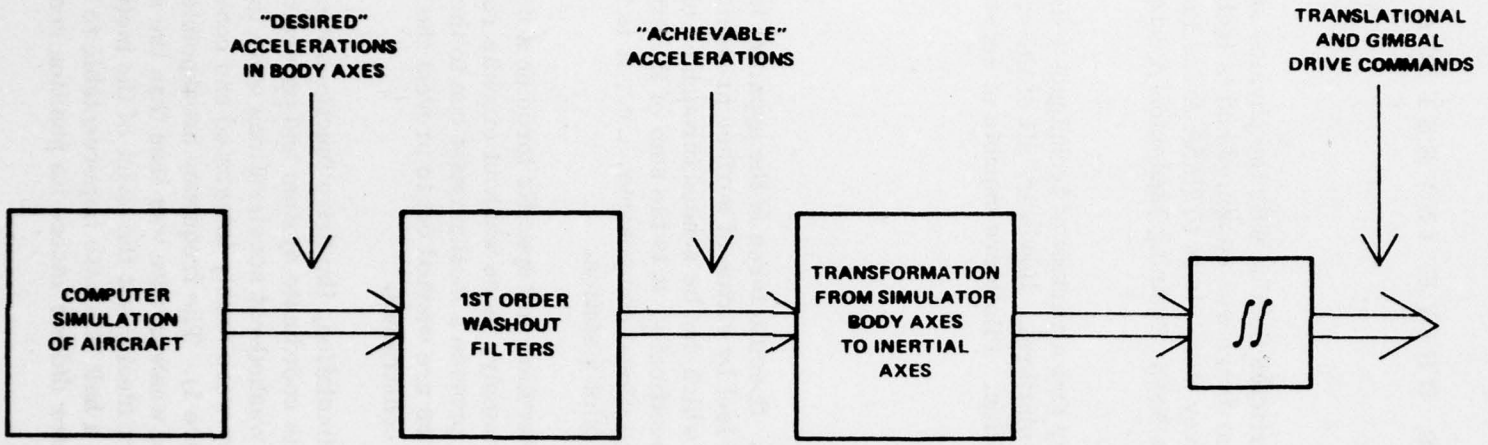

FIGURE 1 - Basic Washout Circuit

Attempted improvements to the original motion drive functions have been in three areas: 1.) the choice of axis system in which the washouts are performed, 2.) the type of washout filter used (first order linear, high order linear, nonlinear adaptive, etc.), and 3.) the use of "tilt" to simulate low frequency specific forces.

Since motion is sensed in a body centered frame of reference it is aesthetically desirable to washout the accelerations in that axis system. However, anomalies associated with washout in one component of the body axis accelerations would then be coupled into three components when they are transformed into the inertial frame of reference. This coupling can produce a degree of simulator drift during operation. Washing out the accelerations after they have been transformed to inertial axes would eliminate the drift problem. However, washing out accelerations in a frame of reference other than the axis system in which the accelerations are sensed may have an effect on the quality of the motion.

Both techniques have been suggested. It has also been suggested that the small angle approximation be employed to linearize the transformation, thereby obviating the question of whether to washout in inertial or body axes.

The second area of modification to the original washout circuits was in the design of the washout filters themselves. First order linear filters have the advantage of simplicity. However, they also have some disadvantages. The frequency cutoff is not sharp for a first order filter. Therefore accelerations at frequencies near the filter breakpoint will suffer large distortions. Another disadvantage is associated with the steady state response of a first order filter to step inputs. If an acceleration step is input to the filter and then doubly integrated, the steady state output will be some nonzero position. For, although the acceleration is washed out, the position is not. A series of acceleration steps, therefore, will eventually cause the simulator to exceed its position constraints.

Second order linear filters have sharper cutoffs than first order filters, but they also will command a steady state nonzero position for an acceleration step.

Third order washout filters have sharp cutoffs and they also insure that the position, as well as the acceleration, will return to zero. However, high order linear filters can have undesirable transient responses.

Other washout filters in use today are of the nonlinear adaptive variety. These nonlinear filters attempt to minimize a cost function designed to produce one-to-one motion whenever possible and to scale down the filter gains whenever the input is too large for the constraints of the motion base. Such filters can produce one-to-one motion simulation a large percentage of the time. However, it may be argued that linear time invariant washouts are more desirable because they allow the pilot to judge different cases by comparing relative changes in the cues.

Rotation angles (tilt) of the cockpit alter the specific force on the pilot since the gravity vector is rotating in a body centered frame of reference. This effect is often used to simulate low frequency specific forces in the lateral and longitudinal directions. Specific forces arising from tilt can be held indefinitely, unlike the force sensations generated by translational drive mechanisms. The common technique for utilizing tilt is shown in figure 2.

Small rotation rate signals are generated that drive the simulator toward an attitude which gives appropriate force cues. The rotation rates must remain below the sensory threshold of the pilot to prevent anomalous rotation cues. It is desired to achieve a specific force sensation by placing the gravity vector g_c in a direction along the desired specific force vector f_c. This is done by rotation the simulator about an axis perpendicular to both f_c and g_c until they are aligned. Figure 3 shows a typical circuit for implementing tilt. The specific force vector is resolved into inertial axes and the cross product $f_c x(-g_c)$ generates the rotation vector which will rotate the simulator to null the cross product and align the desired specific force vector with the gravity vector. Note the provision for a shaping filter (a low pass filter of some sort) which passes only slowly varying force terms to prevent the generation of large anomalous rotation rates. The tilt rates are then summed with the rates from the rotational channels. For a six degree-of-freedom simulator, it is possible to coordinate the translational and rotational channels and reproduce longitudinal and lateral specific forces at all frequencies. The translational drive reproduces the high frequency forces and the rotational drive takes over for the low frequency forces through the use of tilt.

SIMULATION DESIGN

A hybrid simulation design was selected. The digital portion of the program, implemented on a CDC 6600, was responsible for simulation control (real-time operation and input/output functions), and the motion base drive logic. The aircraft simulation resided on an EAI 8800 hybrid analog computer which also acted as an interface between the digital motion base drive logic and the Singer-Link three degree-of-freedom motion base. A digital turbulence model (detailed in Appendix A) was added to increase the realism of the simulation. Figure 4 depicts a block diagram of the simulation elements and interfaces.

The motion base with its helicopter controls and displays in an enclosed cockpit and the aircraft model, a UH-1 helicopter, were borrowed from the Light Airborne Multi-Purpose System (LAMPS) simulation in residence at the NAVAIRDEVCEN simulation facility (see figure 5).

The motion base hydraulics were refurbished with new hydraulic fluid and filters. The accumulator was recharged with nitrogen and the hydraulic system pressure raised to the desired operating level. New servo valves were purchased when an old one was found defective, and the electronic gains were adjusted to obtain optimum response from the system. Appendix B describes the refurbishment of the motion system.

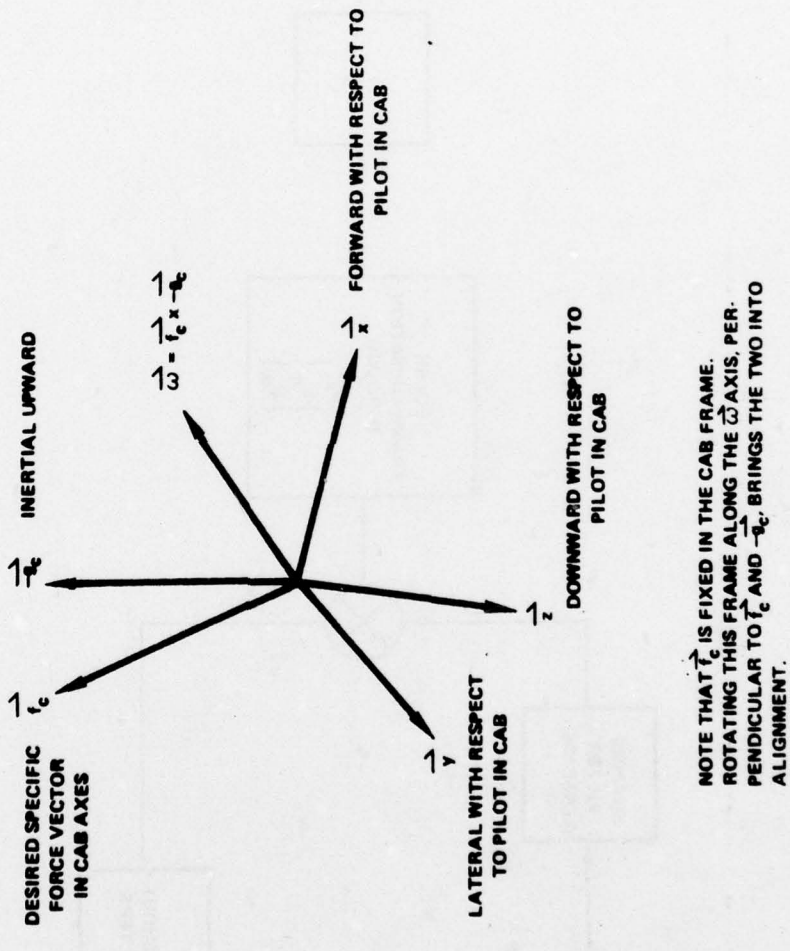

FIGURE 2 - Tilt Geometry

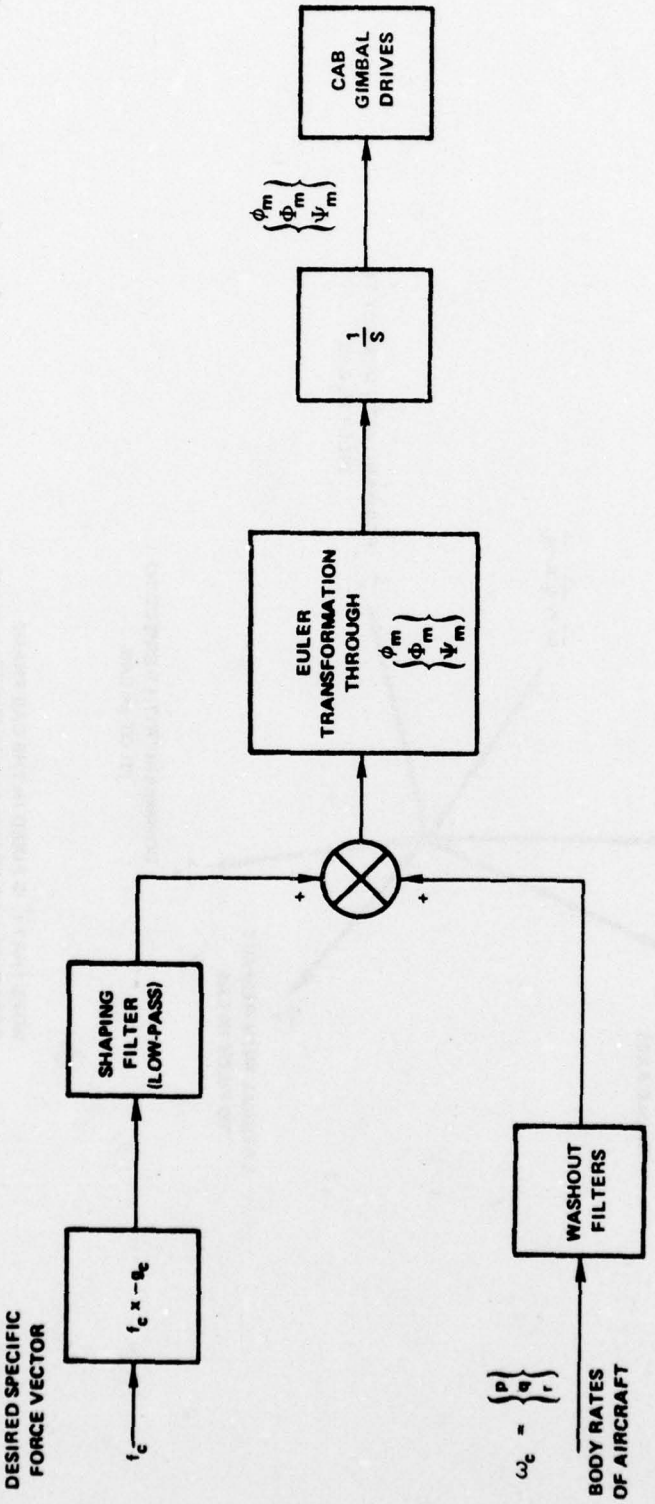

FIGURE 3 - Block Diagram Of Tilt Algorithm

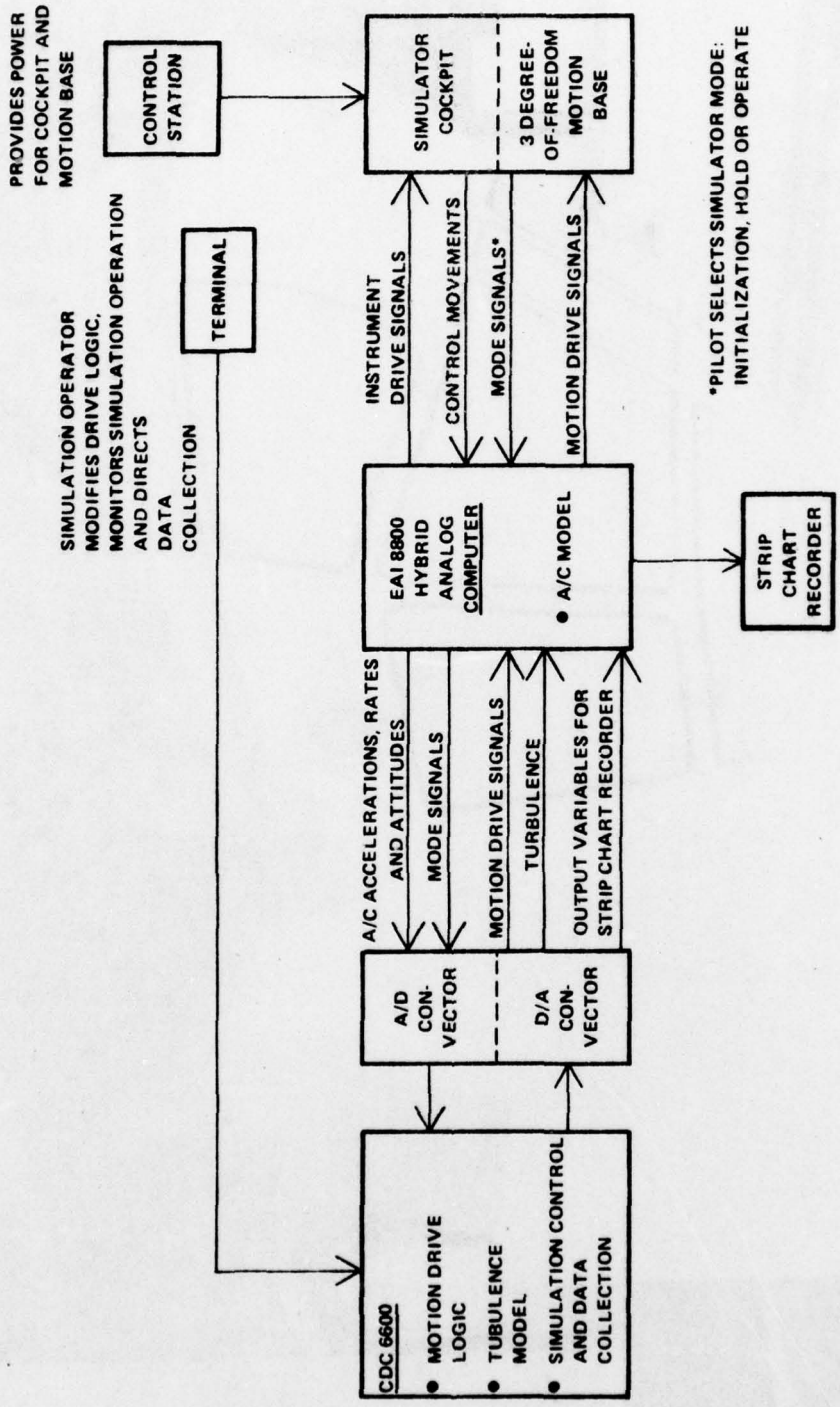

FIGURE 4 - Simulation Block Diagram

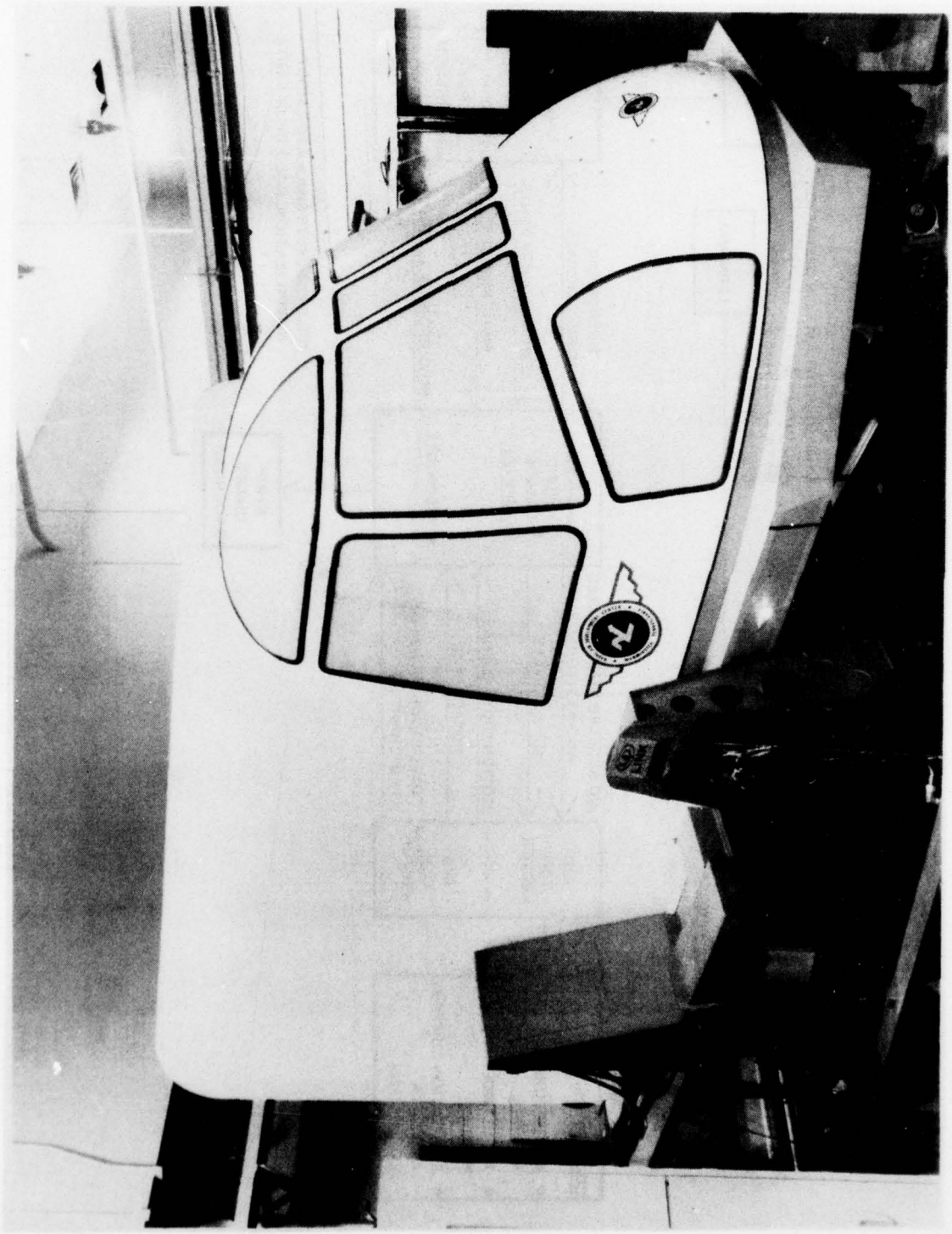

FIGURE 5 - Motion Base With Enclosed Cockpit

The motion base drive logic was designed such that washouts could be performed in inertial axes, body axes or in conjunction with a linear transformation. Washout types were also selectable: first order linear, third order linear, high order linear with tilt or adaptive nonlinear filters.

Because the motion base has only three degrees of freedom (pitch, roll and heave), the utility of tilt could not be fully tested. It has been shown in the past, that tilt algorithms are most effective when linear and rotational drives are "coordinated". Rotational washouts produce anomalous forces which can be eliminated by a coordinated linear drive. Also, specific forces can be simulated at all frequencies by allowing the linear drives to pass high frequency forces and angular drives (through tilt) to simulate low frequency forces.

Because the NAVAIRDEVCEN motion base does not have a longitudinal or lateral linear drive, coordinated drive logic could not be examined. Therefore, the only question concerning tilt that was addressed by this research has to do with the effectiveness of using tilt in the absence of linear drives.

The tilt algorithm used in this study was derived from the drive logic developed by J. B. Sinacori for Northrop Corporation in 1973.[1]

The nonlinear adaptive washout filter was patterned after the algorithm developed by Parrish, Dieudonne, Bowles and Martin for NASA Langley Research Center in 1973.[2] It applies the method of continuous steepest descent to define adaptive washout parameters such that a given cost function is optimized.

EXPERIMENTAL DESIGN

A total of thirteen algorithms were tested. Each of the four washout filter types (first order linear, third order linear, high order with tilt and nonlinear adaptive) were applied in body axes, inertial axes and in conjunction with linear transformations making a total of twelve motion algorithms and no motion was the thirteenth algorithm. A description of each of the twelve motion algorithms is included in Appendix C.

The experiment was performed in three phases. In the first phase a NAVAIRDEVCEN helicopter pilot, LCDR A. Bingley, flew the simulator without motion to check out the helicopter model and suggest changes to make the model more realistic. After

[1] Sinacori, J. B.; "A Practical Approach to Motion Simulation"; AIAA Paper No. 73-931; Sep 1973.

[2] Parrish, R. V., Dieudonne, J. E., Bowles, R. L., and Martin, D. J.; "Coordinated Adaptive Washout for Motion Simulators"; AIAA Paper No. 73-930; Sep 1973.

LCDR Bingley was satisfied with the helicopter model, he flew each of the twelve motion algorithms for the purpose of setting washout parameters. These settings were then used for the rest of the experiment.

The second phase of the experiment tested each of the thirteen algorithms - twelve different motion algorithms and one with no motion. Four NAVAIRDEVCEN helicopter pilots were used in the second phase of the experiment: LCDR A. Bingley, LCDR G. Montgomery, LCDR C. Park and LT F. Porter.

The pilots were given a flying task designed to exercise all the degrees of freedom of the aircraft. Referring to figure 6, the task was a race track pattern with a climb and descent. The run was started with the aircraft heading north at an altitude of 500 feet and an airspeed of 120 knots. The pilot was then asked to execute a 180 degree turn to the left at constant altitude. After leveling out on a southerly heading, he was asked to climb at 500 feet per minute to an altitude of 750 feet. He then leveled out and initiated another constant altitude 180 degrees turn to the left. After leveling out on a northerly heading, he started a descent at 500 feet per minute to an altitude of 500 feet where he leveled out, completing the run. Airspeed was to remain constant throughout the run which lasted approximately 3-1/2 minutes.

Steering commands for flying the pattern were provided by an instrument mounted above the instrument panel. Ideally, motion algorithms should be tested using a Visual Flight Rules (VFR) rather than an Instrument Flight Rules (IFR) task. However, no out-the-window visuals were available for this simulation. The steering command instrument, therefore, was positioned above the instrument panel requiring the pilot to set up a scan pattern similar to one he would use when flying VFR.

Referring to figure 7, the steering command instrument consisted of a horizontal bar, a vertical bar and a ball. The horizontal bar was driven with airspeed error, the vertical bar with heading error and the ball with altitude error.

The pilots practiced with no motion until they were familiar with the instrument, the flying pattern, and the aircraft. Then they practiced with each motion algorithm until they were familiar with it, and data was collected.

The motion algorithms were numbered as follows:

Algorithm Number	Algorithm Type
1	First Order Washout (Linear Transformation)
2	Third Order Washout (Linear Transformation)
3	Nonlinear Adaptive Washout (Linear Transformation)
4	High Order Washout with Tilt (Linear Transformation)
5	First Order Washout (Body Axis)

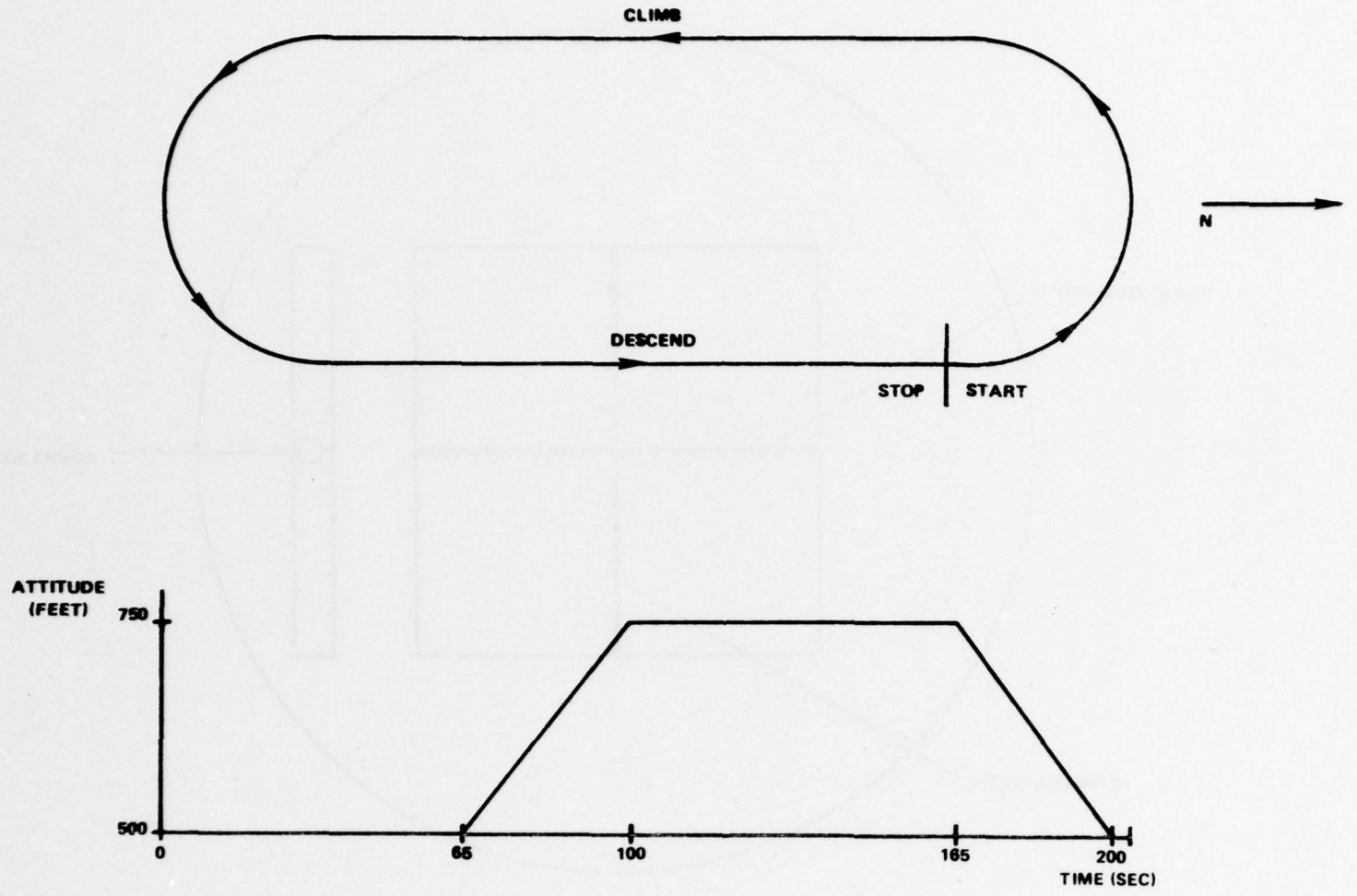

FIGURE 6 - Racetrack Pattern

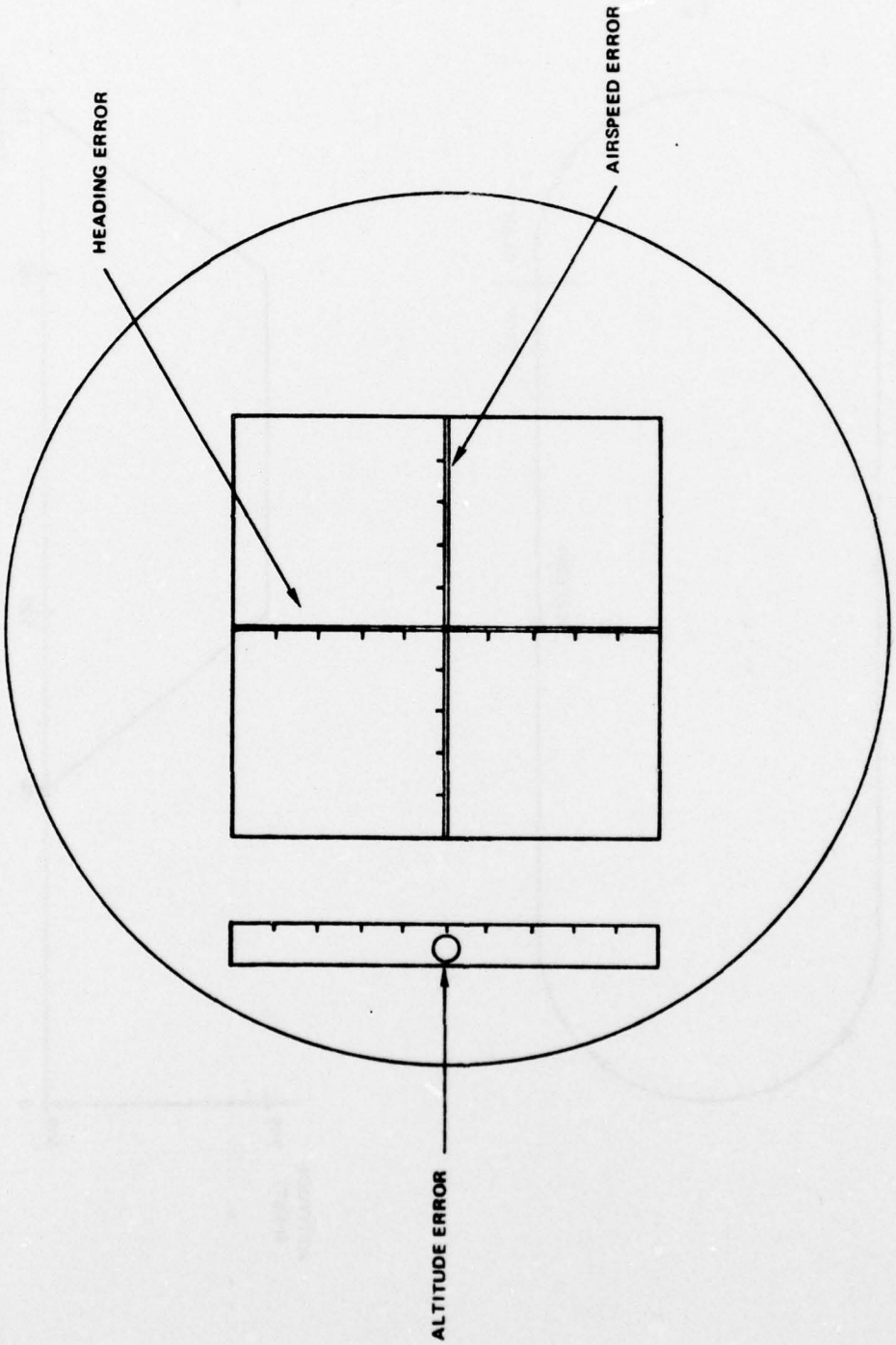

FIGURE 7 - Instrument Providing Flight Task Cues

Algorithm Number	Algorithm Type
6	Third Order Washout (Body Axis)
7	Nonlinear Adaptive Washout (Body Axis)
8	High Order Washout with Tilt (Body Axis)
9	First Order Washout (Inertial Axis)
10	Third Order Washout (Inertial Axis)
11	Nonlinear Adaptive Washout (Inertial Axis)
12	High Order Washout with Tilt (Inertial Axis)
13	No Motion

The order of appearance of these algorithms during the experiment was randomly selected for each pilot to minimize the effect of a "learning curve":

	Pilot #1	Pilot #2	Pilot #3	Pilot #4
Algorithm No.	2	8	13	12
Algorithm No.	13	2	3	1
Algorithm No.	5	11	4	2
Algorithm No.	7	10	8	13
Algorithm No.	8	7	5	7
Algorithm No.	10	6	12	11
Algorithm No.	4	5	7	9
Algorithm No.	11	13	9	5
Algorithm No.	3	3	6	6
Algorithm No.	12	12	2	8
Algorithm No.	1	9	10	4
Algorithm No.	6	1	11	3
Algorithm No.	9	4	1	10

The data collected were the means and variances, computer on-line, for each of nine error parameters. The following formulas were used:

$$\text{Mean of error} = \frac{1}{T} \int_0^T \text{error}(t)\,dt$$

$$\text{Variance of error} = \frac{1}{T} \int_0^T (\text{error}(t))^2 dt - (\text{Mean})^2.$$

The nine error parameters were: Three inertial position errors, three attitude angular errors and three stick positions (x and y cylic control and collective).

The measures of effectiveness were taken to be the variances of the error parameters rather than the means, since the variances of the errors carry more information on the accuracy with which the pilot is flying.

The attitude and position error variances are a measure of total system performance. The variance of the control positions gives insight into the reason for differences in system performance.

Preliminary results of the second phase of the experiment indicated that the error variances were nearly equal when washouts were performed in inertial axes, body axes, or in conjunction with linear transformations. First order linear filters, high order linear filters with tilt and adaptive nonlinear filters produced error variances that were approximately equal while substantially higher variances were observed for third order linear filters.

On the basis of these results, a third phase of the experiment was designed. It was decided to perform the washouts in inertial axes to eliminate the problem of drift. First order filters, high order filters with tilt and adaptive nonlinear filters were chosen to be tested in this phase of the experiment.

Three NAVAIRDEVCEN pilots were used in the third phase: LCDR B. Bowen, LCDR S. Hoxie and LT. F. Porter. It was felt that a larger sample size was needed to distinguish the differences between the three algorithms. Therefore, the pilots flew the three algorithms five times each in the following order:

Pilot #1

Nonlinear Adaptive Washout
First Order Washout
High Order Washout with Tilt

Pilot #2

First Order Washout
High Order Washout with Tilt
Nonlinear Adaptive Washout

Pilot #3

High Order Washout with Tilt
Nonlinear Adaptive Washout
First Order Washout

In addition to the nine error parameters of the second phase of the experiment, data was also collected on the means and variances of three angular rate errors.

A fast fourier transform was performed on the control position time histories showing the frequency content of the stick movements. It was felt that differences in the frequency content could aid in understanding any observed variations in system performance for the three algorithms.

DISCUSSION OF RESULTS

PHASE I

The washout parameters selected in this phase of the experiment and used in the second and third phases are listed in the algorithm descriptions, Appendix C.

PHASE II

The second phase of the experiment investigated washout types and the axis system in which washouts are applied.

The three control variances (x and y cyclic and collective) were added to form a control variance; the three Euler angle error variances were added to form an attitude error variance; and the x, y and z error variances were added to form position error variance. The control, attitude and position error variances were then averaged over the four pilots for washout types and axis system of application. Figures 8 through 10 show the average control, attitude and position error variances for the four different washout types. Figures 11 through 13 are the average control, attitude and position error variances for the three choices for axis system of application.

Control, attitude and position error variances are larger for third order washout filters than for the other three washout filters - first order, high order with tilt and nonlinear adaptive. This difference is seen to be more pronounced for attitude and position error variances than it is for control variances, although the trend is the same for all three measures of effectiveness. The levels of significance for this result were .30 for control variances, .08 for attitude error variances and .10 for position error variances.

The control, attitude and position error variances for axis system of application (figures 11 through 13) show no consistent trend. The level of significance for the control variance difference is .39. For attitude error variance difference the level of significance is .76; and for position error variance difference, the level of significance is .60.

Figures 14 through 16 show the control, attitude and position error variances for runs with motion versus runs with no motion. Smaller variances are evident for runs with motion for control and attitude errors, while that trend is reversed for position error variances. The one-tailed test levels of significance for these results were:

Control Variance - .24
Attitude Error Variance - .39
Position Error Variance - .45

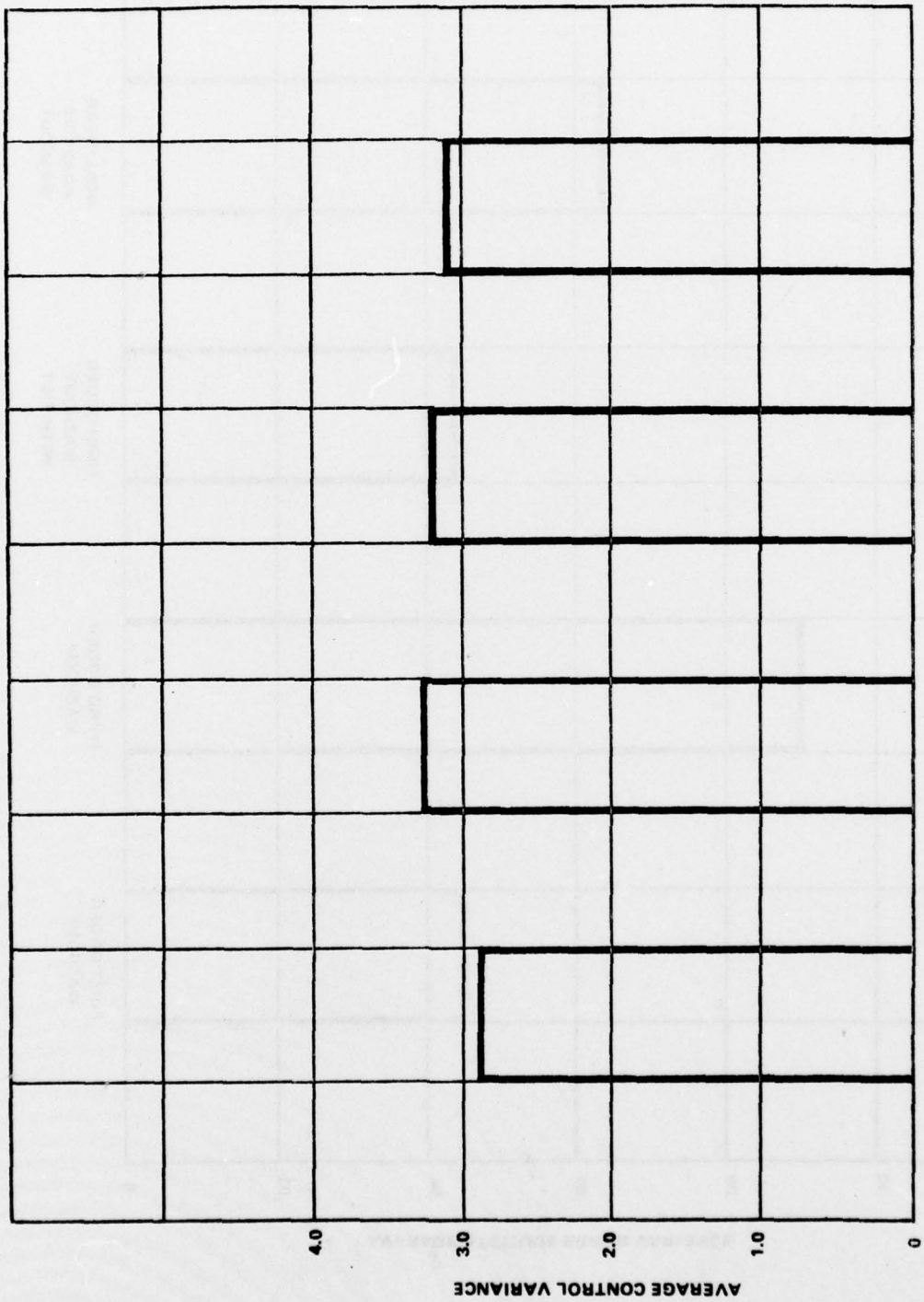

FIGURE 8 - Control Variance For Washout Types

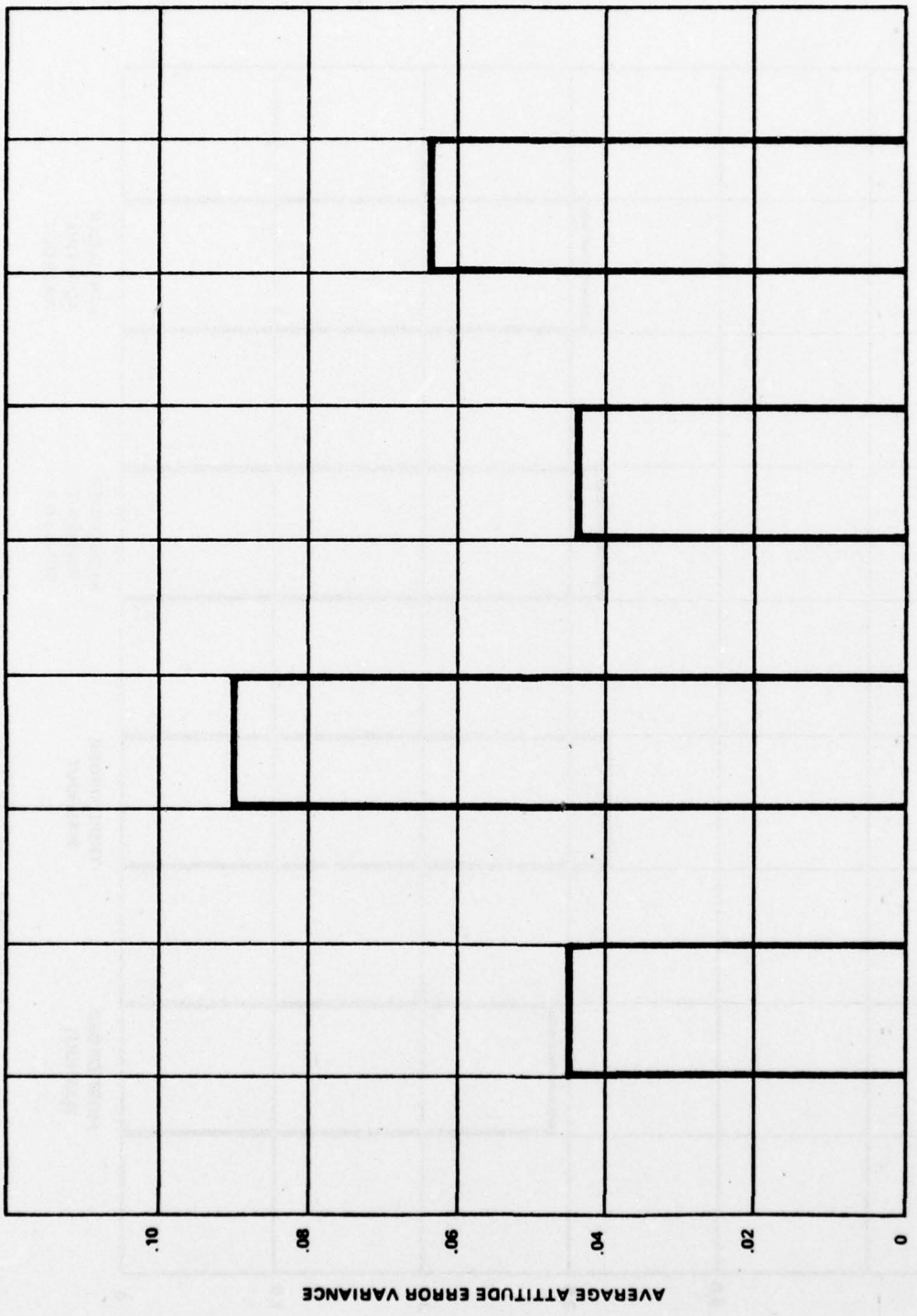

FIGURE 9 - Attitude Error Variance For Washout Types

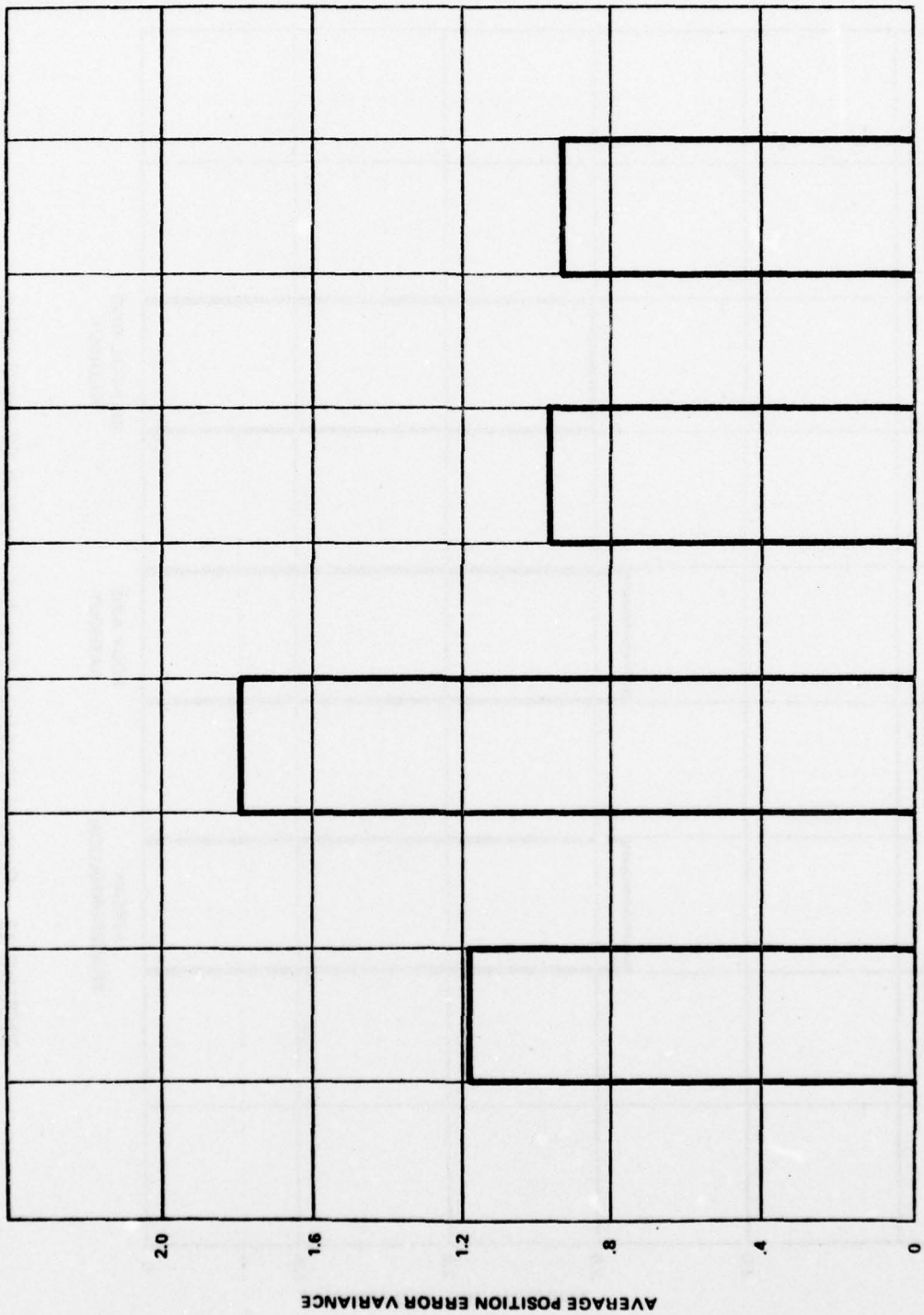

FIGURE 10 - Position Error Variance For Washout Types

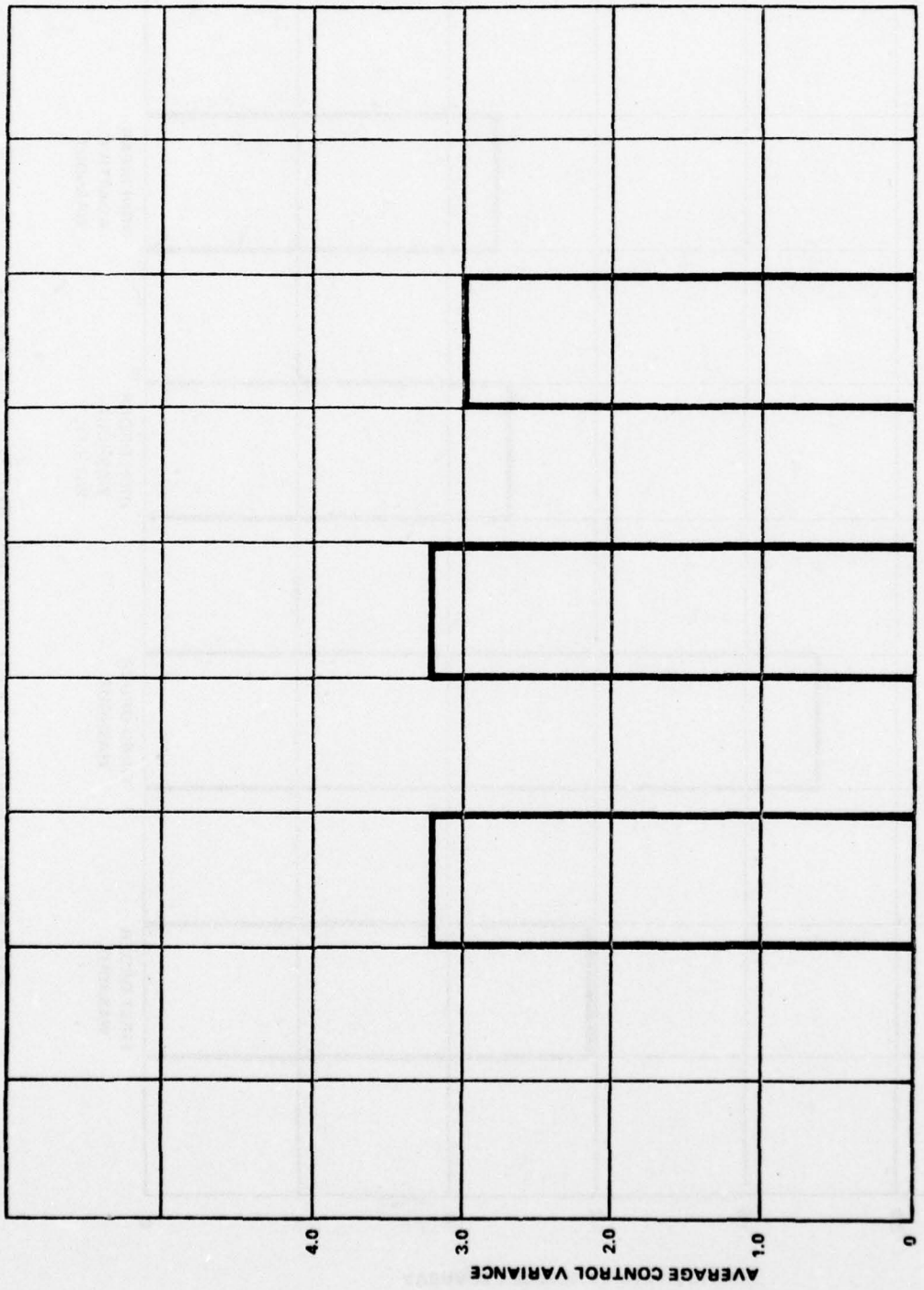

FIGURE 11 - Control Variance For Axis System Of Application

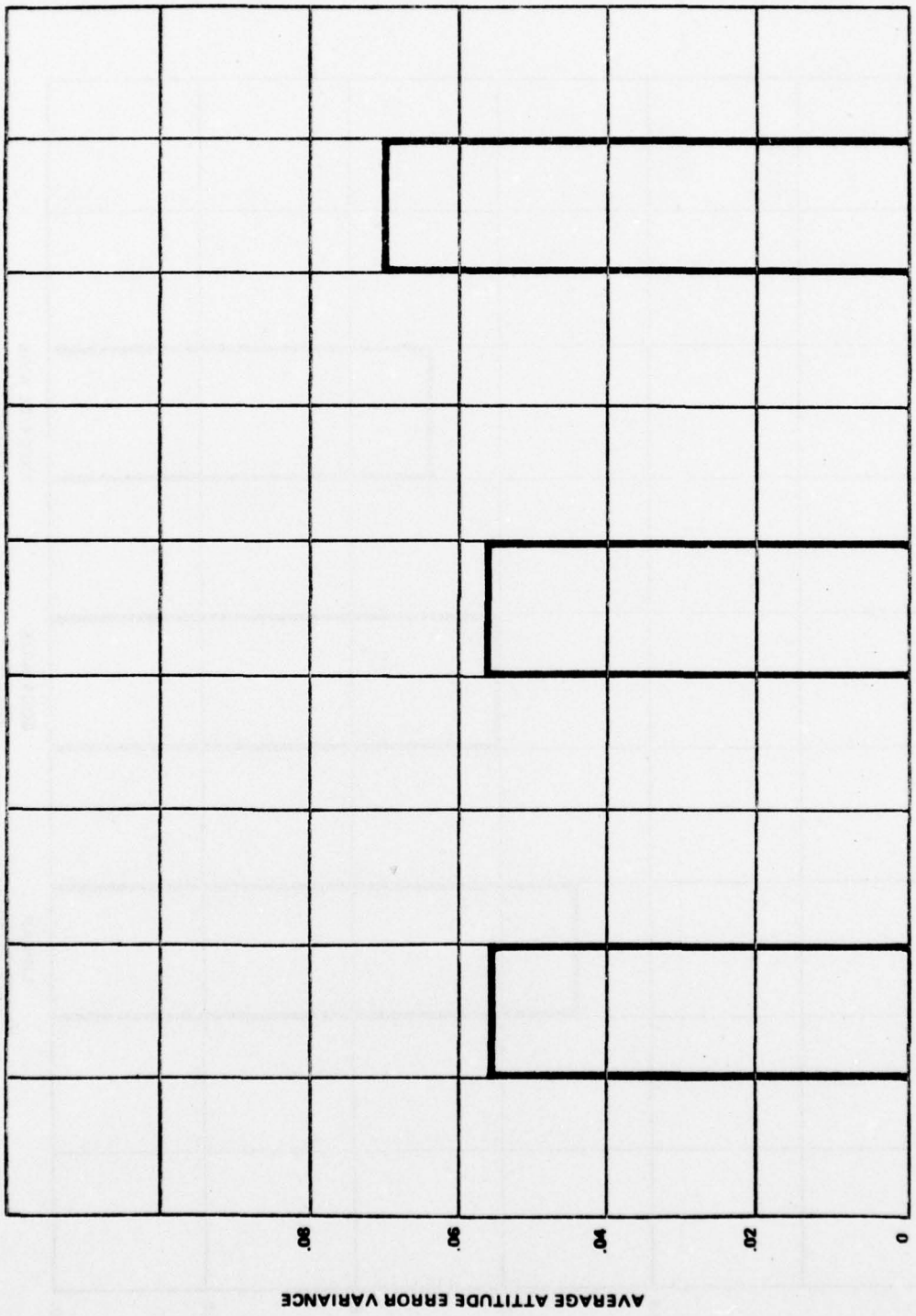

FIGURE 12 - Attitude Error Variance For Axis System Of Application

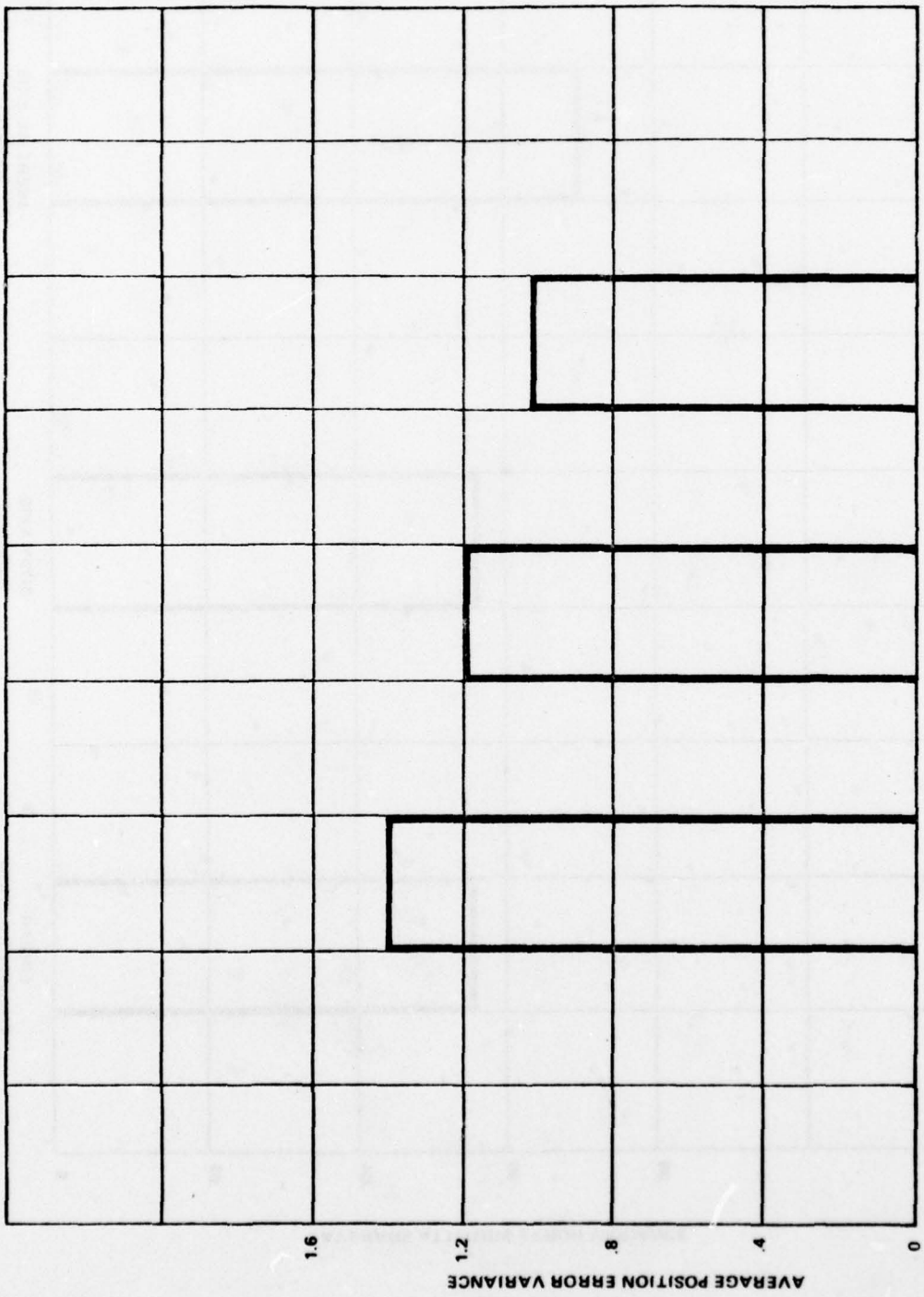

FIGURE 13 - Position Error Variance For Axis System Of Application

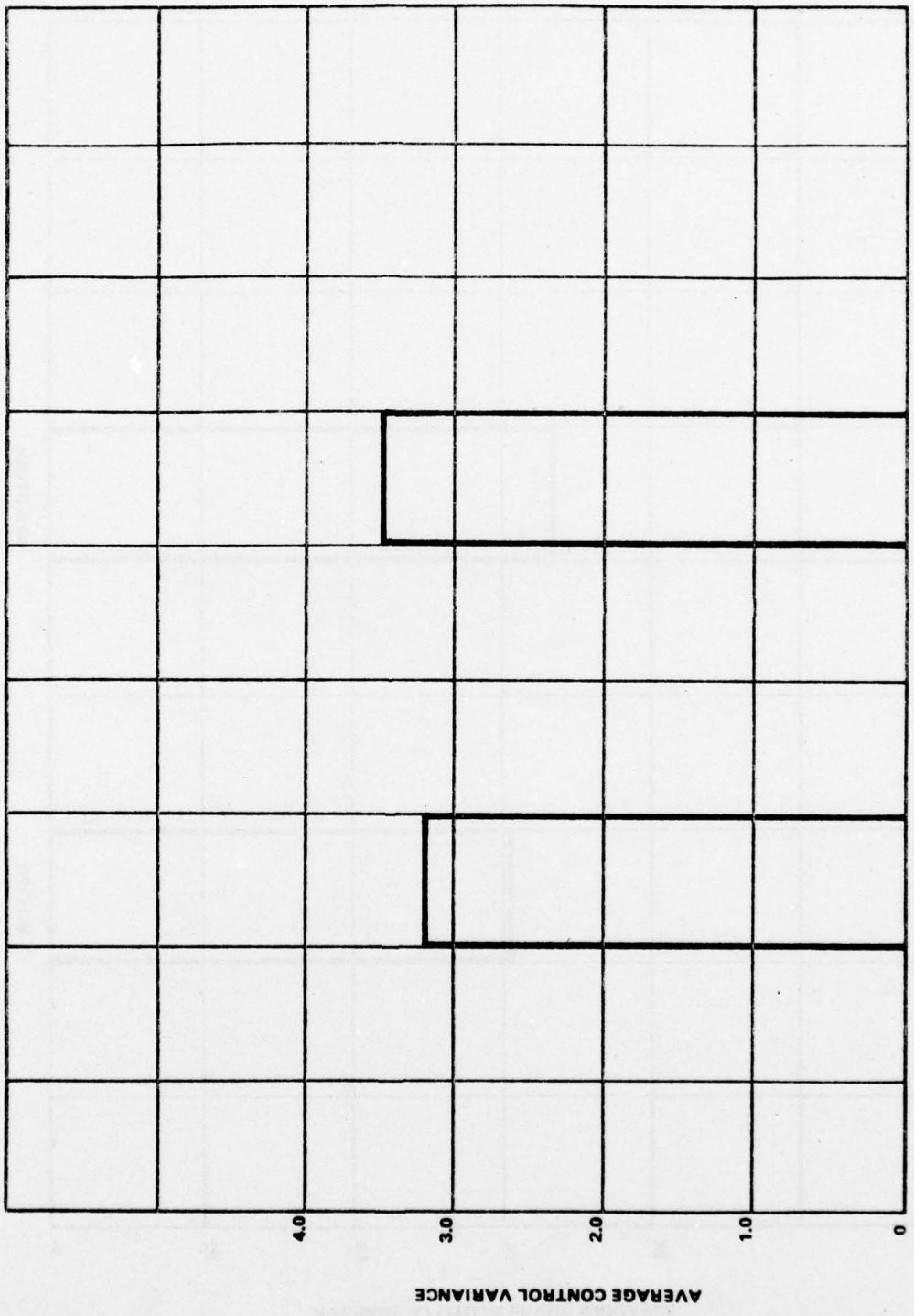

FIGURE 14 - Control Variance For Motion Versus No Motion

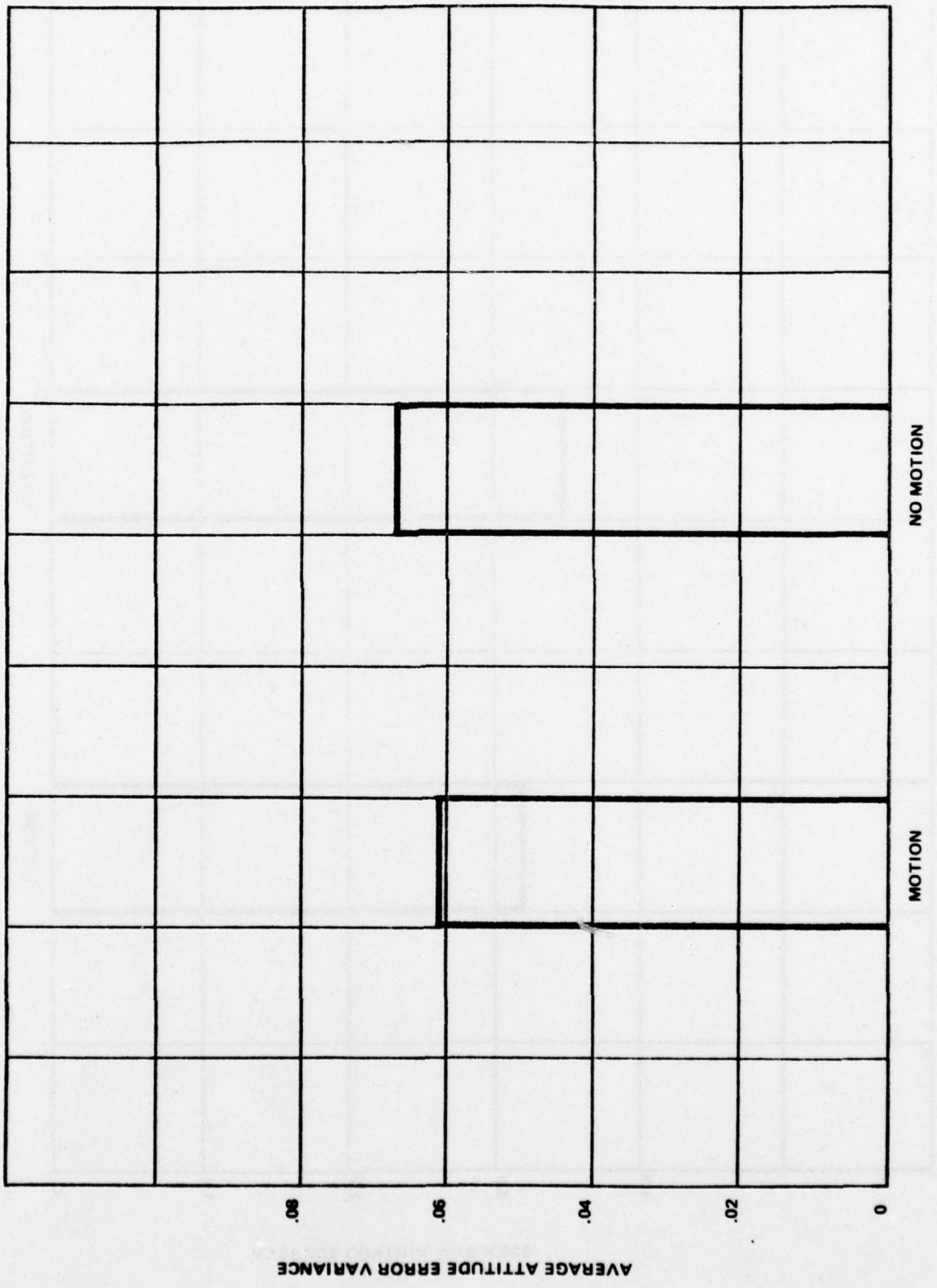

FIGURE 15 - Attitude Error Variance For Motion Versus No Motion

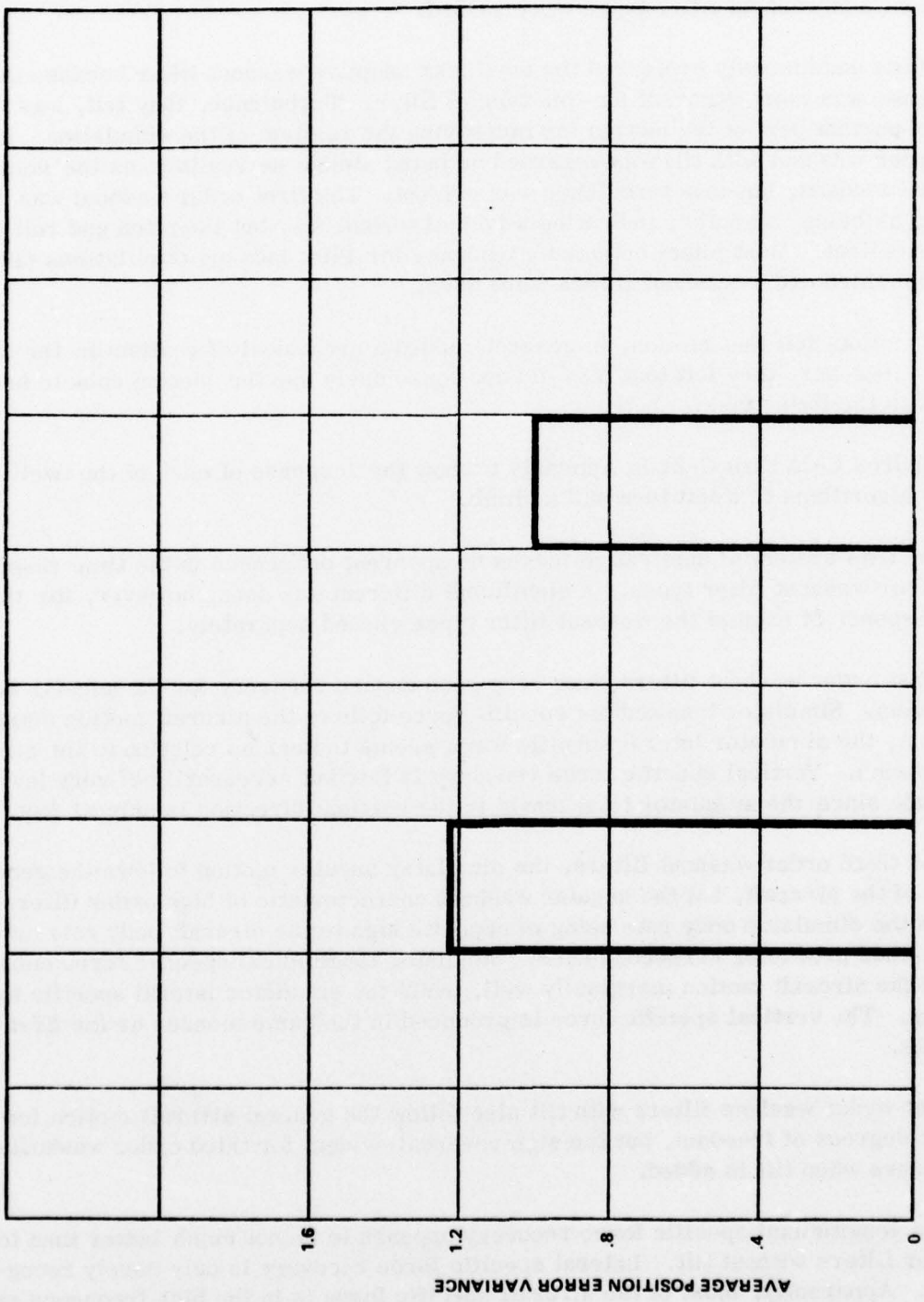

FIGURE 16 - Position Error Variance For Motion Versus No Motion

The pilots could sense no difference in the motion cues when the axis system of application for washouts was varied. However, they felt very definite differences in the cues when washout filter types were varied.

Pilots unanimously preferred the nonlinear adaptive washout filter because the turbulence was most apparent for this type of filter. Turbulence, they felt, was the most important part of the motion for increasing the realism of the simulation. The high order washout with tilt was regarded as being almost as realistic as the nonlinear adaptive washout, but less turbulence was evident. The first order washout was described as being "smooth", indicating a lack of turbulence, but the pitch and roll cues were excellent. Most pilots detected a tendency for Pilot Induces Oscillations (PIO) when the third order washout filters were used.

The pilots felt that motion, in general, added a great deal of realism to the simulation. However, they felt that they did not consciously use the motion cues to help them with the flying task.

Figures C-13 thru C-24 in Appendix C show the response of each of the twelve motion algorithms to a left turn and a climb.

The axis system of application makes no apparent difference in the time response of the four washout filter types. A significant difference is seen, however, for the time response of each of the washout filter types viewed separately.

First order washout filters show very good motion recovery for the angular degrees of freedom. Simulator longitudinal specific force follows the aircraft motion marginally well, but, the simulator lateral specific force seems to bear no relation to the aircraft motion. Vertical specific force recovery is fair but necessarily of very low amplitude since the simulator total travel in the vertical direction is only ±1 foot.

For third order washout filters, the simulator angular motion follows the general motion of the aircraft, but the angular washout characteristic of high order filters results in the simulator body rate being of opposite sign to the aircraft body rate on occasion, thus producing erroneous cues. Simulator longitudinal specific force once again follows the aircraft motion marginally well, while the simulator lateral specific force does not. The vertical specific force is produced in the same manner as for first order washouts.

High order washout filters with tilt also follow the general aircraft motion for angular degrees of freedom, but the sign reversal evident for third order washouts still occurs when tilt is added.

The longitudinal specific force recovery appears to be not much better than for the other filters without tilt. Lateral specific force recovery is only barely recognizable. Apparently, most of the aircraft specific force is in the high frequency range

and is thus being filtered out by the tilt shaping filter. Once again the vertical specific force is handled in the same manner as for the other linear washout circuits.

Angular rate recovery is excellent for nonlinear adaptive washout circuits. High frequency rates are reproduced exactly with washout occurring only for sustained aircraft rates. No evidence of sign reversal is apparent. Simulator longitudinal specific force follows aircraft motion as well or better than the linear washout circuits. Lateral specific force is reproduced much better with the nonlinear adaptive washouts than for any of the linear washouts including the high order washout with tilt. Vertical specific force recovery is very poor. For this degree-of-freedom, the linear washouts performed much better.

PHASE III

The third phase of the experiment further investigated the three washout filter types that appeared nearly equal from the second phase - nonlinear adaptive washout, high order washout with tilt and first order washout.

Control, attitude and position error variances were formed as in the second phase of the experiment. In addition, the body axis x, y and z angular rate error variances were added to form a body rate error variance.

Figures 17 through 20 show the control, body rate, attitude and position error variances averaged over all the pilots' runs for each of the three washout filter types. A consistent trend is seen for control, body rate and attitude error variances. First order washouts show the least error variances, high order washout with tilt show higher error variances. For position error variance, first order washout is still best, however nonlinear adaptive washouts show better position error variance than the high order washout with tilt. Levels of significance for individual comparisons between washout filter types are shown in table I.

Figures 21 through 23 show the average frequency distributions of control movements for first order filters, nonlinear adaptive filters and high order filters with tilt respectively.

Comparisons were made between the different frequency distrubitions by subtracting one spectrum from another and limiting the difference spectrum to zero as a minimum.

The difference spectrums for cyclic x control movements are shown in the following figures:

First Order Washout - Nonlinear Adaptive Washout	Figure 24
Nonlinear Adaptive Washout - First Order Washout	Figure 25
First Order Washout - High Order Washout with Tilt	Figure 26
High Order Washout with Tilt - First Order Washout	Figure 27
Nonlinear Adaptive Washout - High Order Washout with Tilt	Figure 28
High Order Washout with Tilt - Nonlinear Adaptive Washout	Figure 29

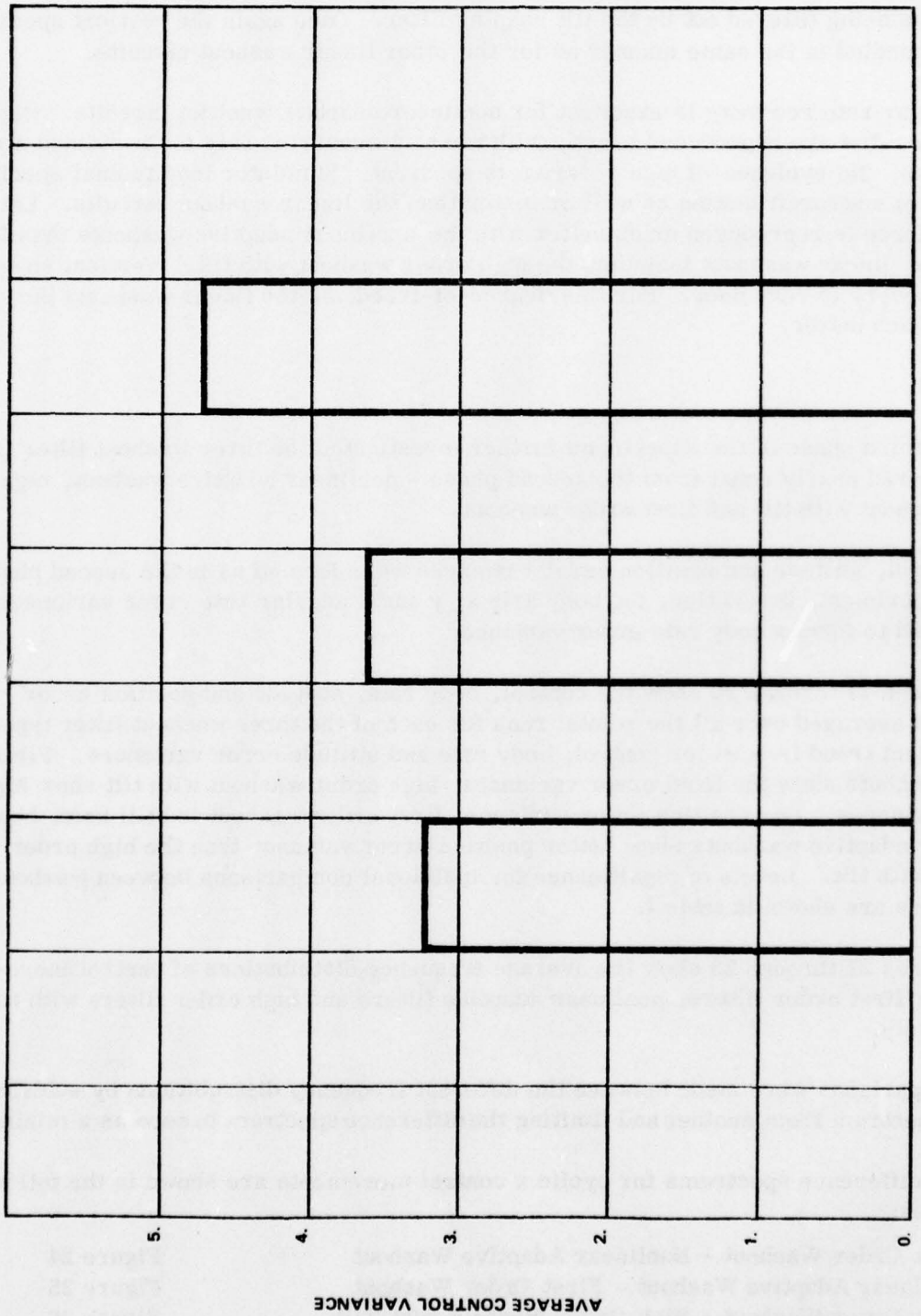

FIGURE 17 - Control Variance For Washout Types (Phase III)

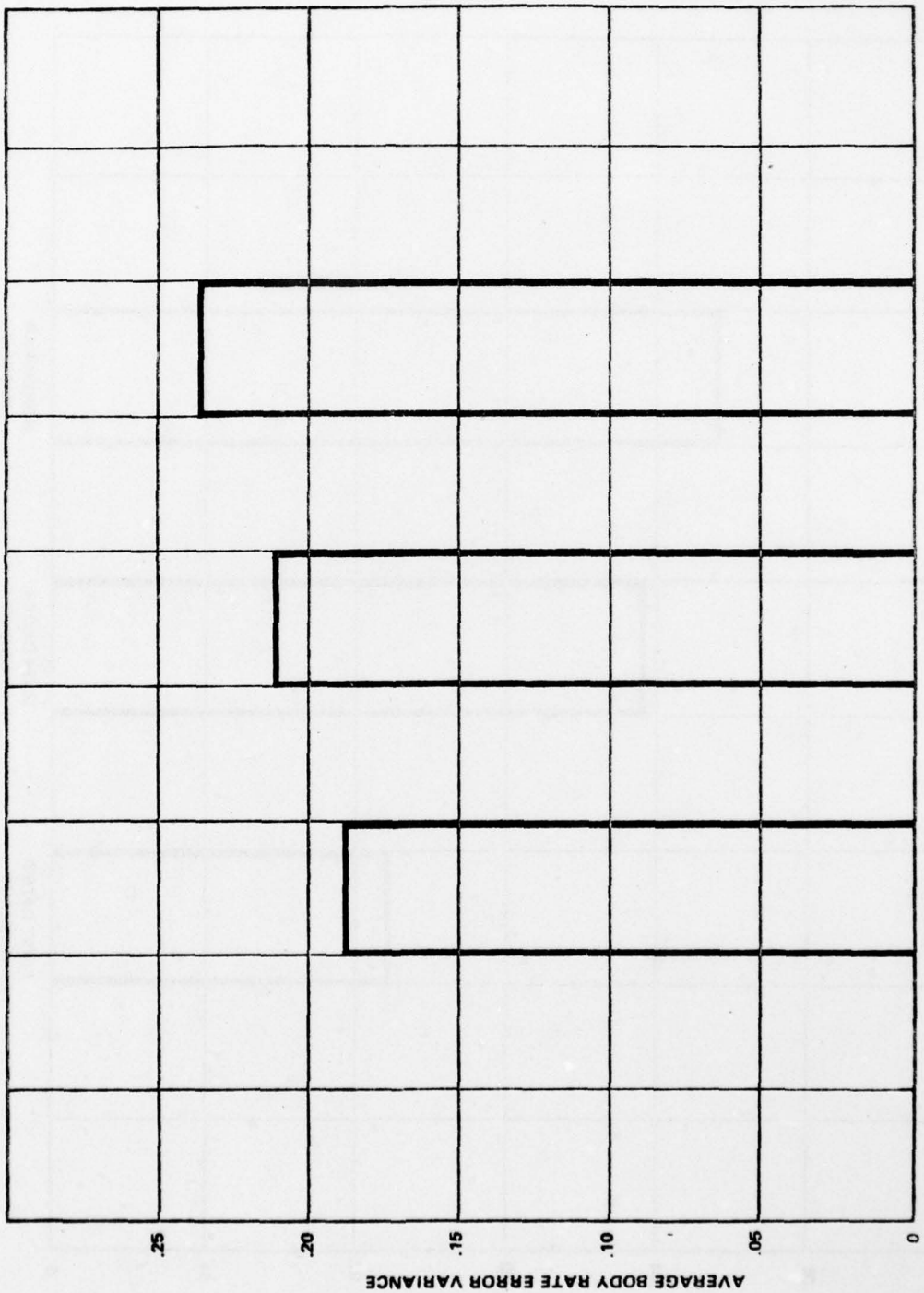

FIGURE 18 - Body Rate Error Variance For Washout Types (Phase III)

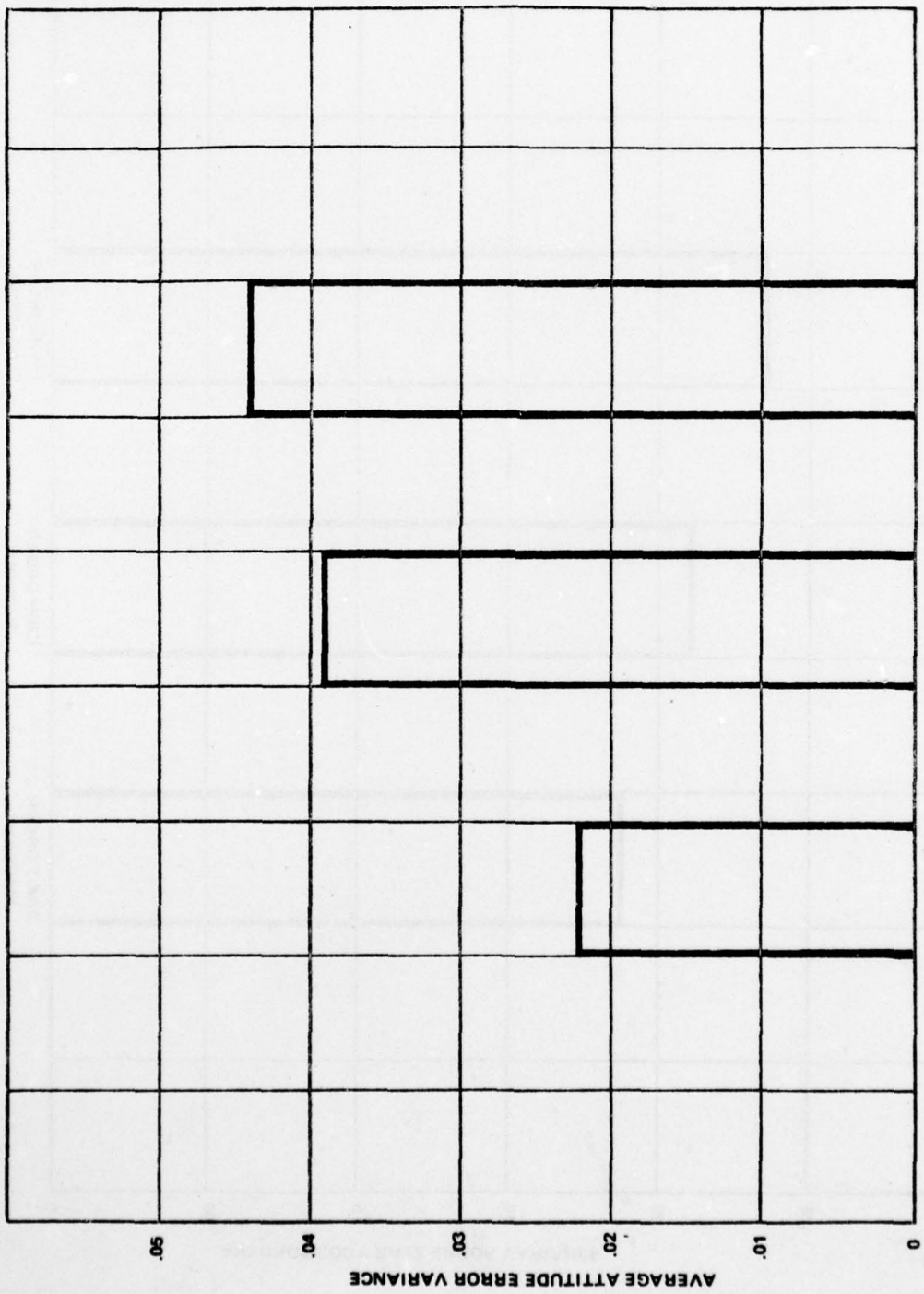

FIGURE 19 - Attitude Error Variance For Washout Types (Phase III)

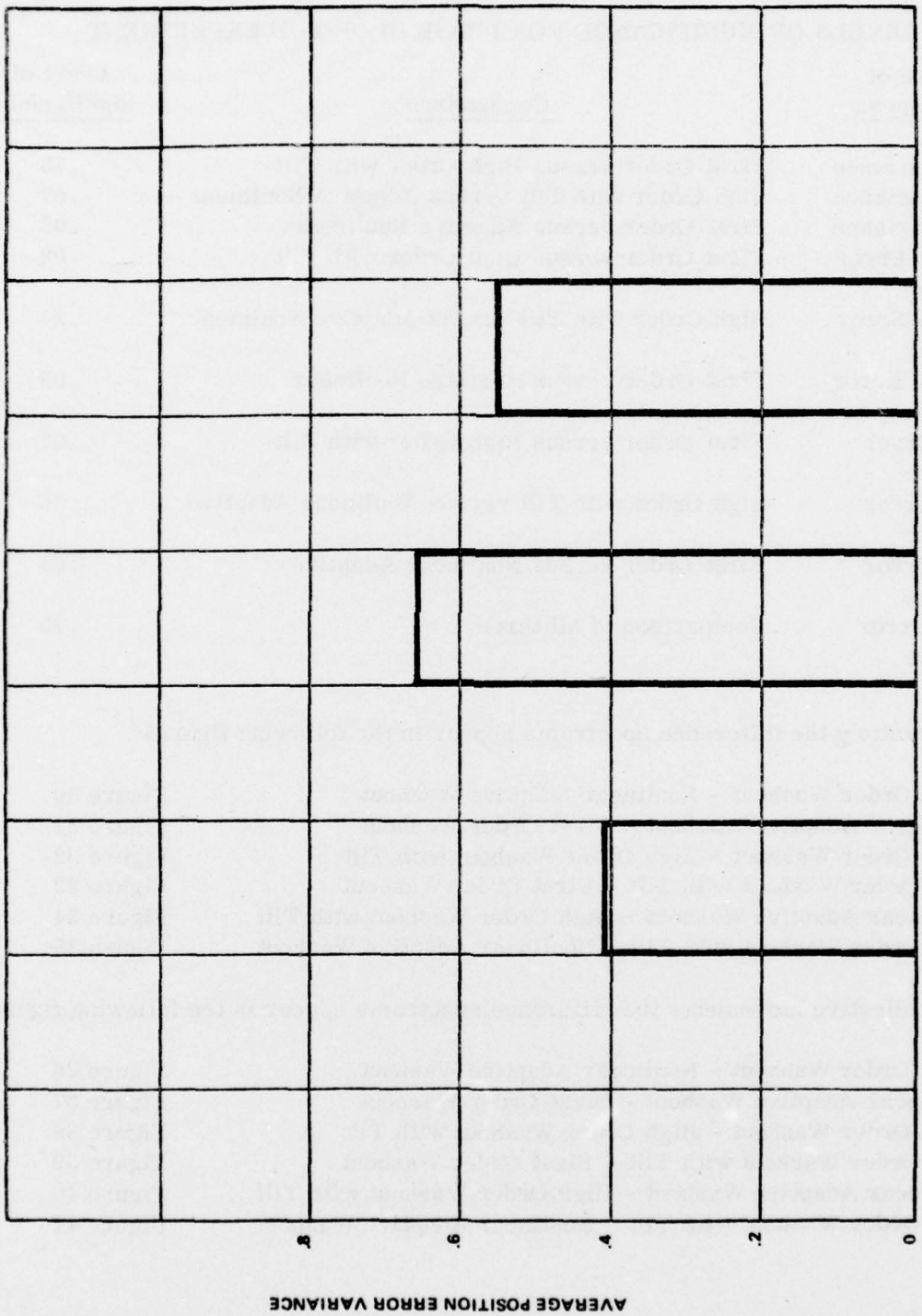

FIGURE 20 - Position Error Variance For Washout Types (Phase III)

TABLE I

LEVELS OF SIGNIFICANCE FOR PHASE III OF THE EXPERIMENT

Measure of Effectiveness	Comparison	Level of Significance
Control Variance	First Order versus High Order with Tilt	.13
Control Variance	High Order with Tilt versus Adaptive Nonlinear	.07
Control Variance	First Order versus Adaptive Nonlinear	.03
Body Rate Error Variance	First Order versus High Order with Tilt	.08
Body Rate Error Variance	High Order with Tilt versus Adaptive Nonlinear	.24
Body Rate Error Variance	First Order versus Adaptive Nonlinear	.03
Attitude Error Variance	First Order versus High Order with Tilt	.07
Attitude Error Variance	High Order with Tilt versus Nonlinear Adaptive	.16
Attitude Error Variance	First Order versus Nonlinear Adaptive	.04
Position Error Variance	Comparison of all three	.75

For cyclic y the difference spectrums appear in the following figures:

First Order Washout - Nonlinear Adaptive Washout	Figure 30
Nonlinear Adaptive Washout - First Order Washout	Figure 31
First Order Washout - High Order Washout with Tilt	Figure 32
High Order Washout with Tilt - First Order Washout	Figure 33
Nonlinear Adaptive Washout - High Order Washout with Tilt	Figure 34
High Order Washout with Tilt - Nonlinear Adaptive Washout	Figure 35

For collective movements the difference spectrums appear in the following figures:

First Order Washout - Nonlinear Adaptive Washout	Figure 36
Nonlinear Adaptive Washout - First Order Washout	Figure 37
First Order Washout - High Order Washout with Tilt	Figure 38
High Order Washout with Tilt - First Order Washout	Figure 39
Nonlinear Adaptive Washout - High Order Washout with Tilt	Figure 40
High Order Washout with Tilt - Nonlinear Adaptive Washout	Figure 41

FIGURE 21 - Frequency Content Of Control Movements For First Order Washout

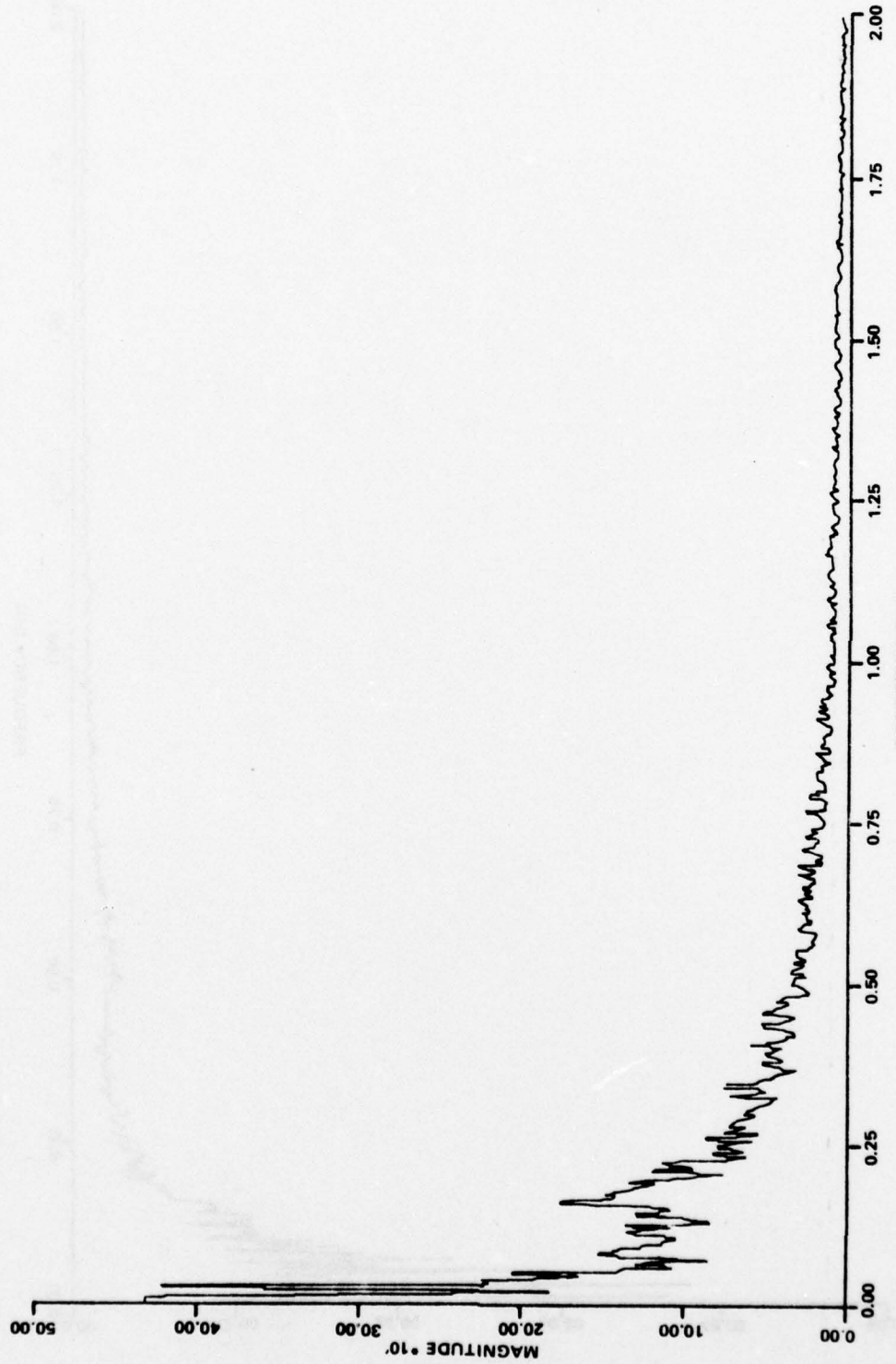

FIGURE 21 - Frequency Content Of Control Movements For First Order Washout (Con't)

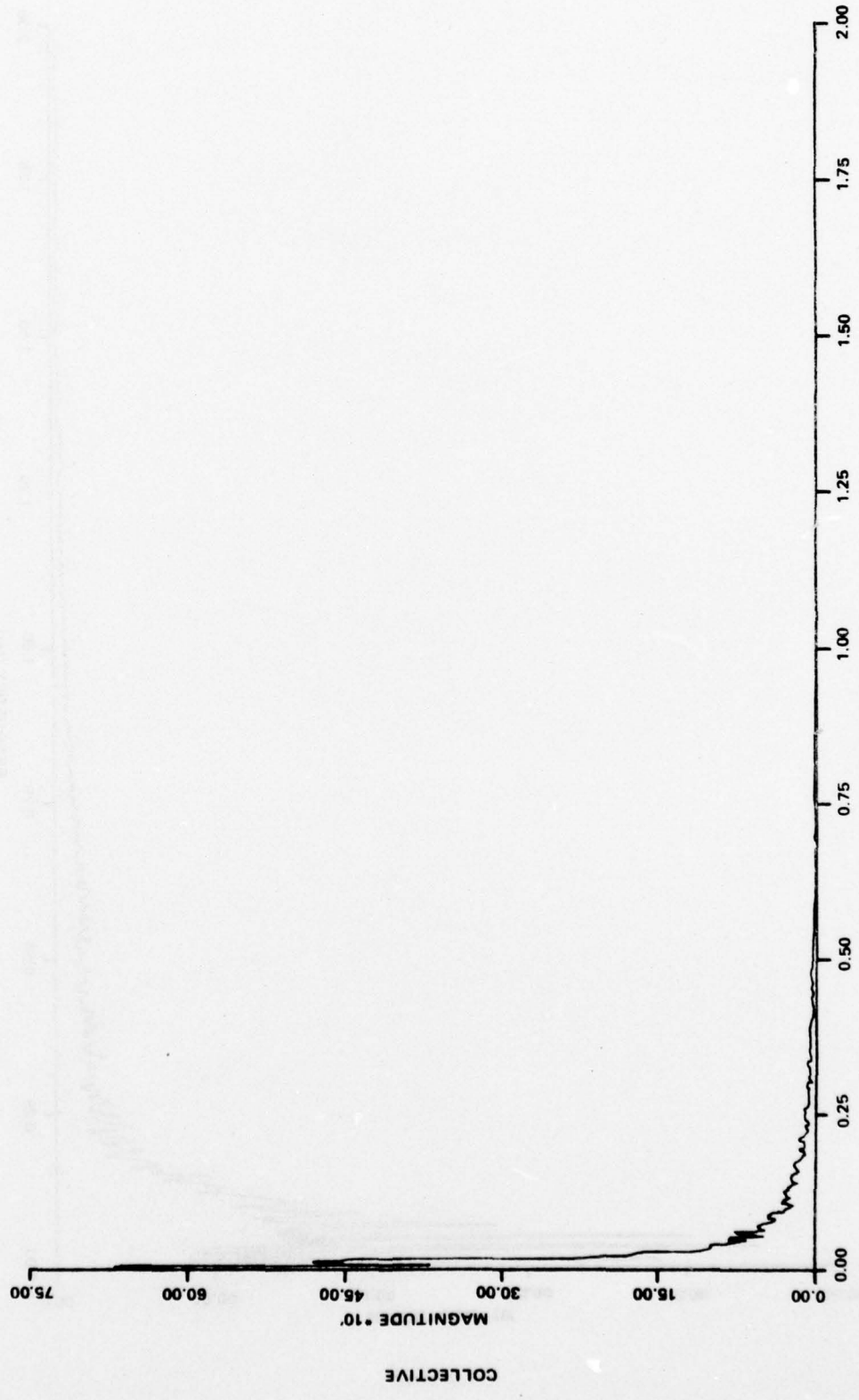

FIGURE 21 - Frequency Content Of Control Movements For First Order Washout (Con't)

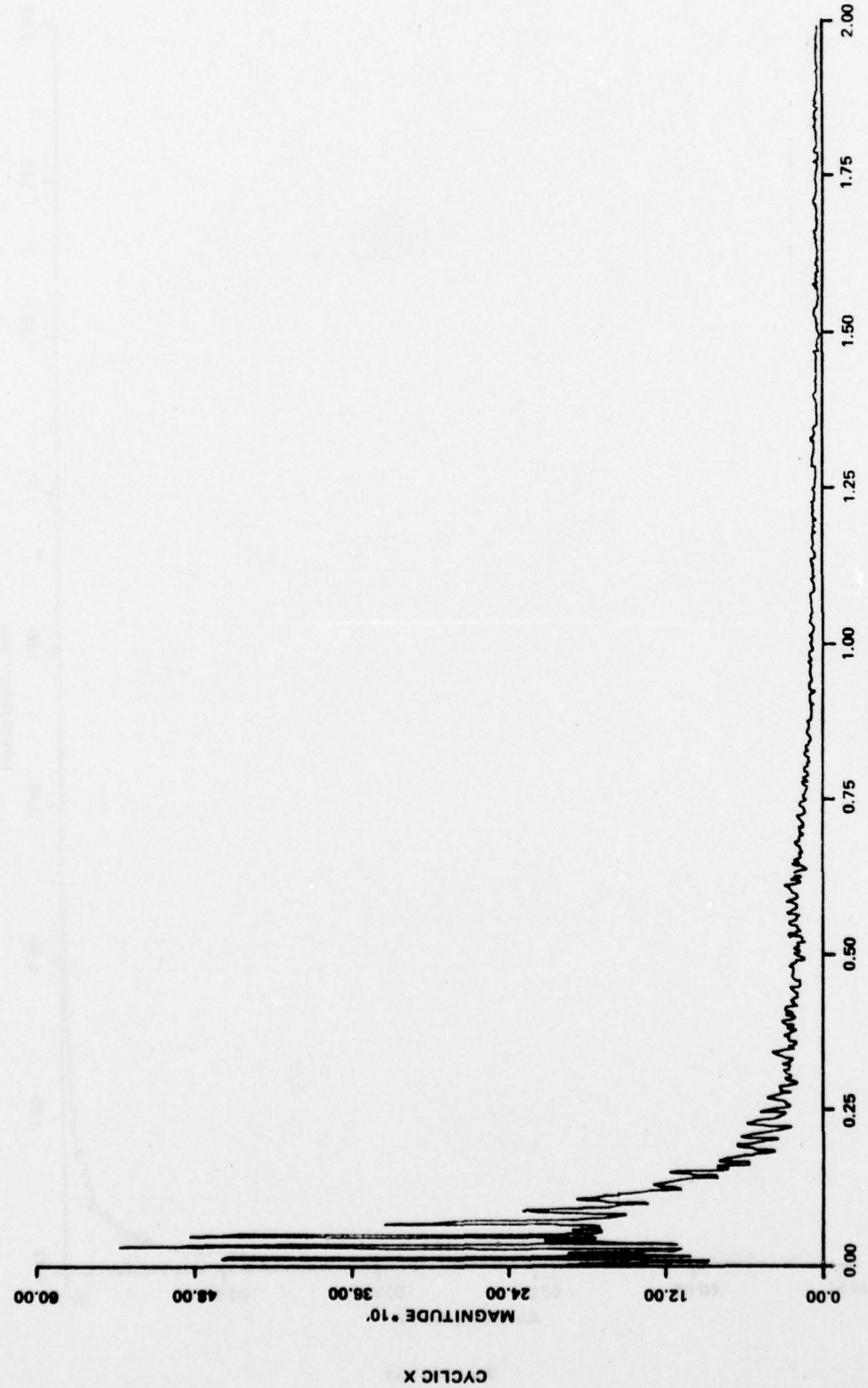

FIGURE 22 - Frequency Content Of Control Movements For Nonlinear Adaptive Washout

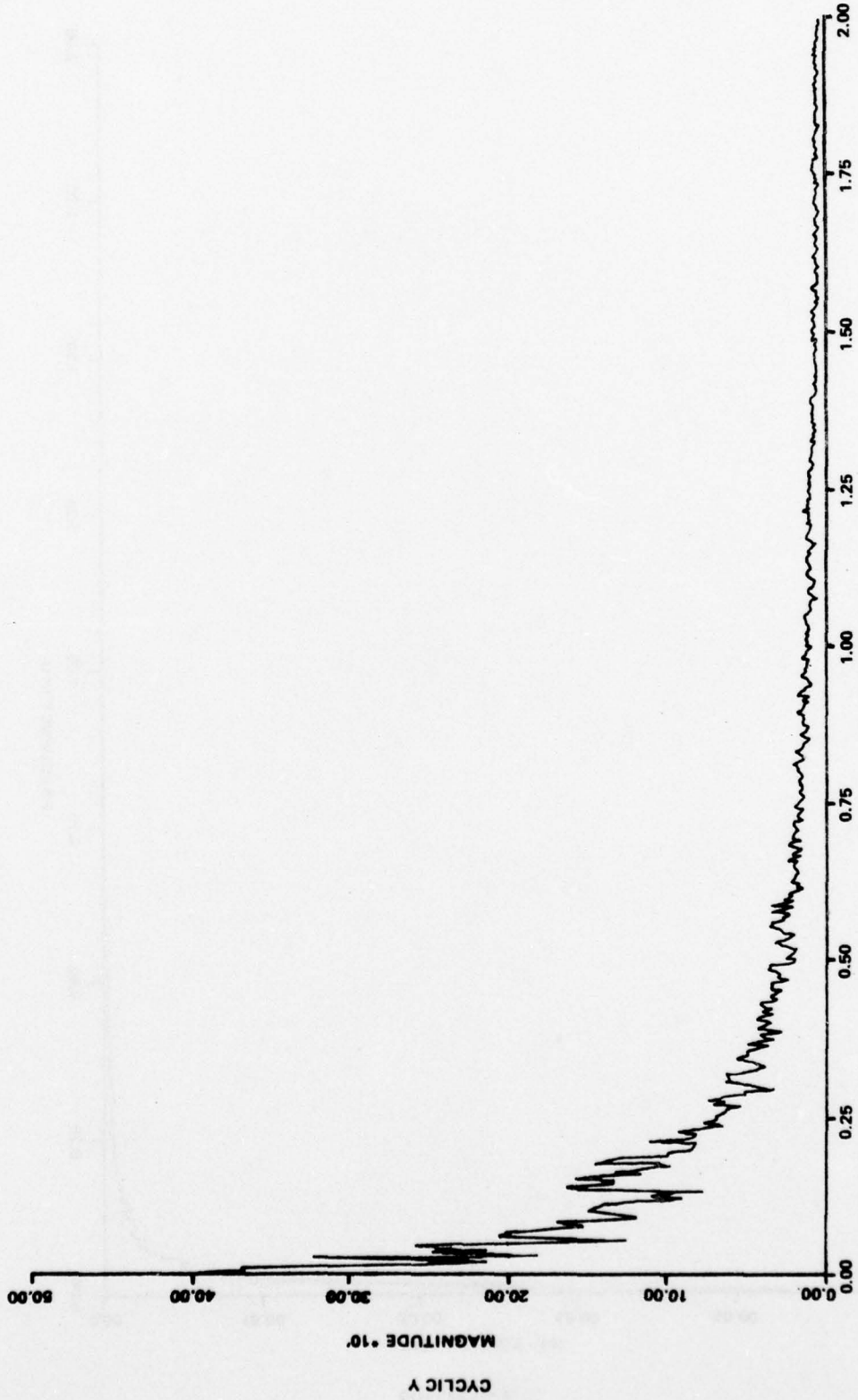

FIGURE 22 - Frequency Content Of Control Movements For Nonlinear Adaptive Washout (Con't)

FIGURE 22 - Frequency Content Of Control Movements For Nonlinear Adaptive Washout (Con't)

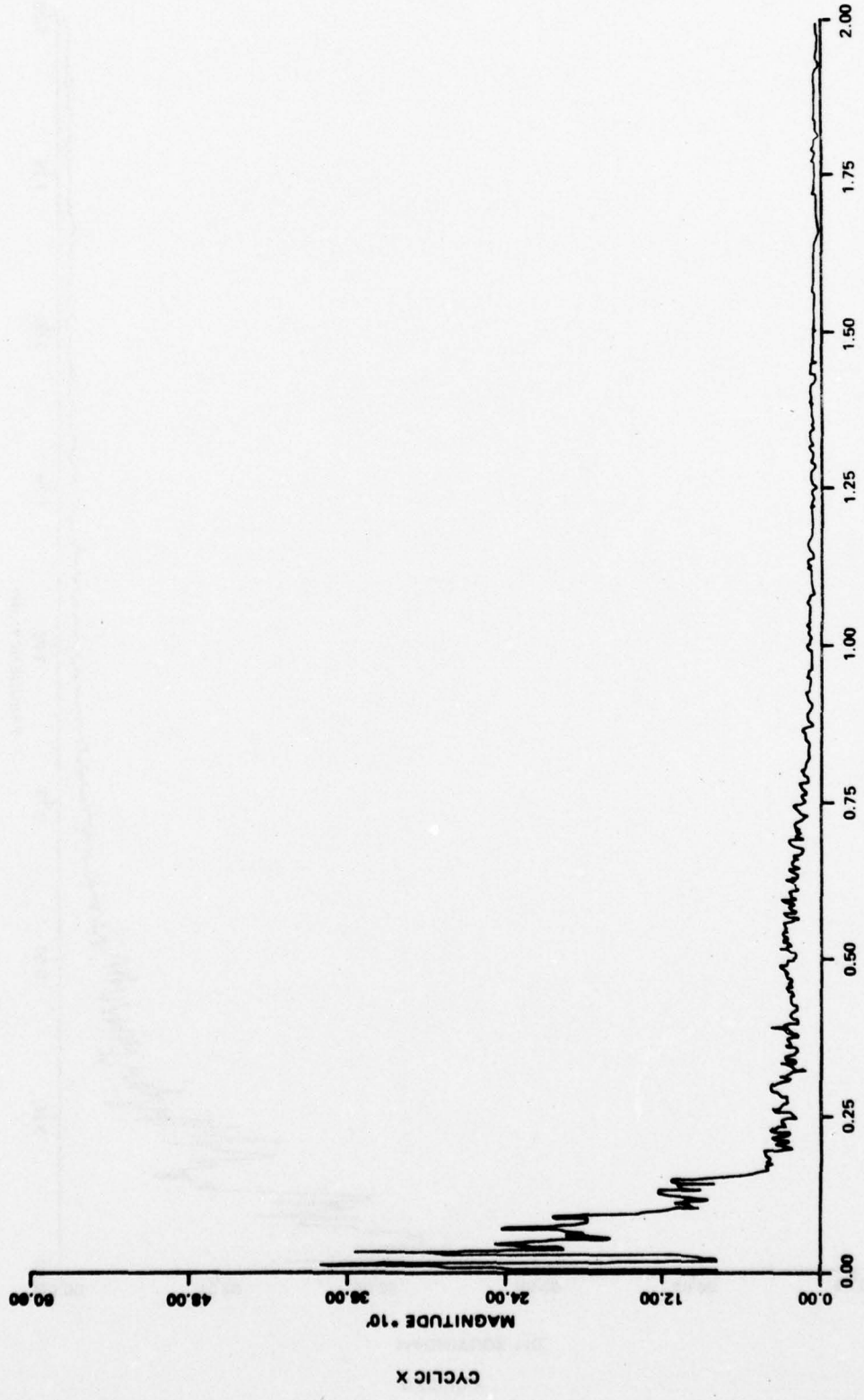

FIGURE 23 - Frequency Content Of Control Movements For High Order Washout With Tilt

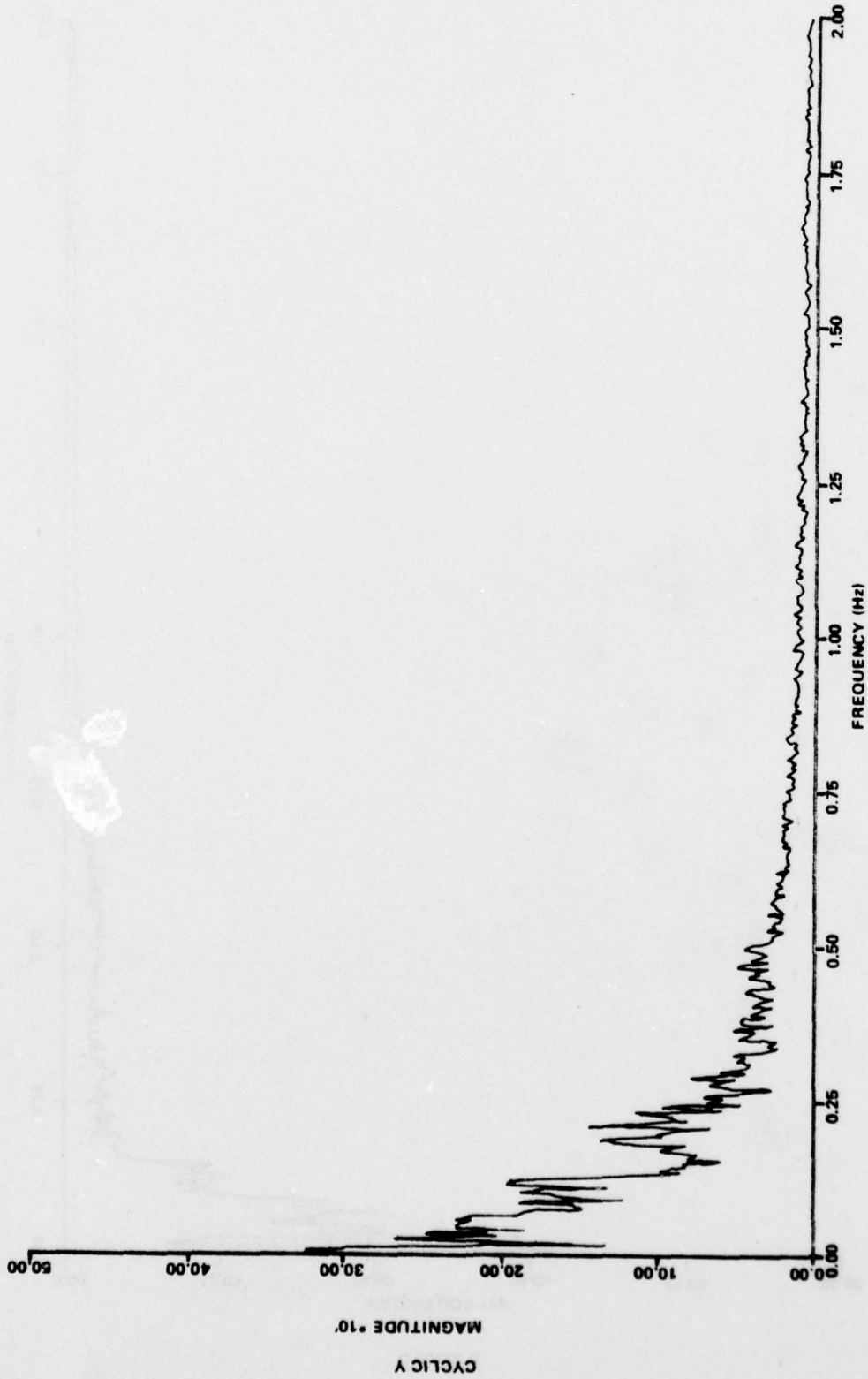

FIGURE 23 - Frequency Content Of Control Movements For High Order Washout With Tilt (Con't)

FIGURE 23 - Frequency Content Of Control Movements For High Order Washout With Tilt (Con't)

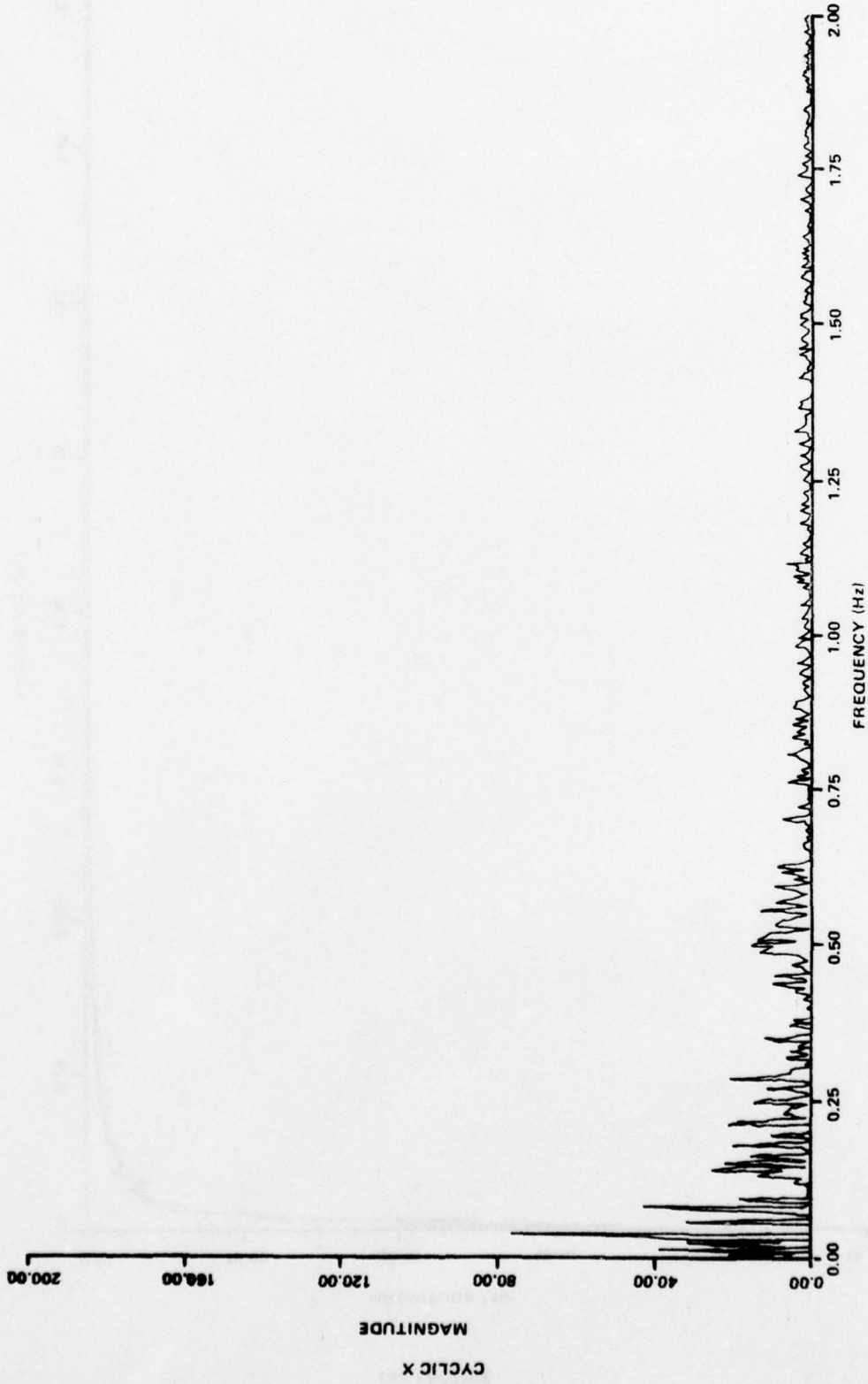

FIGURE 24 - Cyclic X Difference Spectrum For First Order Washout Minus Nonlinear Adaptive Washout

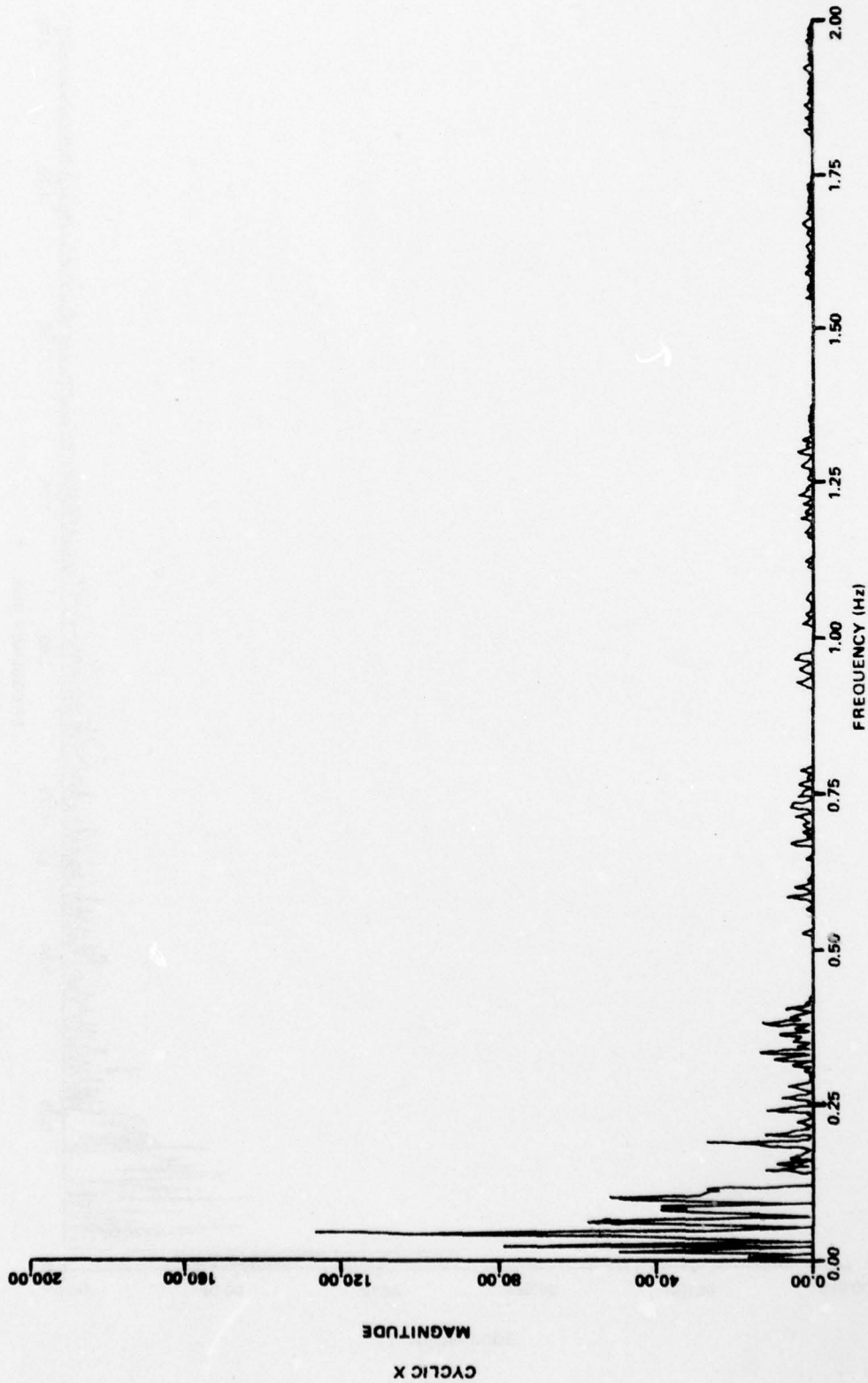

FIGURE 25 - Cyclic X Difference Spectrum For Nonlinear Adaptive Washout Minus First Order Washout

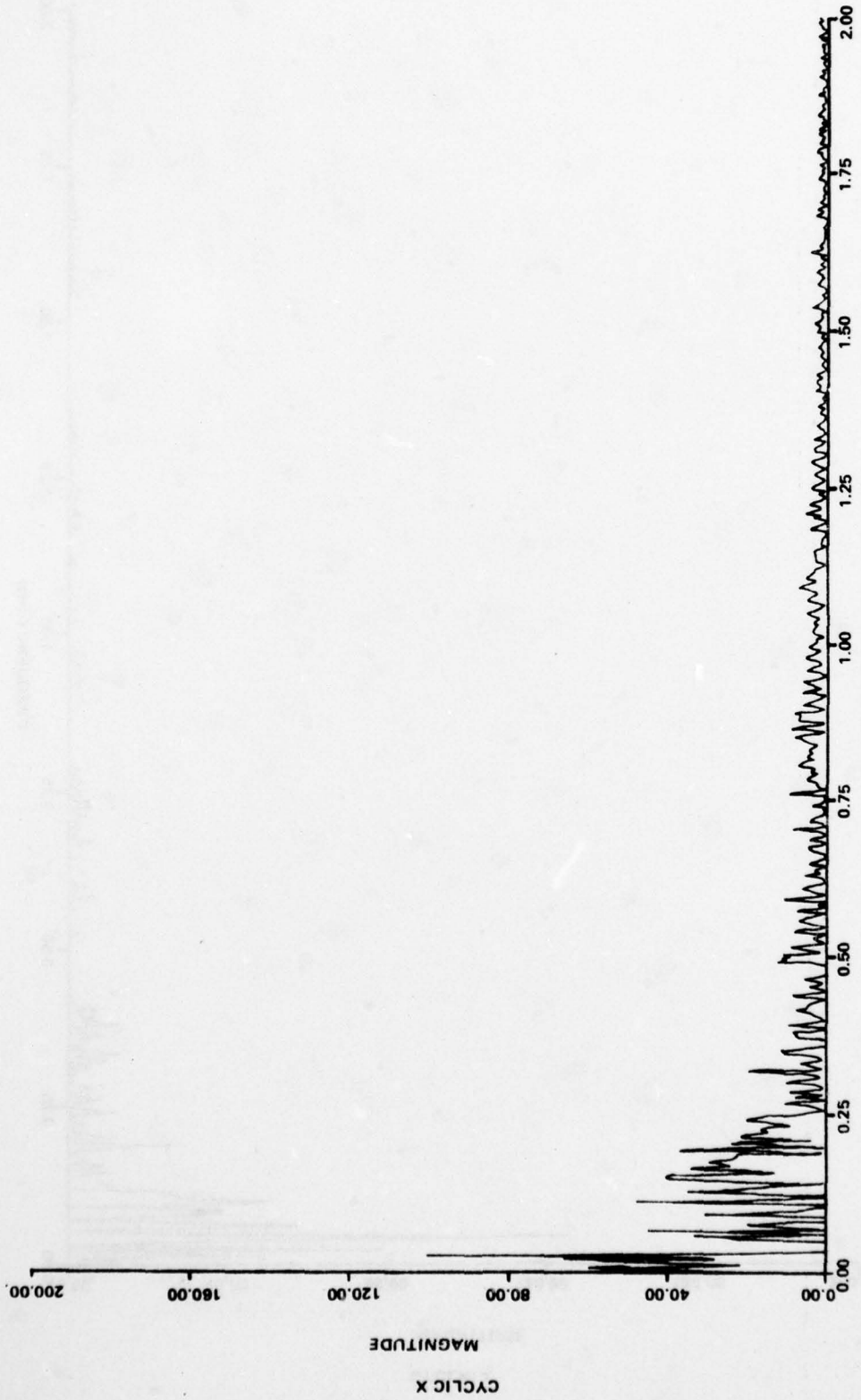

FIGURE 26 - Cyclic X Difference Spectrum For First Order Washout Minus High Order Washout With Tilt

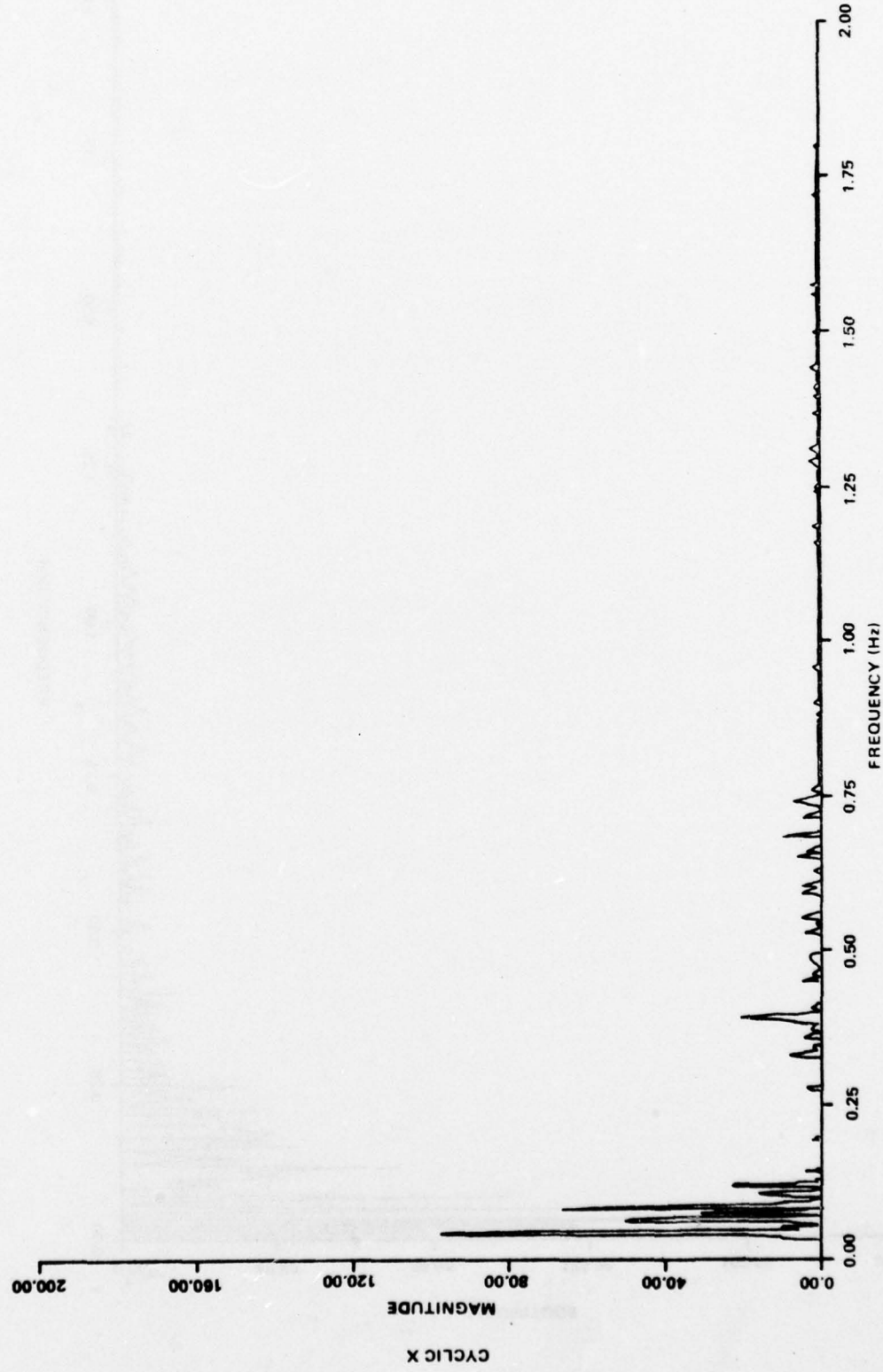

FIGURE 27 - Cyclic X Difference Spectrum For High Order Washout With Tilt Minus First Order Washout

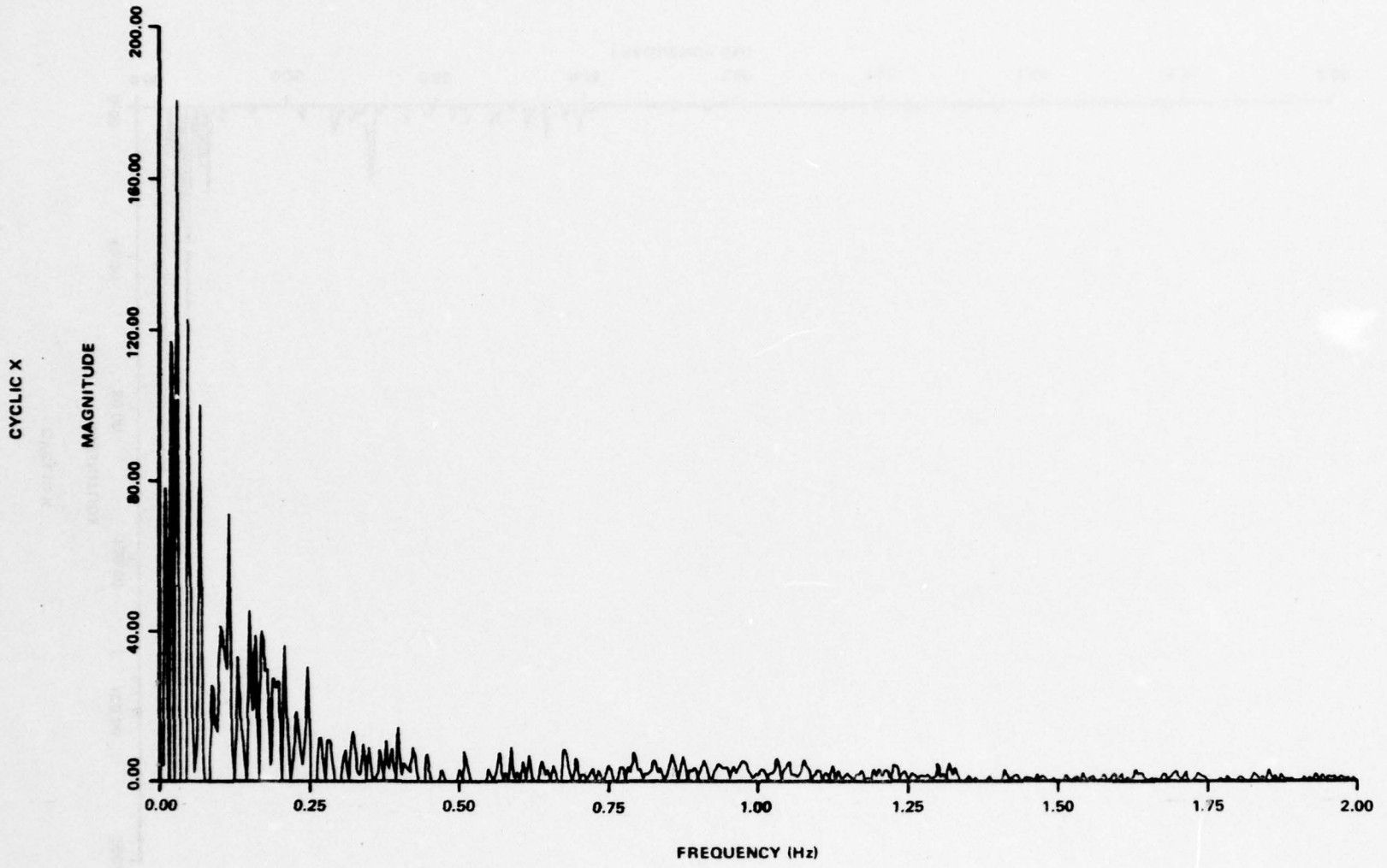

FIGURE 28 - Cyclic X Difference Spectrum For Nonlinear Adaptive Washout Minus High Order Washout With Tilt

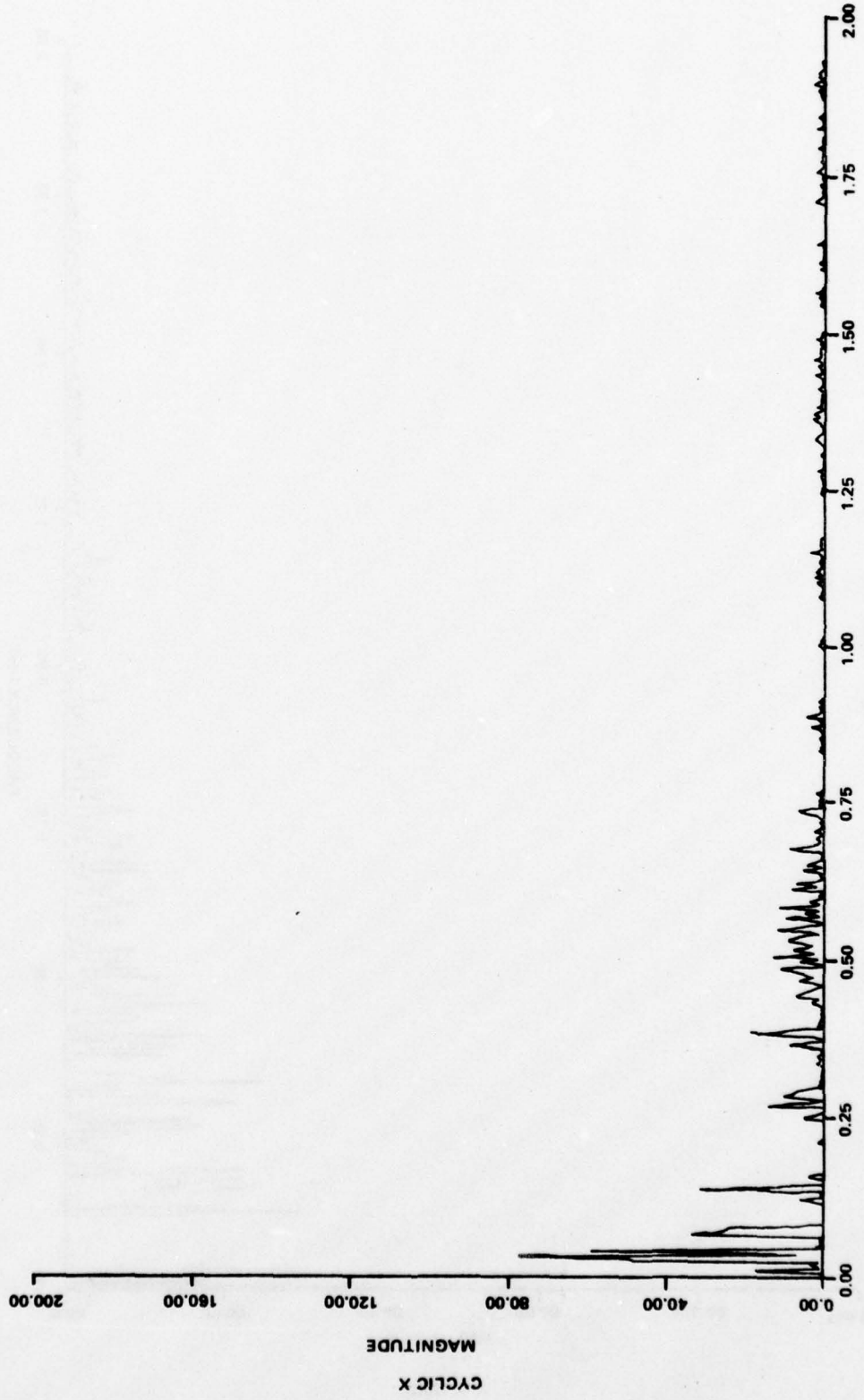

FIGURE 29 - Cyclic X Difference Spectrum For High Order Washout With Tilt Minus Nonlinear Adaptive Washout

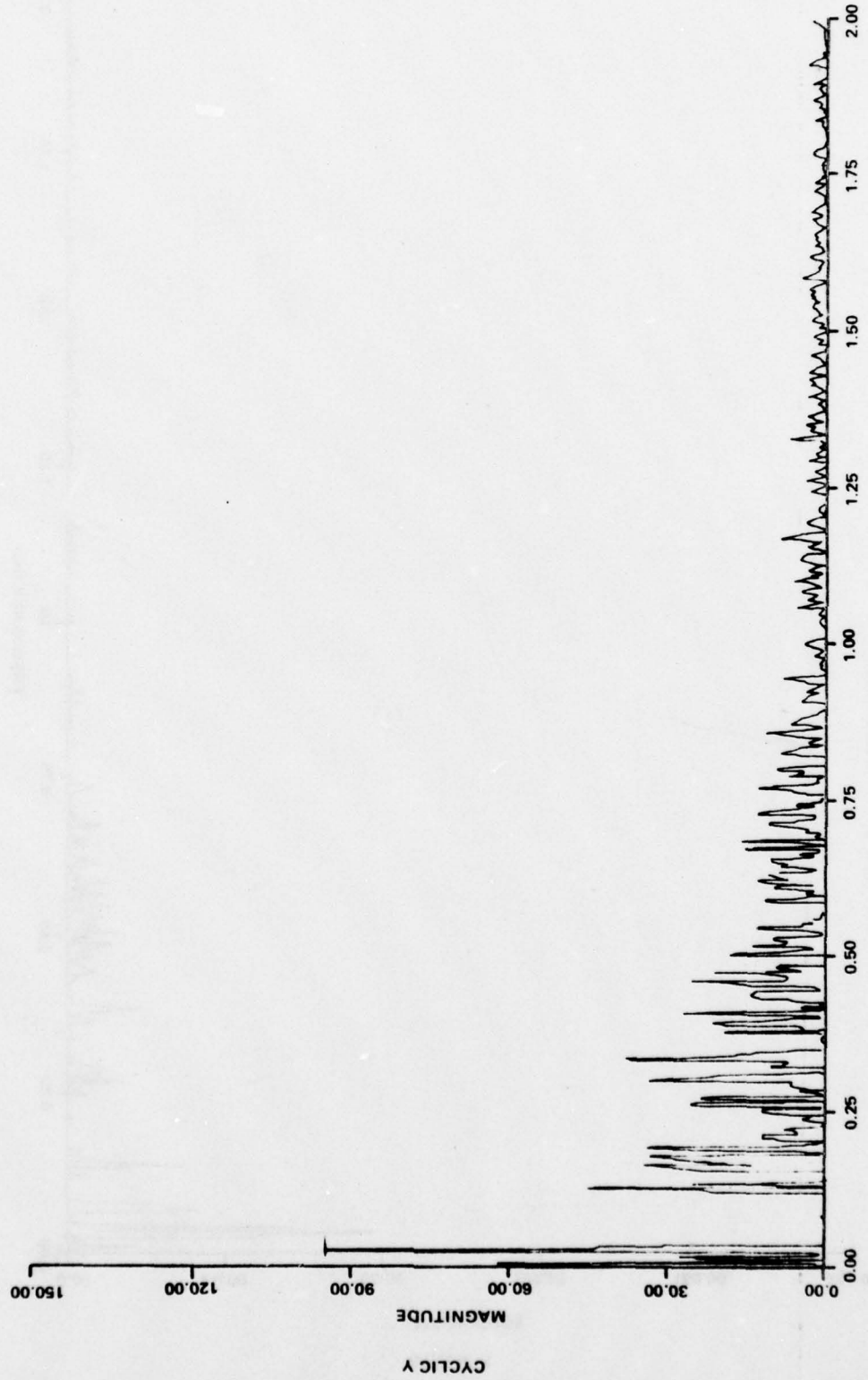

FIGURE 30 - Cyclic Y Difference Spectrum For First Order Washout Minus Nonlinear Adaptive Washout

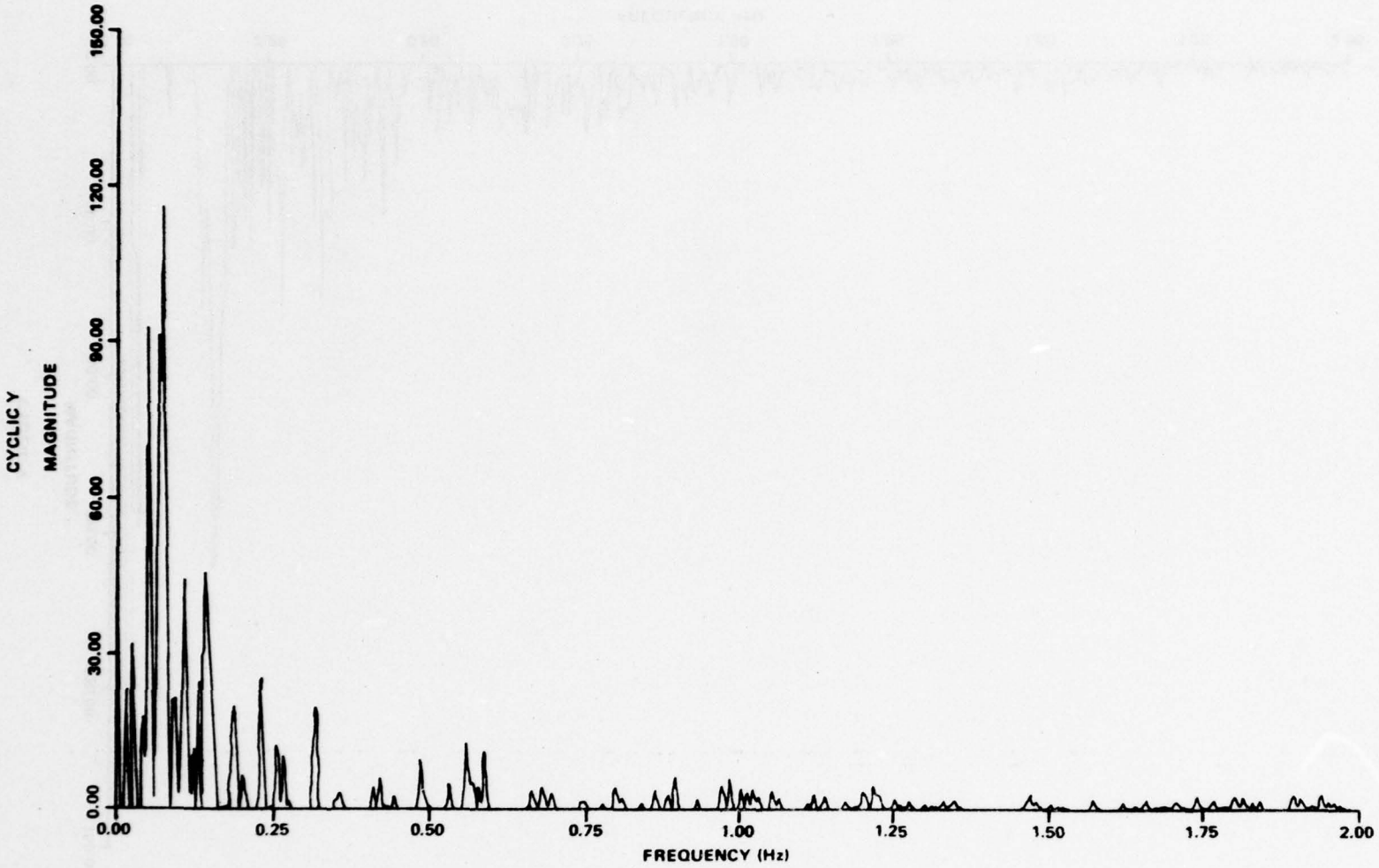

FIGURE 31 - Cyclic Y Difference Spectrum For Nonlinear Adaptive Washout Minus First Order Washout

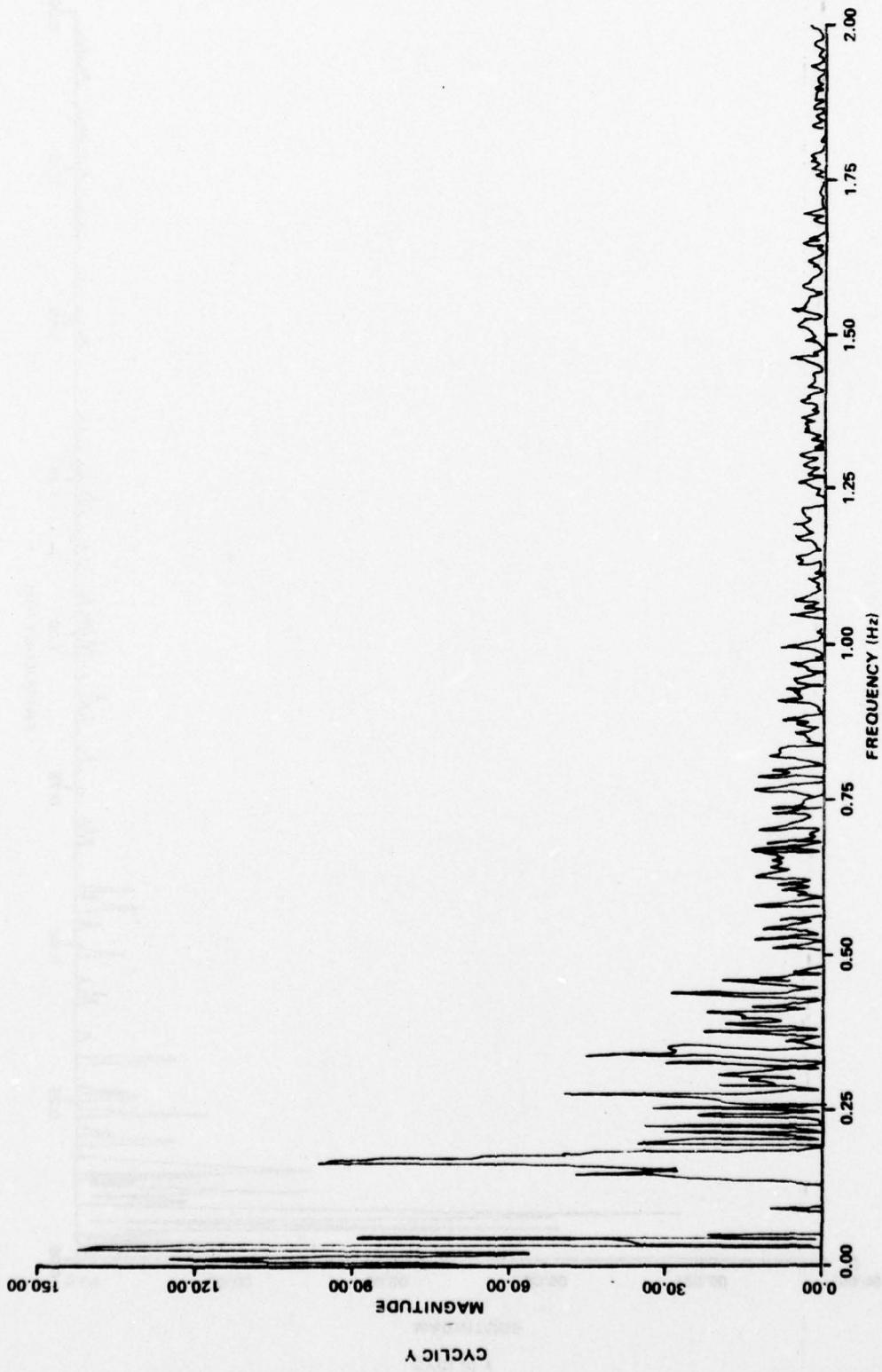

FIGURE 32 - Cyclic Y Difference Spectrum For First Order Washout Minus High Order Washout With Tilt

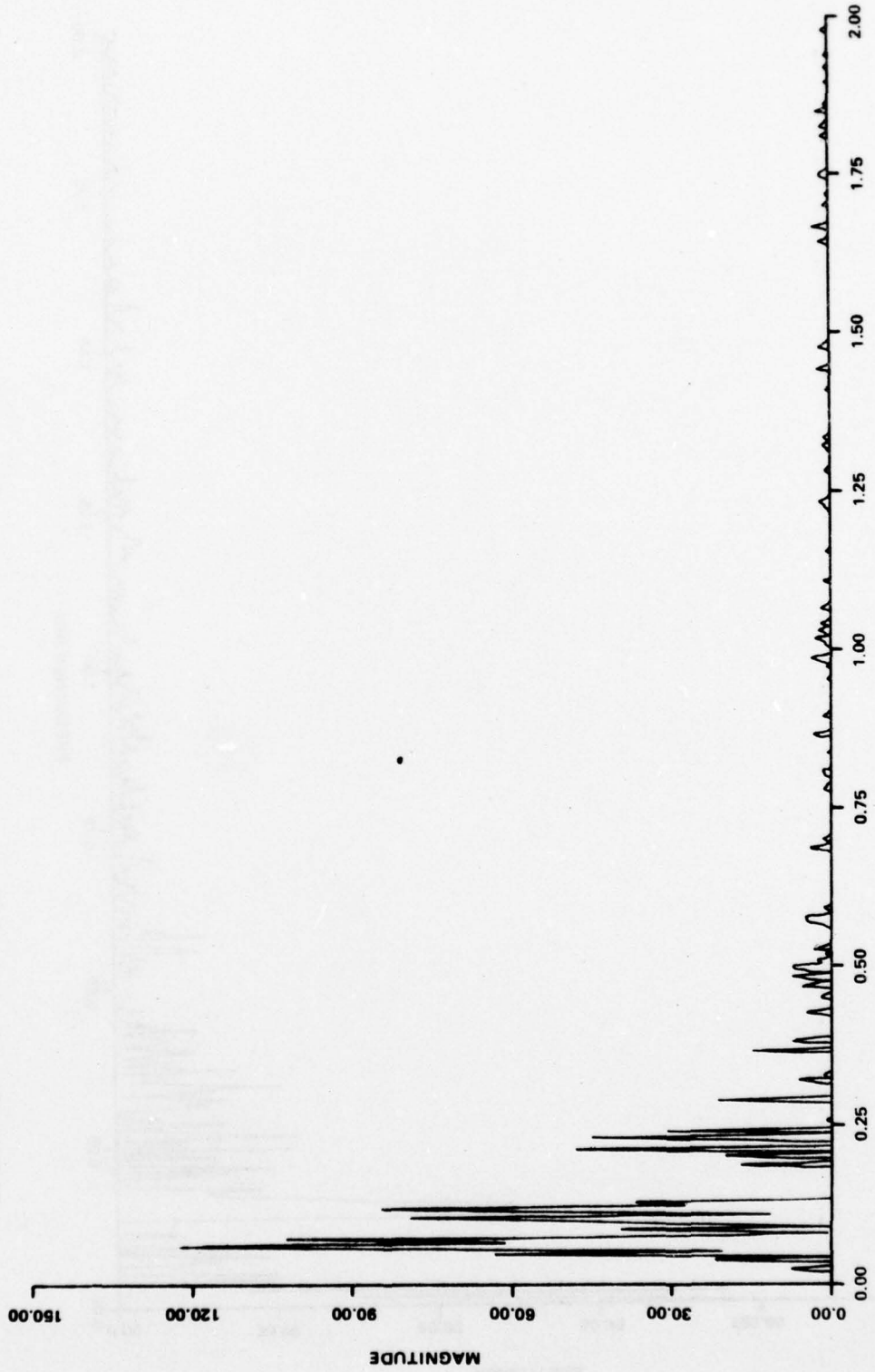

FIGURE 33 - Cyclic Y Difference Spectrum For High Order Washout With Tilt Minus First Order Washout

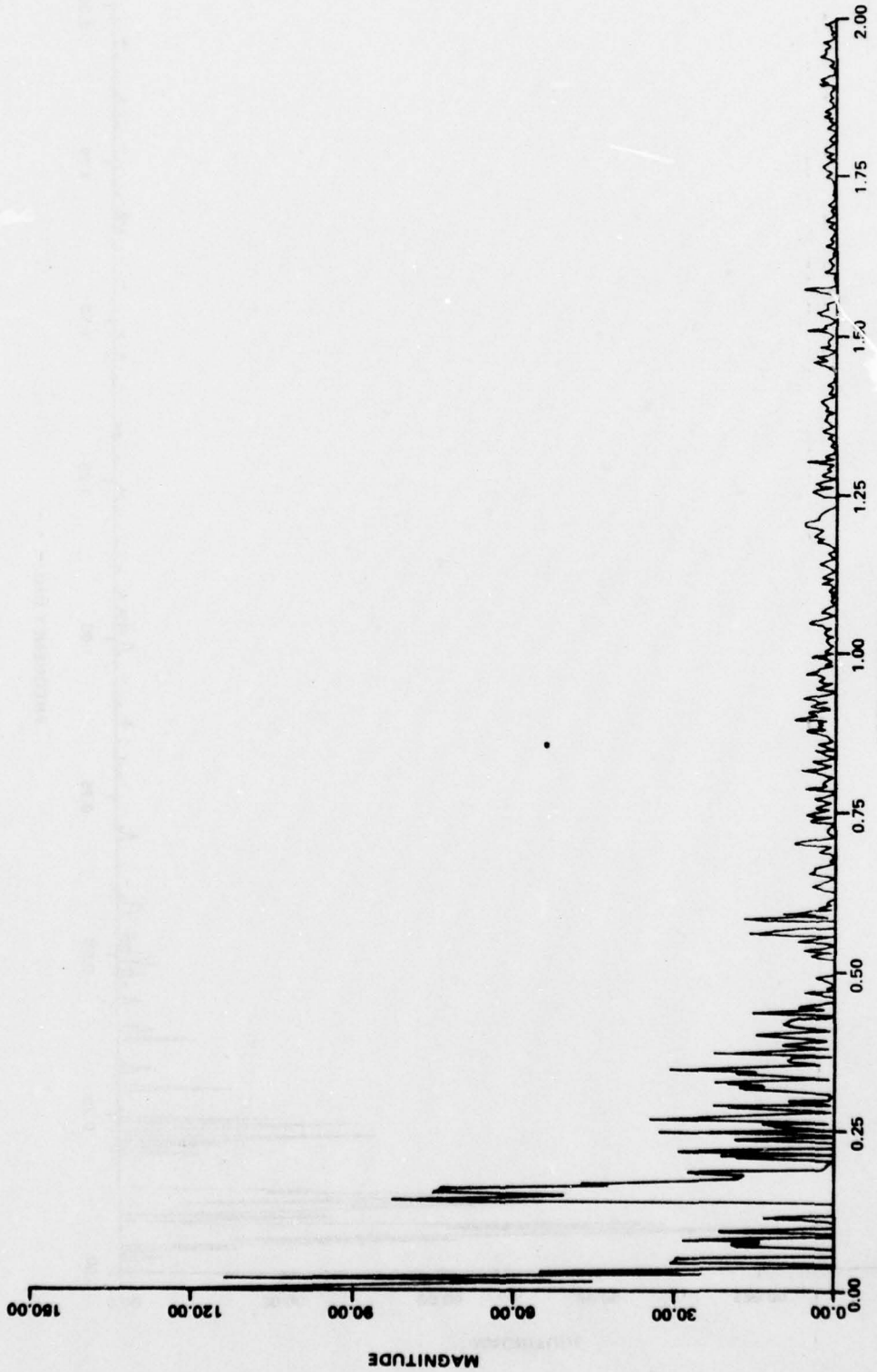

FIGURE 34 - Cyclic Y Difference Spectrum For Nonlinear Adaptive Washout Minus High Order Washout With Tilt

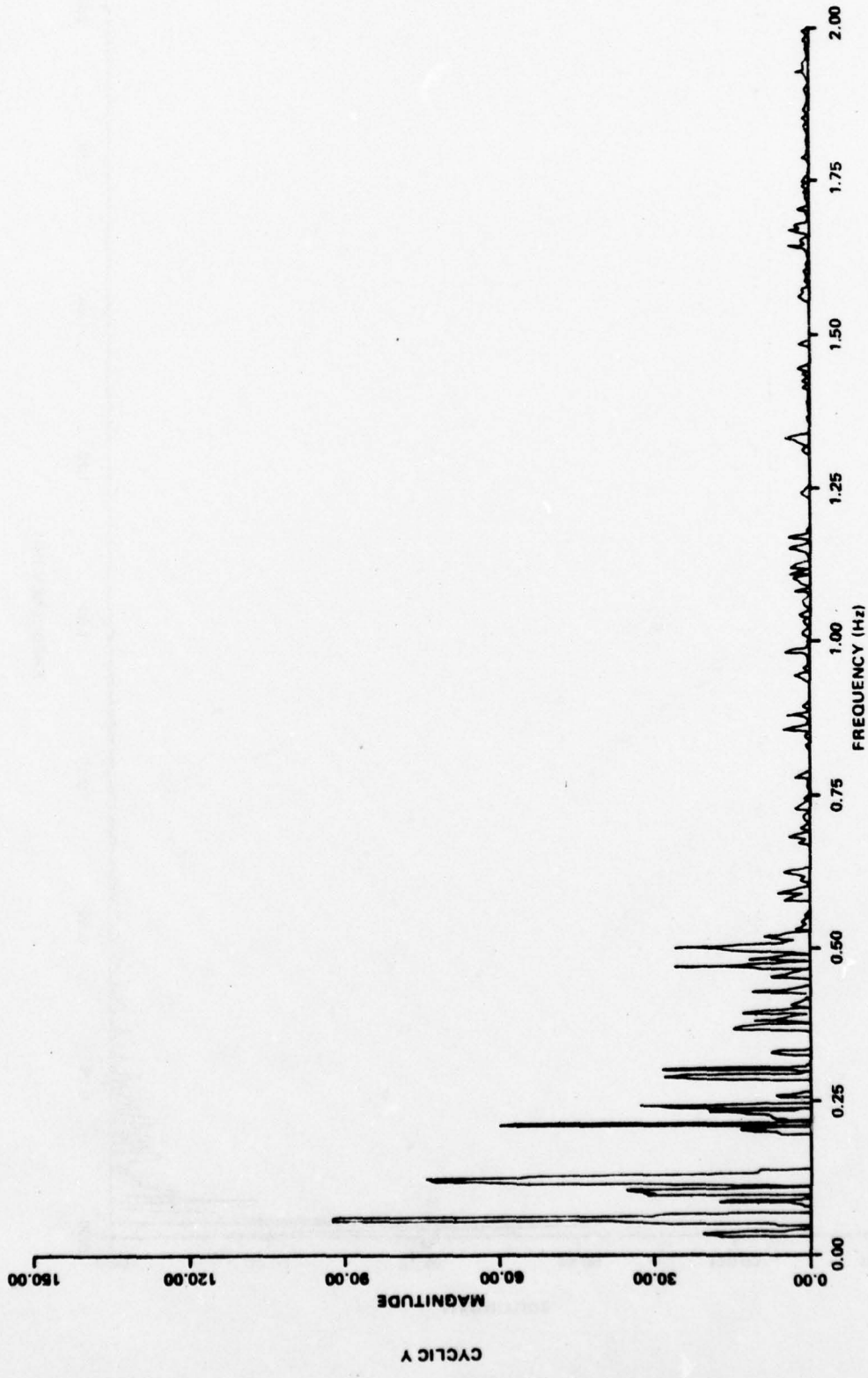

FIGURE 35 - Cyclic Y Difference Spectrum For High Order Washout With Tilt Minus Nonlinear Adaptive Washout

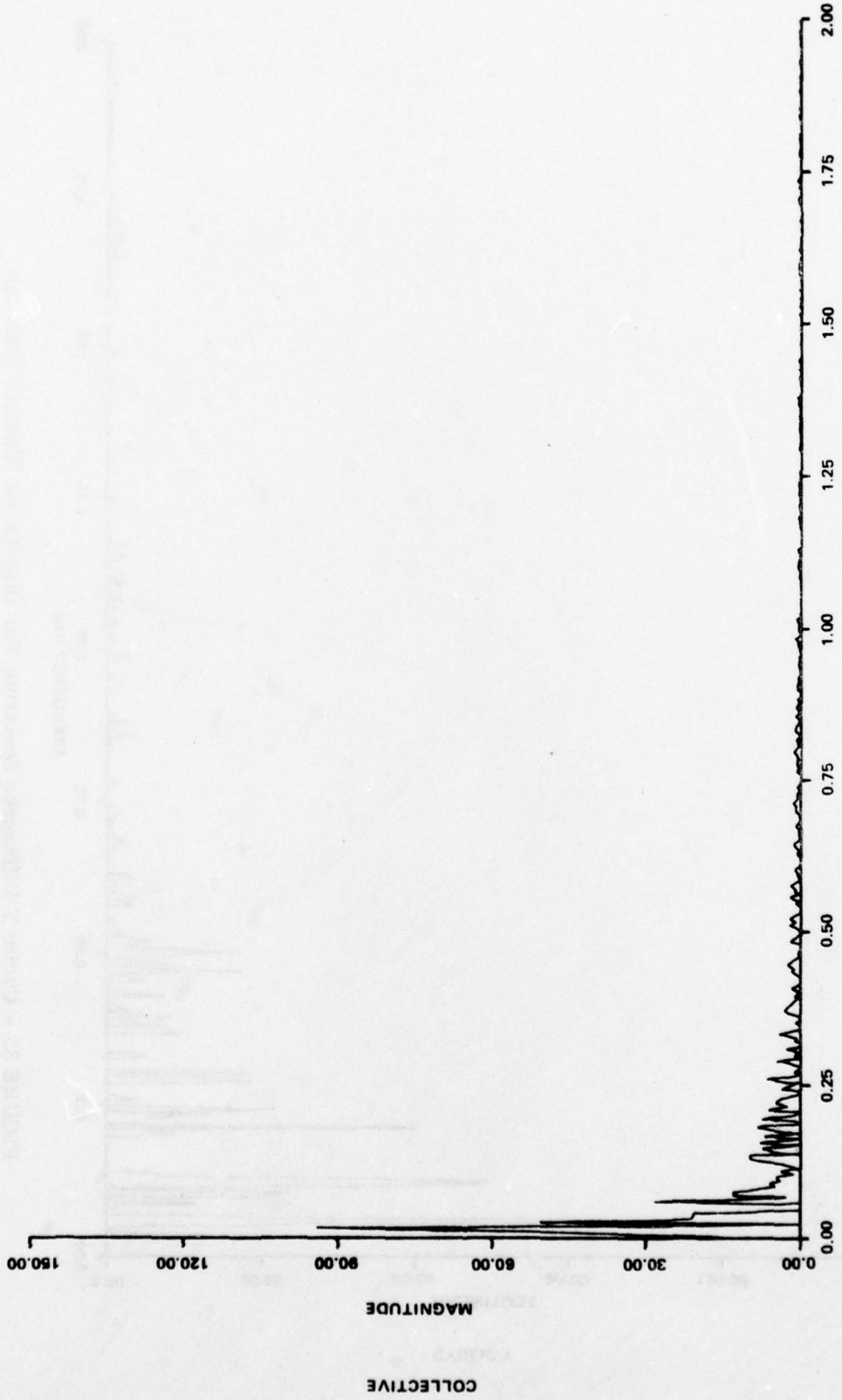

FIGURE 36 - Collective Difference Spectrum For First Order Washout Minus Nonlinear Adaptive Washout

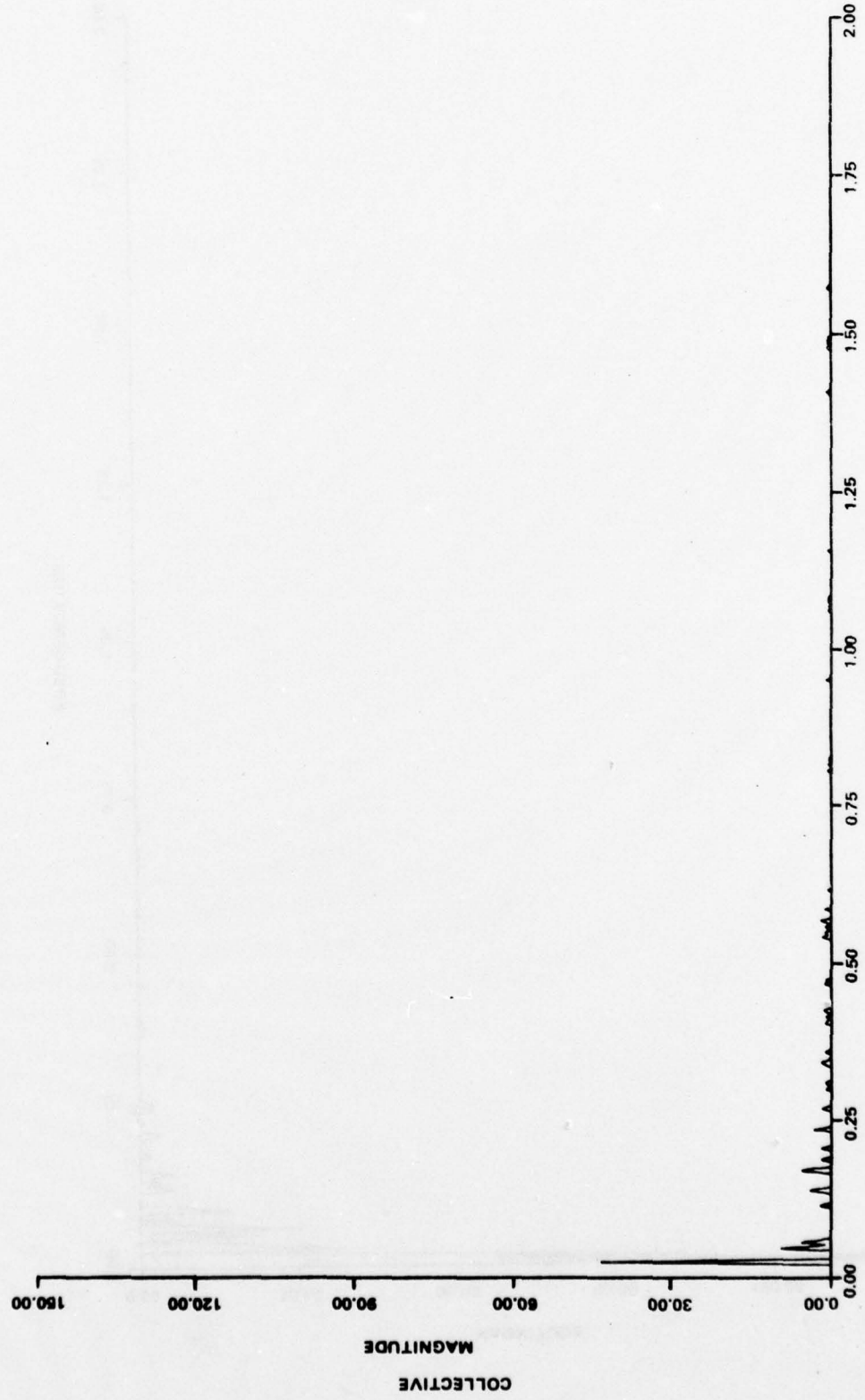

FIGURE 37 - Collective Difference Spectrum For Nonlinear Adaptive Washout Minus First Order Washout

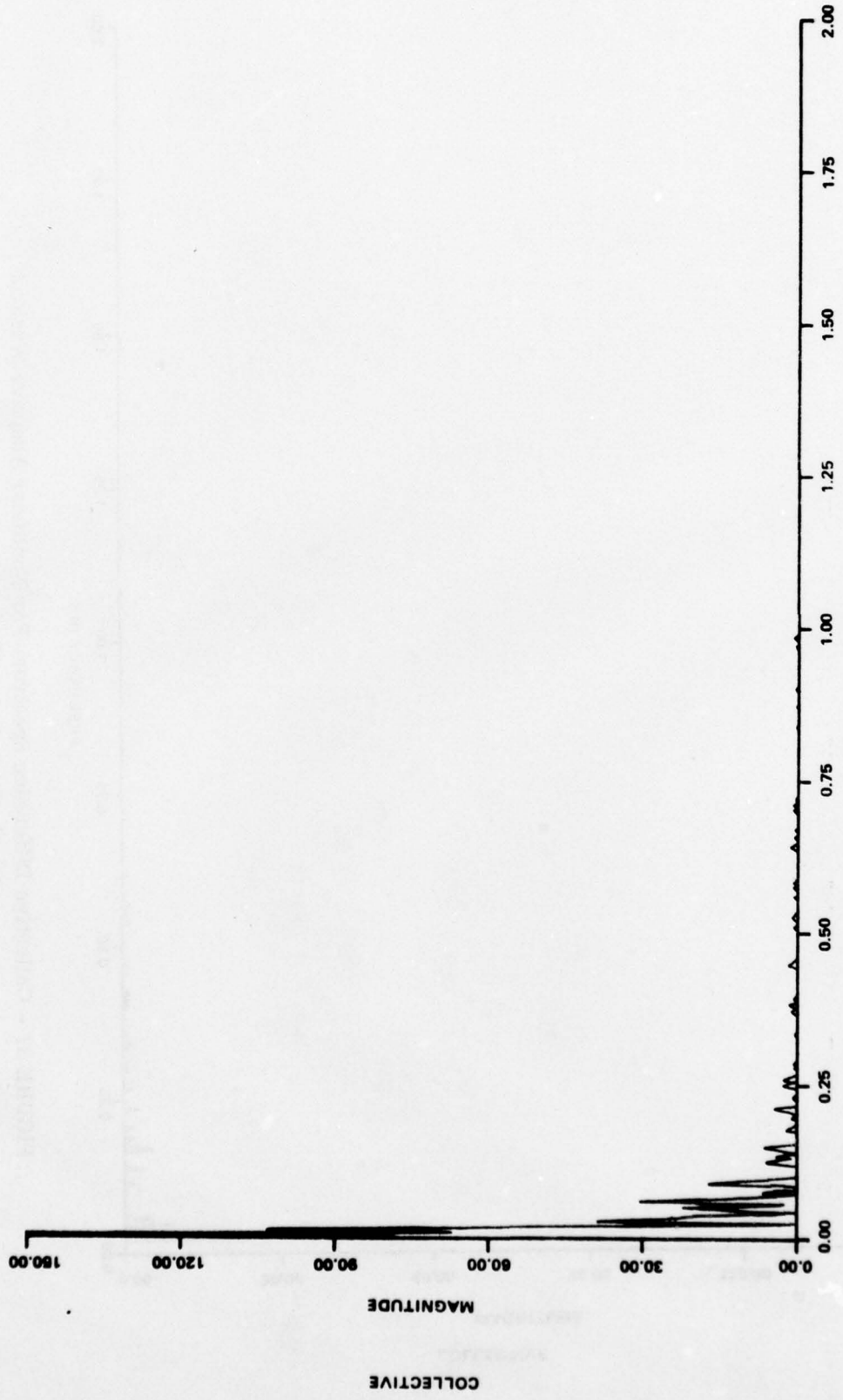

FIGURE 38 - Collective Difference Spectrum For First Order Washout Minus High Order Washout With Tilt

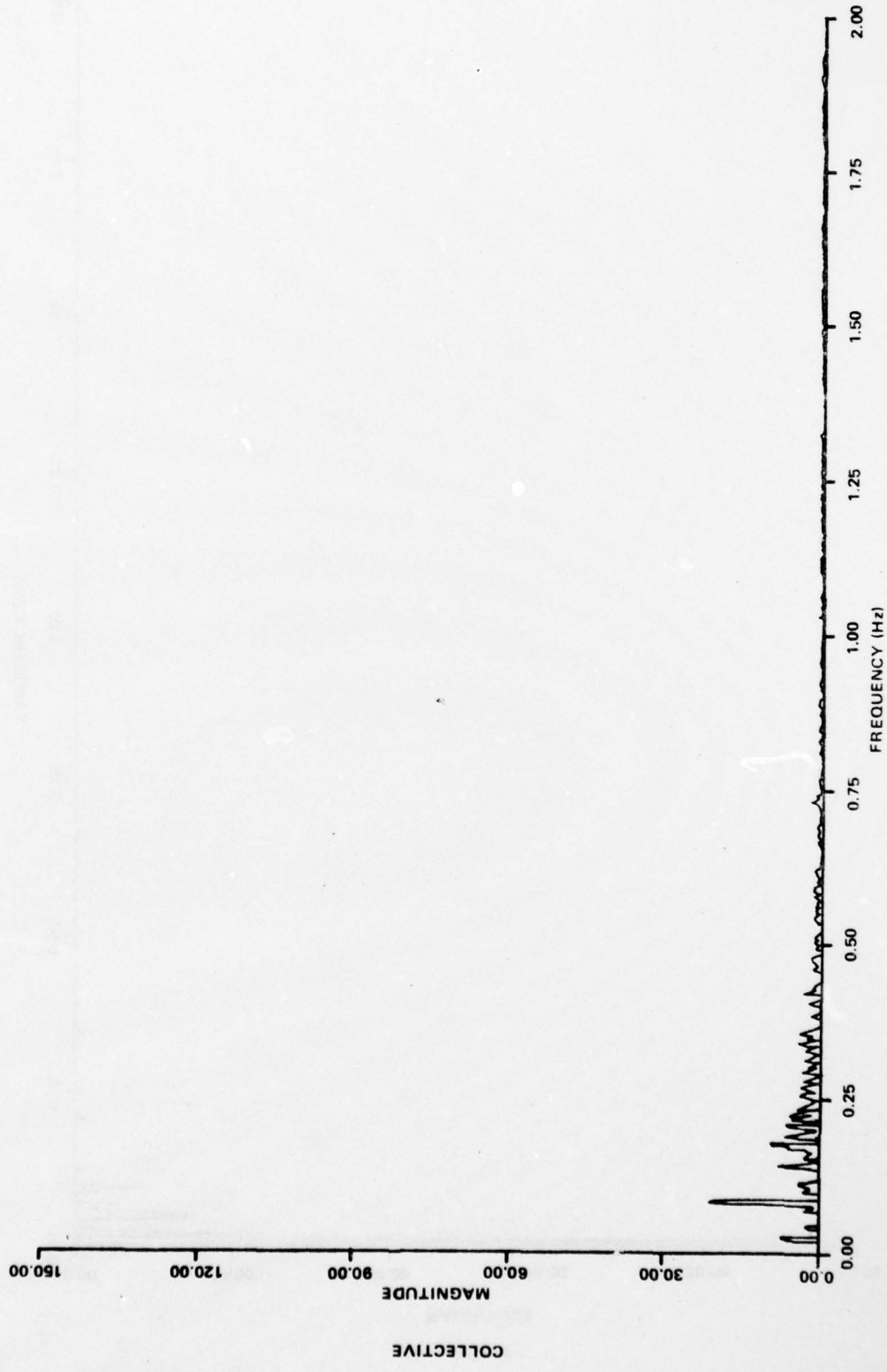

FIGURE 39 - Collective Difference Spectrum For High Order Washout With Tilt Minus First Order Washout

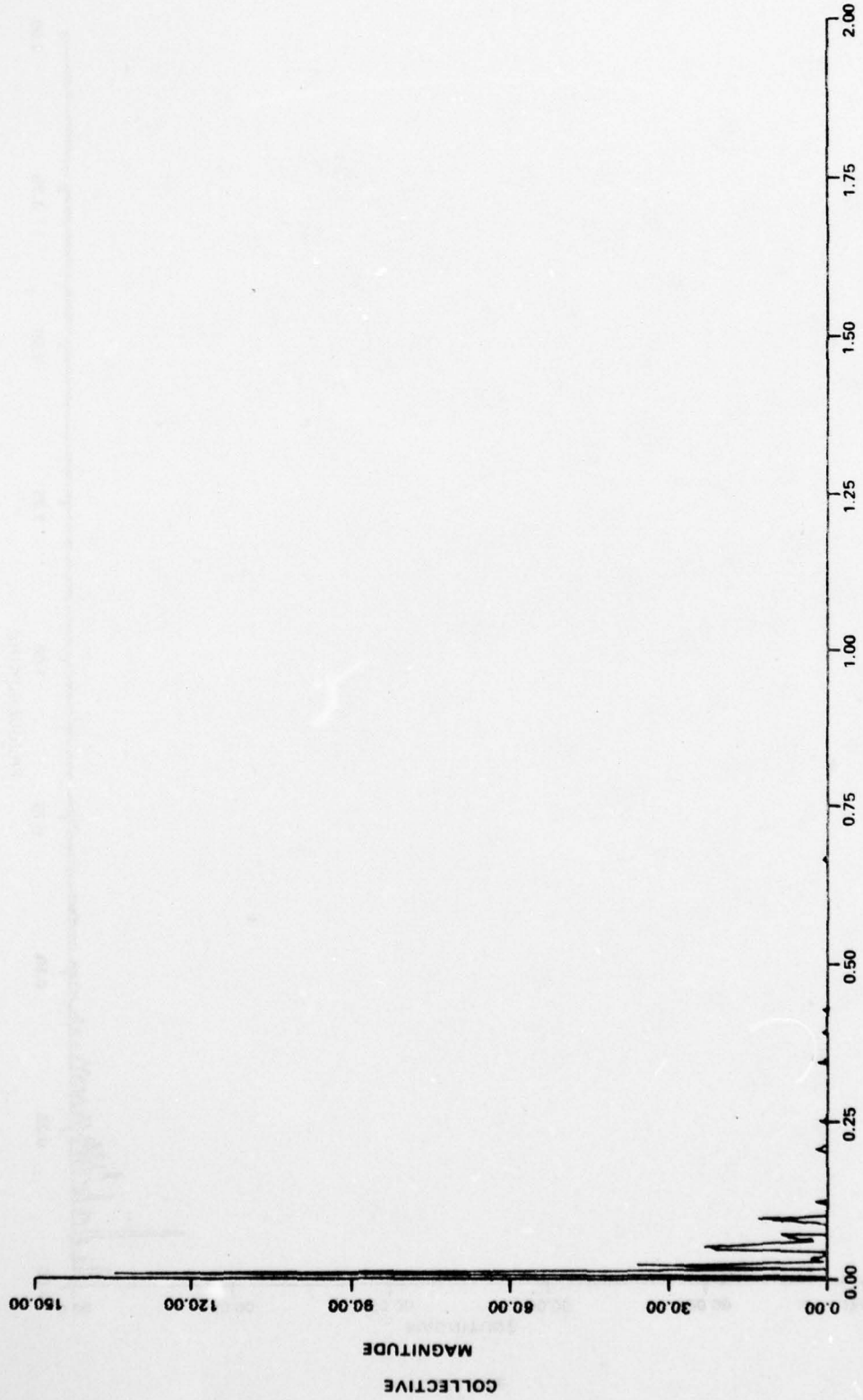

FIGURE 40 - Collective Difference Spectrum For Nonlinear Adaptive Washout Minus High Order Washout With Tilt

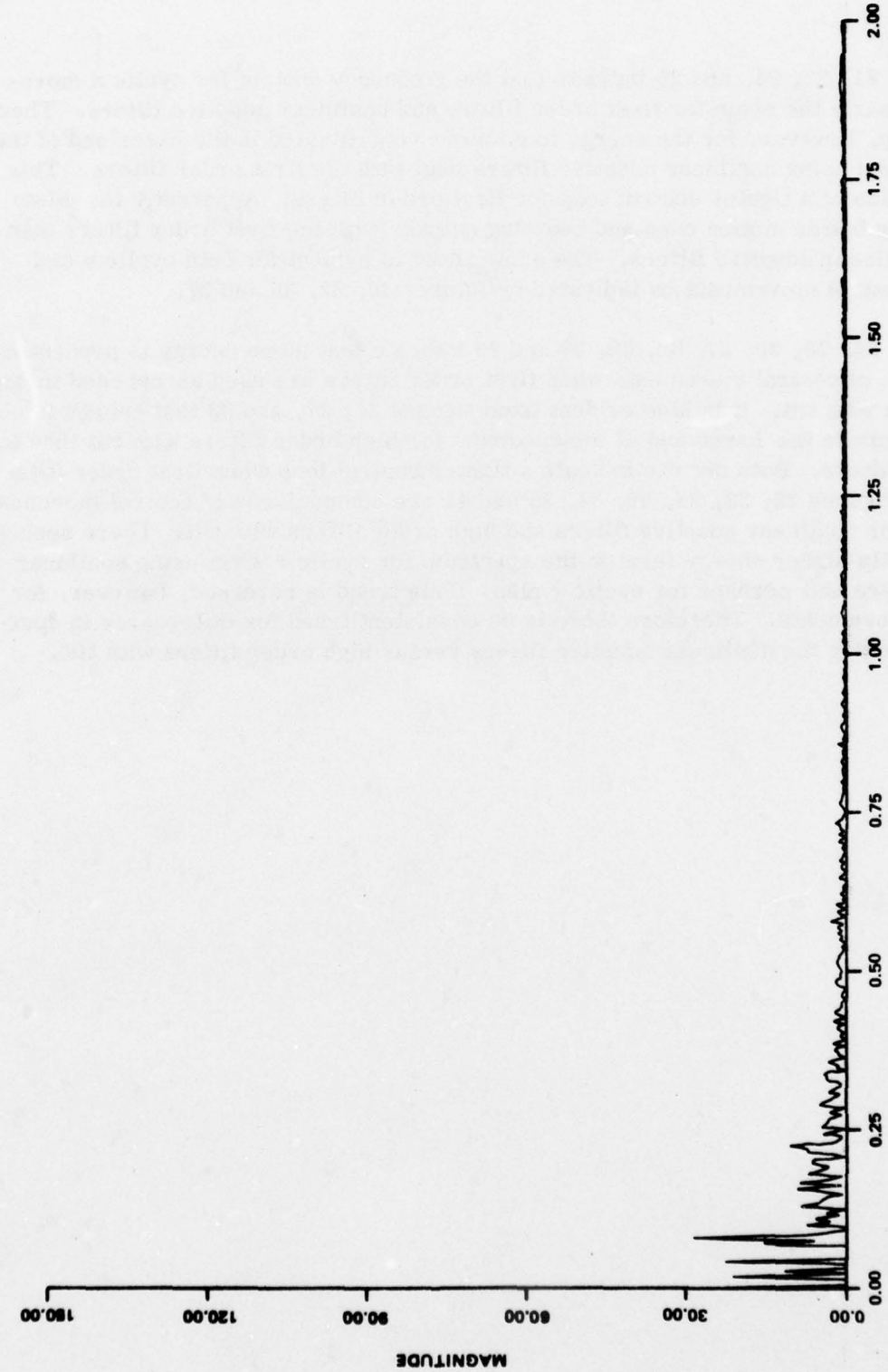

FIGURE 41 - Collective Difference Spectrum For High Order Washout With Tilt Minus Nonlinear Adaptive Washout

Figures 21, 22, 24, and 25 indicate that the frequency content for cyclic x movements are nearly the same for first order filters and nonlinear adaptive filters. There is a tendency, however, for the energy to be more concentrated in the lower end of the spectrum when using nonlinear adaptive filters than with the first order filters. This is an indication of a tighter control loop for first order filters. Apparently the pilots are receiving better motion cues and reacting quicker with the first order filters than with the nonlinear adaptive filters. The same trend is evident for both cyclic y and collective control movements as indicated by figures 30, 32, 36 and 37.

Figures 21, 23, 26, 27, 32, 33, 38 and 29 indicate that more energy is present in the spectrum of control movements when first order filters are used as opposed to high order filters with tilt. It is also evident from figures 26, 27, and 33 that energy is concentrated more in the lower end of the spectrum for high order filters with tilt than for first order filters. Both results indicate a tighter control loop when first order filters are used. Figures 22, 23, 28, 29, 34, 35 and 41 are comparisons of control movement spectrums for nonlinear adaptive filters and high order filters with tilt. There seems to be a slightly higher energy level in the spectrum for cyclic x when using nonlinear adaptive filters and perhaps for cyclic y also. This trend is reversed, however, for collective movements. Therefore there is no consistent trend for differences in spectrums when using the nonlinear adaptive filters versus high order filters with tilt.

CONCLUSIONS AND RECOMMENDATIONS

From the pilot comments, results of the statistical tests and the time histories of the motion algorithms, it is apparent that the axis system of application for washout filters has no effect on the accuracy with which pilots fly the aircraft. Indeed, the axis system transformations may be linearized by applying the small angle approximation without jeopardizing the quality of the motion.

The results of the second phase also indicate that high order washout filters without tilt should be avoided for three-degree-of-freedom motion bases. The anomalous specific force cues that result from angle washout (a characteristic of high order filters without tilt) are probably the cause for pilot induced oscillations and resulting higher error variances that occur when this type of washout is used.

The fact that no significant difference in performance can be observed for runs with motion as opposed to runs without motion is probably a result of the flying task used in this experiment. Visual flight tasks are better for measuring the relative merit of washout circuits than instrument flight tasks. Since no out-the-window visuals were available for this simulation, the steering commands were given by an instrument positioned above the instrument panel in an attempt to require the pilot to set up a scan pattern similar to the one he would use when flying a visual task. This apparently was not totally successfully, because the pilots indicated that they still flew as if it were an instrument flying task. Motion is not as important a cue when flying instruments as it is when flying a visual flight task such as carrier landing or terrain following. For the flight task used in this experiment, the pilots felt that motion was valuable more from a standpoint of adding realism to the simulation rather than from giving them additional cues for flying the aircraft.

The results of Phase III show conclusively that first order washout filters provided the best motion cues to the pilot for the flying task, aircraft type and motion base hardware used in this experiment.

Smaller variances for control movements, body rate errors and attitude errors can be attributed to a tightening of the control loop when using first order filters as evidenced by the frequency distributions of the control movements.

Results concerning nonlinear adaptive washouts and high order washouts with tilt are inconclusive. The time histories in Appendix C indicate that first order filters provide better motion recovery than the two linear filters for all except the vertical degree of freedom. However, the error variances indicate that nonlinear adaptive filters did not provide the best motion cues in the experiment. Reference[3] offers a possible

[3] Graham, D. K., Hickey, L. K., and Vaden, V. C.; "A Rational for Moving Base Flight Simulation and a Preliminary Statement of the Motion Requirements"; The Boeing Company; Oct 1968.

explanation of this seeming contradiction. Flight in turbulent air is listed as an example of a type of motion which actually hinders the pilot when flying his aircraft. Turbulence was passed most effectively by the nonlinear adaptive filters, less effectively by the high order filters with tilt and least effectively by the first order filters. It is possible that confusion caused by the turbulence was responsible for the poor performance of nonlinear adaptive washouts in this experiment.

Addition of tilt to the high order washouts did not appreciably improve the specific force recovery and is therefore not recommended for simulation of helicopter motion on three degree-of-freedom motion bases. The frequency of specific forces encountered in helicopter motion is too high to be passed by the tilt shaping filter. Therefore, the anomalous rotation cues caused by the high order rotational washout cannot be counteracted by tilt.

Once again the pilots indicated that nonlinear adaptive filters produced the most realistic motion because the turbulence was most apparent when using that kind of filter. However, they felt that all three filter types (first order, nonlinear adaptive and high order with tilt) produced good quality motion simulation.

Position error variance was not found to be a sensitive measure of effectiveness for comparing motion algorithms. It is suggested that future studies of this sort could benefit by collecting data on body rates and accelerations, linear velocities and accelerations, and control movements.

ACKNOWLEDGEMENTS

Many people contributed to the successful completion of this project. In particular, the author wishes to express his appreciation to the following people for their support: Mr. J. G. Douvillier of NASA Ames Research Center, Moffett Field, California for sharing his knowledge of the history of motion base drive function; Mr. W. Harris of the Naval Training Equipment Center, Orlando, Florida for his suggestions on analysis techniques; Mr. R. A. Yurik of the NAVAIRDEVCEN Systems Simulation Division, System Directorate, for his invaluable help with the analog portion of the simulation program; and Mr. M. Brandt of the NAVAIRDEVCEN Fluid System Section, Aircraft and Crew System Technology Directorate, for his assistance in analyzing motion system hardware problems and refurbishing the system.

BIBLIOGRAPHY

Baarspul, M., and Van de Moesdijk, G. A. J.; "Moving - Base Visual Flight Simulator of the Department of Aerospace Engineering", Delft University of Technology, Netherlands; Aug 1976.

Parrish, V., Dieudonne, J. E., Bowles, R. L., and Martin, D. J., Jr.; "Coordinated Adaptive Washout for Motion Simulators"; NASA Langely Research Center; Jan 1975.

Ince, F., Williges, R. C., and Roscoe, S. N.; "Aircraft Simulator Motion and the Order of Merit of Flight Attitude and Steering Displays"; University of Illinois at Urbana-Champaign; Aug 1975.

Jacobson, I. D. and Joshly, D. S.; "Modelling Atmospheric Turbulence for a Motion-Base Simulator"; University of Virginia, Charlottsville, VA.; Oct 1975.

Koonce, J. M.; "Effects of Ground-Based Aircraft Simulator Motion Conditions Upon Prediction of Pilot Proficiency; Parts I and II;" Apr 1974.

Valverde, H. H.; "Review of Flight Simulator Transfer of Training Studies;" Air Force Human Research Laboratory, Wright-Patterson Air Force Base, Ohio; Dec 1973.

Sinacori, J. B.; "A Practical Approach to Motion Simulation"; AIAA Paper No. 73-931; Sep 1973.

Conrad, B., Schmidt, S. F. and Douvillier, J. G.; "Washout Circuit Design for Multi-Degrees-of-Freedom Moving Base Simulators"; AIAA Paper No. 73-929; Sep 1973.

Stewart, J. D.; "Human Preception of Angular Acceleration and Implications in Motion Simulation"; NASA Ames Research Center; Apr 1971.

Schmidt, S. F. and Conrad, B.; "A Study of Techniques for Calculating Motion Drive Signals for Flight Simulators"; NASA Ames Research Center; Jul 1971.

Conrad, B. and Schmidt, S. F.; "Motion Drive Signals for Piloted Flight Simulators"; NASA Ames Research Center; Feb 1970.

Sinacori, J. B.; "Validation of Ground Based Simulation"; Northrup Aircraft Division, Hawthorne, CA.; Jul 1970.

Graham, D. K., Hickey, L. K. and Vaden, V. G.; "A Rationale for Moving Base Flight Simulation and a Preliminary Statement of the Motion Requirements"; The Boeing Company; Oct 1968.

APPENDIX A

DIGITAL TURBULENCE MODEL

APPENDIX A

DIGITAL TURBULENCE MODEL

The vertical component of turbulent air as seen by a moving aircraft has a power spectral density given by:

$$\Phi_V(\omega) = \overline{W_g^2} \quad \frac{L}{\pi} \quad \frac{1 + 3\left(\frac{LW}{V_A}\right)^2}{\left[1 + \left(\frac{LW}{V_A}\right)^2\right]^2}$$

where:

$\overline{W_g^2}$ is the mean square value of the vertical gust - a simple measure of the intensity of the turbulence.

L is the scale of the turbulence - a measure of the average eddy size, it indicates the frequency at which the spectrum breaks from a flat spectrum to one that decreases rapidly.

V_A is the forward velocity of the aircraft.

Reference[4], a report dealing with the simulation of atmospheric turbulence, indicates that vertical gust turbulence may be simulated by passing white Gaussian noise through a filter having the following transfer function:

$$\sqrt{\frac{10L}{V_A}}\left[\frac{1 + \sqrt{3}\left(\frac{L}{V_A}\right) S}{1 + \frac{L}{V_A} S^2}\right]$$

Experimental data indicates the L is of the order of 1000 feet. With respect to the intensity of the turbulence, a root mean square value of 15 feet/sec was used in this simulation. The intensity of turbulence is known to be subject to random fluctuations.

[4] R. Berkowitz and J. Loftus; "Simulation of Atmospheric Turbulence"; U. S. Naval Air Development Center, Report ACLTN No. 62-147-02; Feb 1962.

At low altitude, root mean square values of vertical gust velocities seem to have a Rayleigh probability distribution. No data is available concerning the rate of change of the intensity of turbulence, however, an average period of 30 seconds seems reasonable and was used in this simulation.

Therefore, the root mean square vertical gust velocity was generated by first sampling a Rayleigh distribution with a mean of 15 ft/sec and passing the random variable through a low pass filter with the following characteristics:

$$\frac{1}{30\ S + 1}$$

The value thus derived is $\overline{W_g^2}$ and is used to sample a Gaussian distribution. The random variable derived from this sample is then passed through the filter mentioned previously which reproduces the spectrum of atmospheric vertical gust turbulence.

Reference[5], in the chapter on flight in turbulent air, suggests that the vertical gust velocity be input to the aircraft model in the following manner. Three aircraft state variables are most affected by vertical gusts: the angle of attack, roll rate and pitch rate. Perturbations to these quantities caused by vertical gust can be generated as follows and added to the aircraft simulation:

$$\alpha_g = -W_g/V_A$$

$$P_g = -\dot{W}_g/V_A$$

$$Q_g = \dot{W}_g/V_A$$

where:

α_g is the angle of attack perturbation due to vertical gusts.

P_g is the roll rate perturbation due to vertical gusts.

Q_g is the pitch rate perturbation due to vertical gusts.

W_g is the instantaneous vertical gust velocity.

[5] B. Etkin; "Dynamics of Flight -- Stability and Control"; John Wiley and Sons, Inc.; 1959.

APPENDIX B

MOTION BASE HYDRAULIC MAINTENANCE

APPENDIX B

MOTION BASE HYDRAULIC MAINTENANCE

The motion base drive investigation required the integration of generic helicopter flight motion equations with the Link three-degree-of-freedom motion base system. The following description of motion base hydraulic maintenance is an excerpt from a technical memorandum written by Mr. T. Thomas of the Performance Simulation Division.

The motion system was found to require some hydraulic refurbishment in order that the system could be fully utilized. The following symptoms were noted:

1. The hydraulic pressure on the sequence valve was down from 3000 psi to about 1400 psi.

2. The motion of the three actuator legs was not fully responsive. If an input signal was given to an actuator leg, an unreasonable delay time was noted before the actuator leg was driven to the commanded position. For example the right actuator leg drive at a maximum speed of about 3.5 inches per second.

3. The motion of the three actuator legs did not occur at the same rate.

4. The motion of the three actuator legs was jerky.

The Fluid System Section (code 30211) of the Air Vehicle Technology Department was consulted regarding these hydraulic problems. Mr. J. F. Ohlson (Ext 2834) heads this section. Their technicians inspected the motion system and made several suggestions regarding the motion systems condition and refurbishment. The main relief valve (tag number 10 on the unit) was warm during the motion base operation which meant that hydraulic fluid was being spilled out of this relief valve and not through the required sequence valve (tag number 7 on the unit). The main relief valve was adjusted but the system pressure could not be raised above 1500 psi utilizing just this relief valve adjustment. It was thought that this relief valve might be remaining open and therefore required cleaning and the replacement of the valves O rings.

Mr. Ohlson agreed to allow one of his hydraulic technicians to spend one week analyzing the motion systems problems and refurbishing the system where necessary. The technician assigned to the job was Mr. M. Brandt (Ext. 2062).

The following things were done to the motion system in an attempt to improve its performance.

1. The main relief valve (No. 10) was taken apart, cleaned, inspected and the O rings replaced.

2. The right, left and rear cylinder filters were replaced. It was observed that the rear cylinder bowl was slightly dirty and the old filters were discolored. The filter number and spec is 9C4330-00-277-3274, QPL elements, 10 micron 25 abs, ANG235-4A.

3. The hydraulic fluid reservoir holding about 50 gallons of oil was pumped out. The oil utilized by the Singer Company was identified as micronic 745 oil. The military uses MIL-H-5606C hydraulic fluid (Stock No. 9G-9150-00-223-4134) in their aircraft. Sixty-five gallons of this 5606C type oil was obtained from the Center's stock. The 5606C and the 745 type oils are compatible according to Mr. Larry Almy of the Singer Company. (His telephone number is 1-607-772-3363). The oil removed from the reservoir smelled burnt which might indicate that the water cooling system might not be adequate.

4. A new drain spigot was placed on the bottom of the reservoir to facilitate future removal of oil from the reservoir.

5. The front plate on the reservoir was removed and the metal strainer taken out of the reservoir. The strainer was cleaned and put back into the reservoir.

6. The old 745 type oil was flushed out of the hydraulic lines leading from the pump assembly to the motion system and back to the reservoir. This was accomplished by removing the main return line from the motion system, turning on the pump and motion systems and forcing the fluid out of the main return line into a 55 gallon empty drum. Before turning on the pump and motion system, the reservoir was filled about half way with new 5606C type fluid. It was observed that one inch of the reservoir indicator tube is equal to about six gallons of hydraulic fluid.

The pump and motion system were then turned on. As the motion base moved upward the old 745 oil flowed into the 55 gallon waste drum. Since the 745 oil has a brownish yellow color and the new 5606C oil has a redish color, it was easy to observe when all the old oil was flushed out of the motion base hydraulic lines.

Each intake line to the right, left and rear actuators was cracked open separately to insure that any air in the lines would be removed. With the motion base on, it was observed that in addition to a slight amount of hydraulic fluid leaking out of the intake lines, bubbles also were observed. Before the air was removed from the actuator intake lines the right actuator would not move. This very well may have been caused by a vapor lock condition in the right actuators solenoid system. More hydraulic fluid was added to the reservoir until the glass measuring gage was full. The total system requires about 65 gallons of hydraulic fluid.

7. The hydraulic filters were again replaced with new filters.

8. The hydraulic valve system was then adjusted to see if the system pressure could be increased to 3000 psi. The Singer Company Hydraulic Troubleshooting Manual was utilized for this operation. The steps described in the manual were followed to increase the system pressure to 3000 psi. The procedure in the manual is fairly good but it helps to know something about hydraulic systems to supplement some of the manuals steps. For example, step 5 describes the method of increasing the system pressure to 3400 psi in order that the main relief valve (No. 10) can be adjusted to its proper pressure. This is accomplished by adjusting the sequence valve (No. 5). Adjusting the sequence valve (No. 5) to its maximum only increased the system pressure to 2000 psi. Adjusting the main relief valve (No. 10) raised the system pressure to 3400 psi. The sequence valve (No. 5) was then adjusted back to 3000 psi (Step No. 8 in the manual).

9. A thermometer system was added to the reservoir so that the oil temperature can be observed during continual motion system operation. This will indicate the adequacy of the motion systems cooling system.

10. The motion system required a new solenoid valve in the left actuator leg. A high pitch squeal was detected whenever the left actuator was driven. The solenoid valve was replaced with an old Moog type solenoid valve that had been used in the motion system a couple of years ago. Actually the right solenoid valve was put on the left actuator leg and the old Moog solenoid valve was put on the right actuator leg.

The motion system was checked to see if there was any improvement in performance of the motion system after refurbishment. The system showed only a slight improvement in performance and the jerky motion of the actuator legs was still detected.

The motion systems accumulator pressure is required to be set at 1400 psi. The valve on the top of the accumulator was found to have a leak and consequently the accumulator pressure was down to just about 0 psi. The valve was replaced and the accumulator was recharged with nitrogen to the required 1400 psi. Mr. Phil Porter (Ext. 2638) of the Equip/Inst Shop Branch is the technician that charged the accumulator.

The motion system was again checked to see if there was any improvement in performance. The system now showed a marked improvement in performance and the jerky motion of the actuator legs was eliminated. The right and rear legs were driven at a maximum velocity of about 14 inches per second. There was still some slight performance problems with the right actuator leg. The rear actuator solenoid valve was put on the right actuator leg and a different old Moog type solenoid valve was put on the rear actuator leg. The right actuator leg appears to operate fairly well but the rear actuator leg drove with a jerky motion. A third old solenoid valve was put on the rear actuator leg and this time all three actuator legs appeared to have improved performance.

The motion system was again checked to see if there was any improvement in performance. The system showed acceptable performance for all three actuator legs. The maximum velocity of all three actuator legs was about 14 inches per second.

The final step in the refurbishment of the motion base was the adjustment of the electronic gains in the actuator leg servo systems.

Optimal adjustment of the electronic gains resulted in actuator leg responses similar to a second order system. For the front legs, the gains could be adjusted to achieve a 3 dB bandwidth of 1 Hz. The rear leg experienced high frequency oscillations when the 3 dB bandwidth was increased to .75 Hz or greater.

APPENDIX C

WASHOUT CIRCUIT DESCRIPTIONS

APPENDIX C

WASHOUT CIRCUIT DESCRIPTIONS

Each of the twelve motion algorithms investigated in the second phase of the experiment are described herein. Included in each description is a block diagram illustrating the computational flow for the algorithm.

Euler transformation $[E]$, axis transformation $[F]$ and $[F]^T$, and simulator transformation from pitch, roll and heave command to leg commands are detailed at the end of this appendix.

FIRST ORDER WASHOUT (BODY AXIS)

Figure C-1 is a block diagram of a first order body axis washout circuit for a three degree-of-freedom motion base. The aircraft body axis roll and pitch rates (P_A and Q_A) represent the desired angular motion for the simulator. The P_A and Q_A signals are passed through first order washout filters with gains Kp and Kq both equal to 0.5 and frequency breakpoints W_F and W_Q equal to 0.5 rate/sec. The output of the washout filters, P_1 and Q_1, represent the achievable body axis roll and pitch rates for the simulator.

Note that R_1, the body axis yaw rate, must be calculated from Q_1 and the tangent of ϕ_M, the Euler roll angle of the simulator, to assure that Ψ_M, the Euler yaw angle of the simulator, will always be zero.

P_1, Q_1 and R_1, the achievable body axis rates for the simulator, are resolved into Euler angular rates based on the current simulator attitude. As mentioned above, $\dot{\Psi}_M$ will always be zero. The Euler roll and pitch rates, $\dot{\phi}_M$ and $\dot{\Theta}_M$ are integrated to produce the roll and pitch angle commands, ϕ_M and Θ_M.

The Z axis linear drive represents the third degree of freedom. $\dot{W}_{P_O}$ is the aircraft vertical acceleration and represents the desired vertical acceleration for the simulator. The acceleration due to gravity, G, is added to $\dot{W}_{P_O}$ to insure that only deviations of vertical acceleration from one G are washed out. The vertical acceleration deviation is passed through a third order washout filter with constants $C3_Z = 1.77$, $C4_Z = 1.56$ and $C5_Z = .125$. The full travel of the simulator Z axis is very limited, thus necessitating the use of a third order washout. The third order washout filter will wash out position as well as acceleration, thereby limiting the travel of the simulator more effectively than a lower order washout filter. $\ddot{Z}_2$, the achievable vertical acceleration deviation from one G, is then doubly integrated and multiplied by a gain factor of $K_Z = .1$ to produce Z_2, the simulator Z axis command.

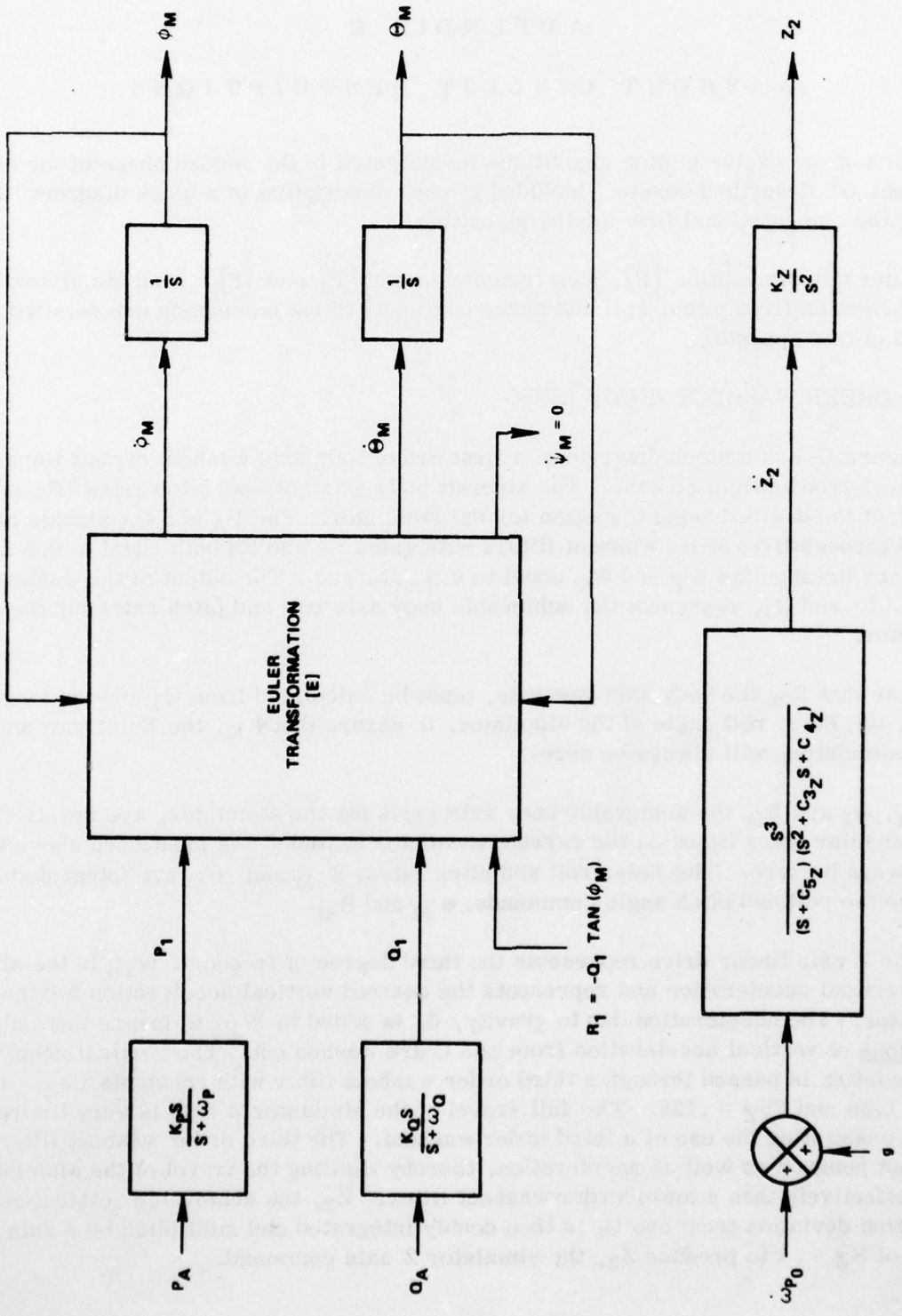

FIGURE C-1 - First Order Body Axis Washout Circuit

The roll, pitch and heave commands (ϕ_M, Θ_M and Z_2) must then be transformed to simulator leg commands. The equations for performing this transformation are listed at the end of this appendix.

FIRST ORDER WASHOUT (INERTIAL AXIS)

Figure C-2 shows a block diagram of a first order inertial axis washout circuit. The desired body rates, P_A and Q_A, are first transformed to desired Euler angular rates, $\dot{\phi}_1$ and $\dot{\Theta}_1$. Once again R_A is calculated to insure that $\dot{\Psi}_1$ will always be zero. The desirable Euler angular rates are passed through first order washout filters with characteristics $K_P = K_R = 0.5$ and $W_P = W_R = 0.5$ to obtain the achievable rates $\dot{\phi}_M$ and $\dot{\Theta}_M$. Integration of the achievable rates produces the simulator roll and pitch command, ϕ_M and Θ_M. The vertical acceleration is identical to that of the first order body axis washout circuitry.

FIRST ORDER WASHOUT (LINEAR TRANSFORMATION)

Figure C-3 is a block diagram of a linearized first order washout circuit. The desired roll and pitch rates, P_A and Q_A, are passed through first order washout filters cascaded with integrations to yield the simulator roll and pitch commands, ϕ_M and Θ_M. The vertical acceleration is once again identical to that for the other first order washout circuits.

THIRD ORDER WASHOUT CIRCUIT (BODY AXIS)

Figure C-4 is a block diagram of a third order body axis washout circuit. P_A and Q_A are passed through third order washout filters with characteristics: $K_P = K_R = .6$, $W_{2P} = W_{2R} = .3$, $W_{3P} = W_{3R} = .3$ and $Z_{3P} = Z_{3R} = 1.0$. The output of the filters, P_1 and Q_1 are transformed to Euler angular rates, $\dot{\phi}_M$ and $\dot{\Theta}_M$, and integrated to yield the simulator roll and pitch commands, ϕ_M and Θ_M. The vertical acceleration for third order washout circuits is handled in the manner as the first order washout circuits.

THIRD ORDER WASHOUT CIRCUIT (INERTIAL AXIS)

Figure C-5 is a block diagram of a third order inertial axis washout circuit. P_A and Q_A are first transformed to the Euler angular rates, $\dot{\phi}_1$ and $\dot{\Theta}_1$, before being passed through third order washout filters cascaded with integrations to yield the simulator roll and pitch commands.

THIRD ORDER WASHOUT CIRCUIT (LINEAR TRANSFORMATION)

A linearized third order washout circuit is shown in figure C-6. P_A and Q_A are passed directly through third order washout filters cascaded with integrations to yield the simulator roll and pitch commands.

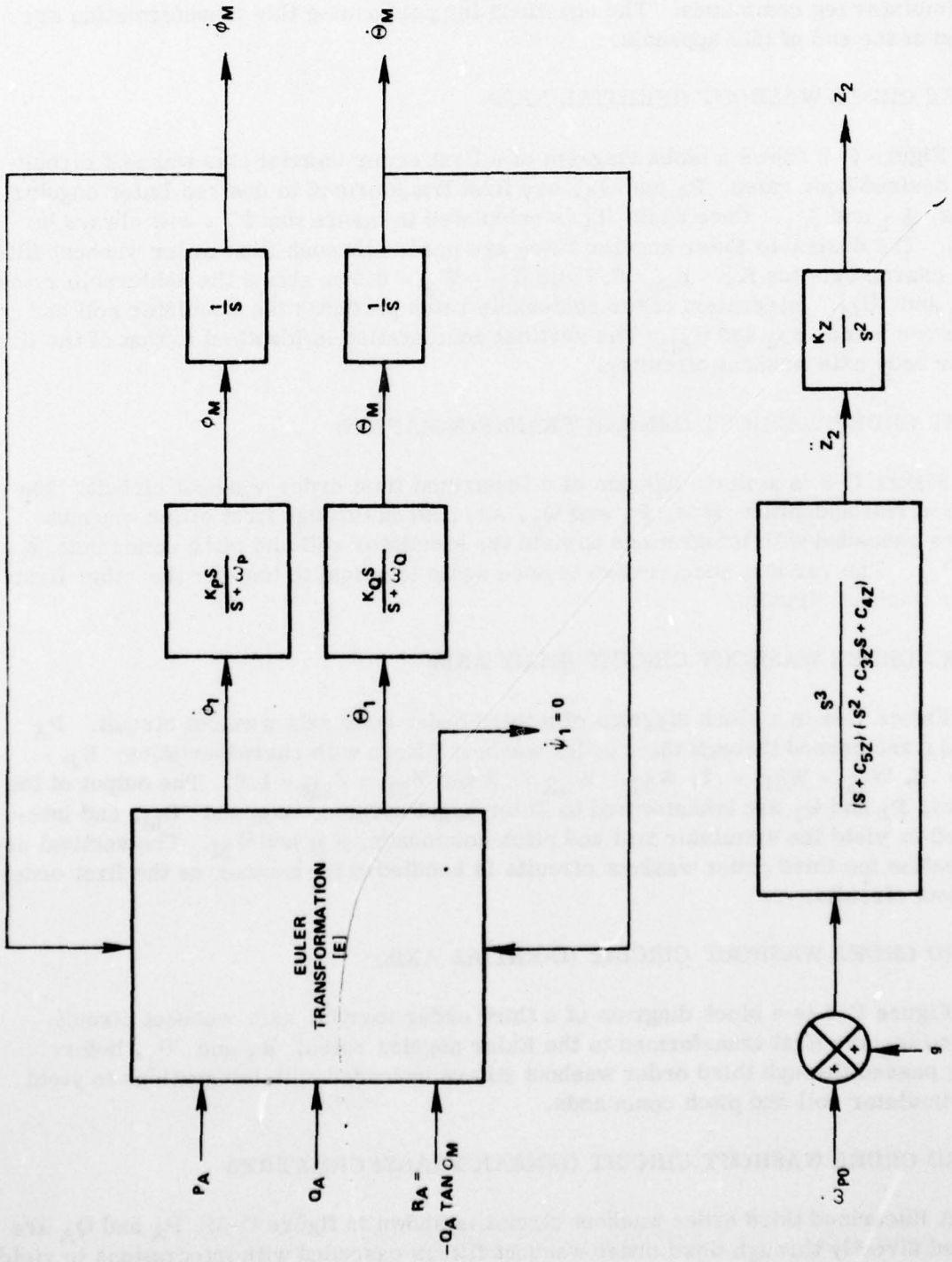

FIGURE C-2 - First Order Inertial Axis Washout Circuit

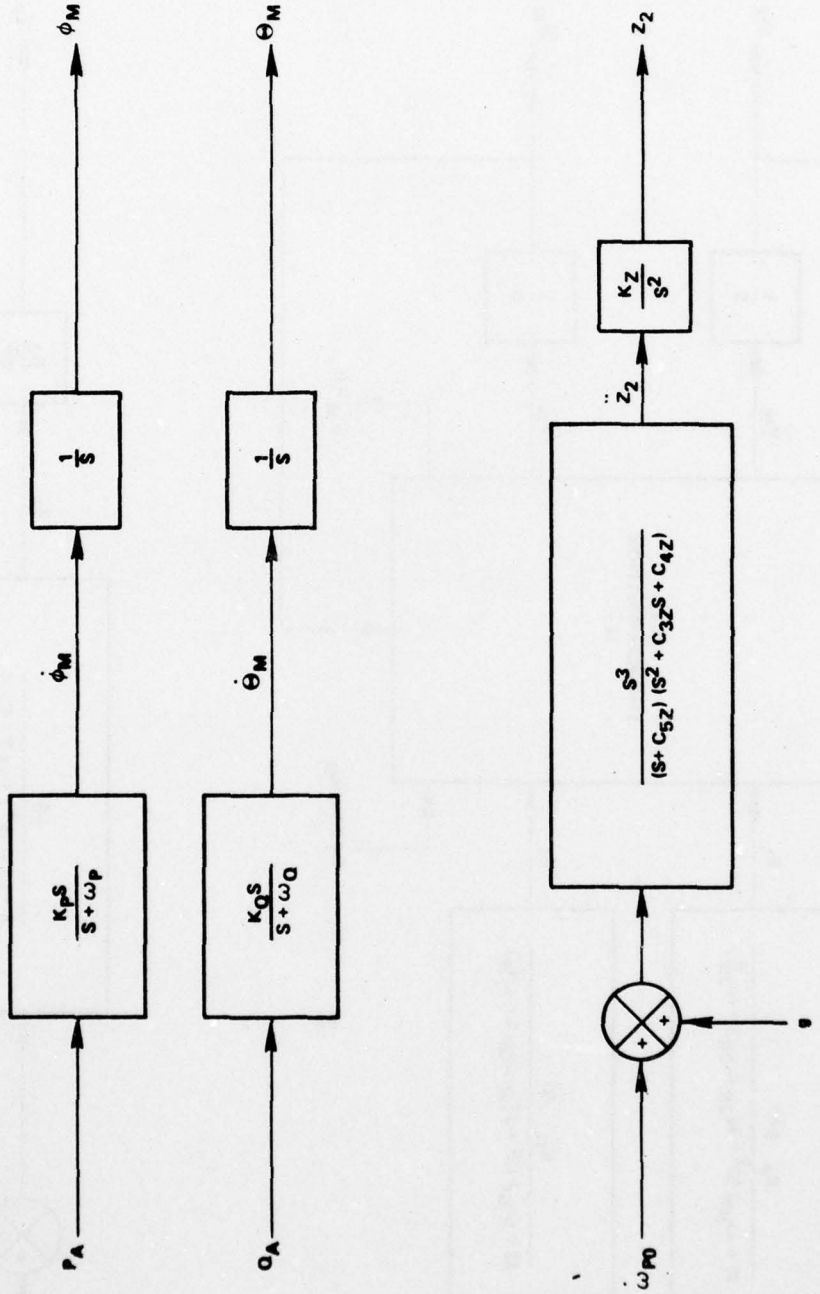

FIGURE C-3 - Linearized First Order Washout Circuit

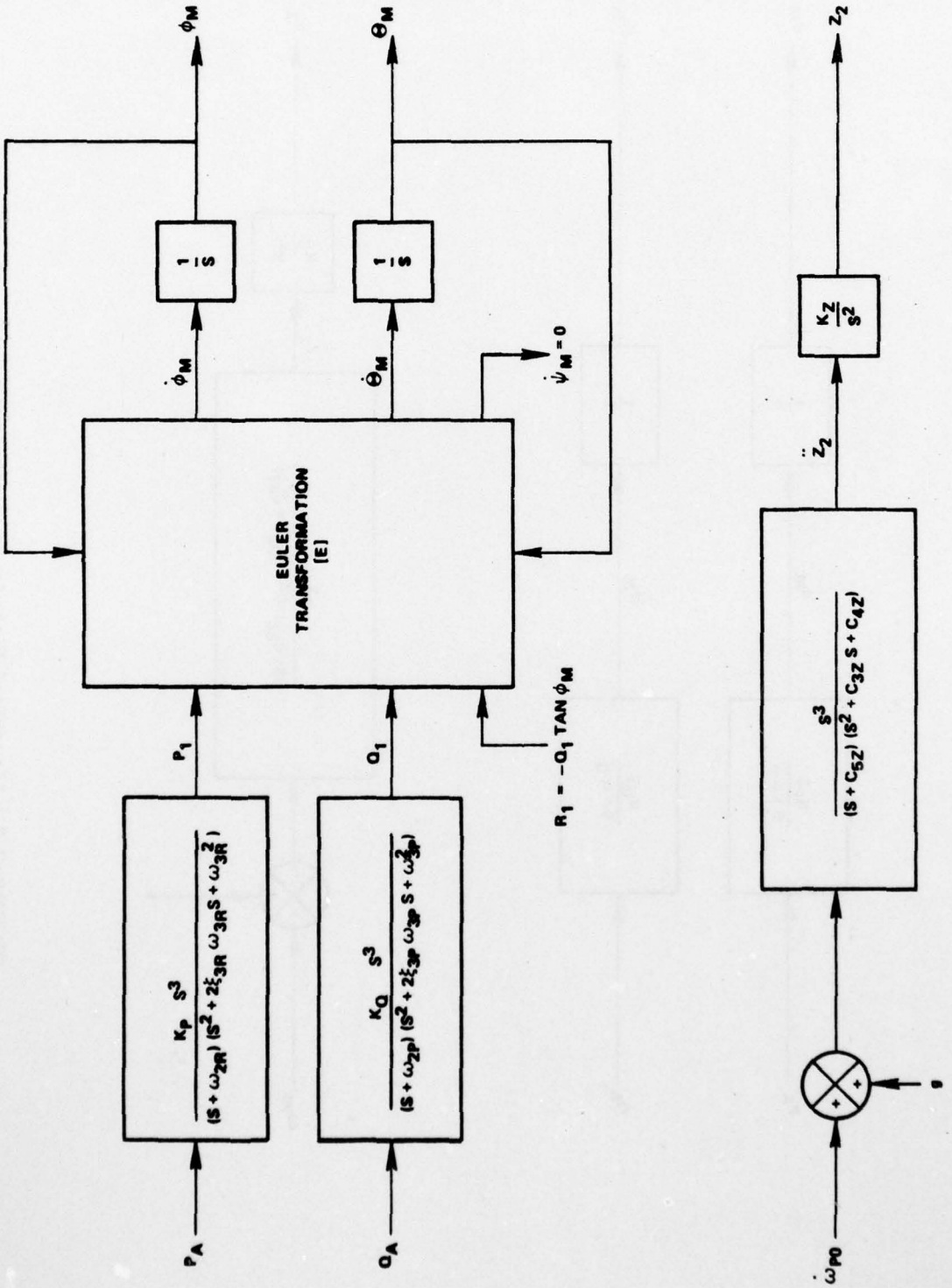

FIGURE C-4 - Third Order Body Axis Washout Circuit

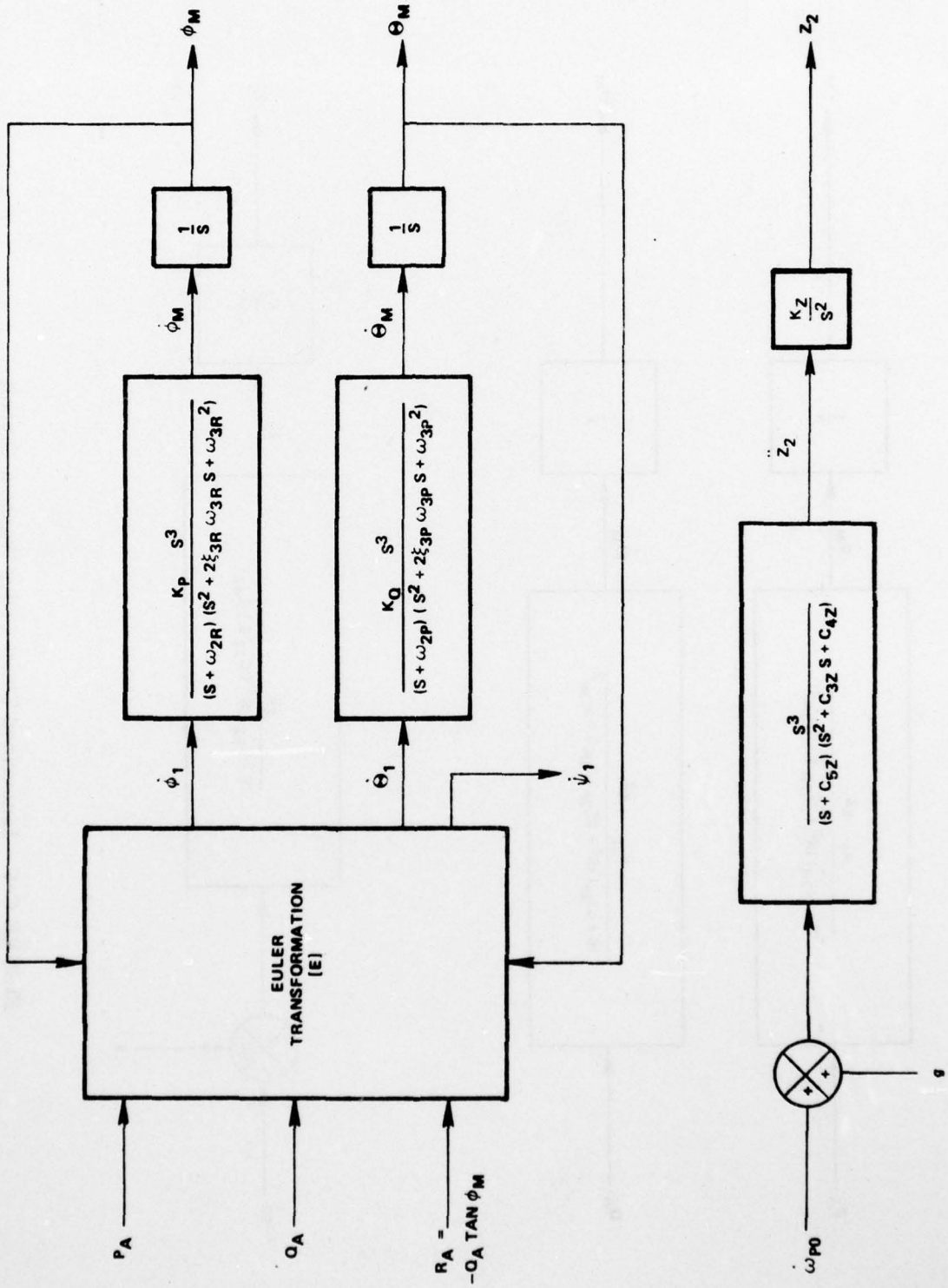

FIGURE C-5 - Third Order Inertial Axis Washout Circuit

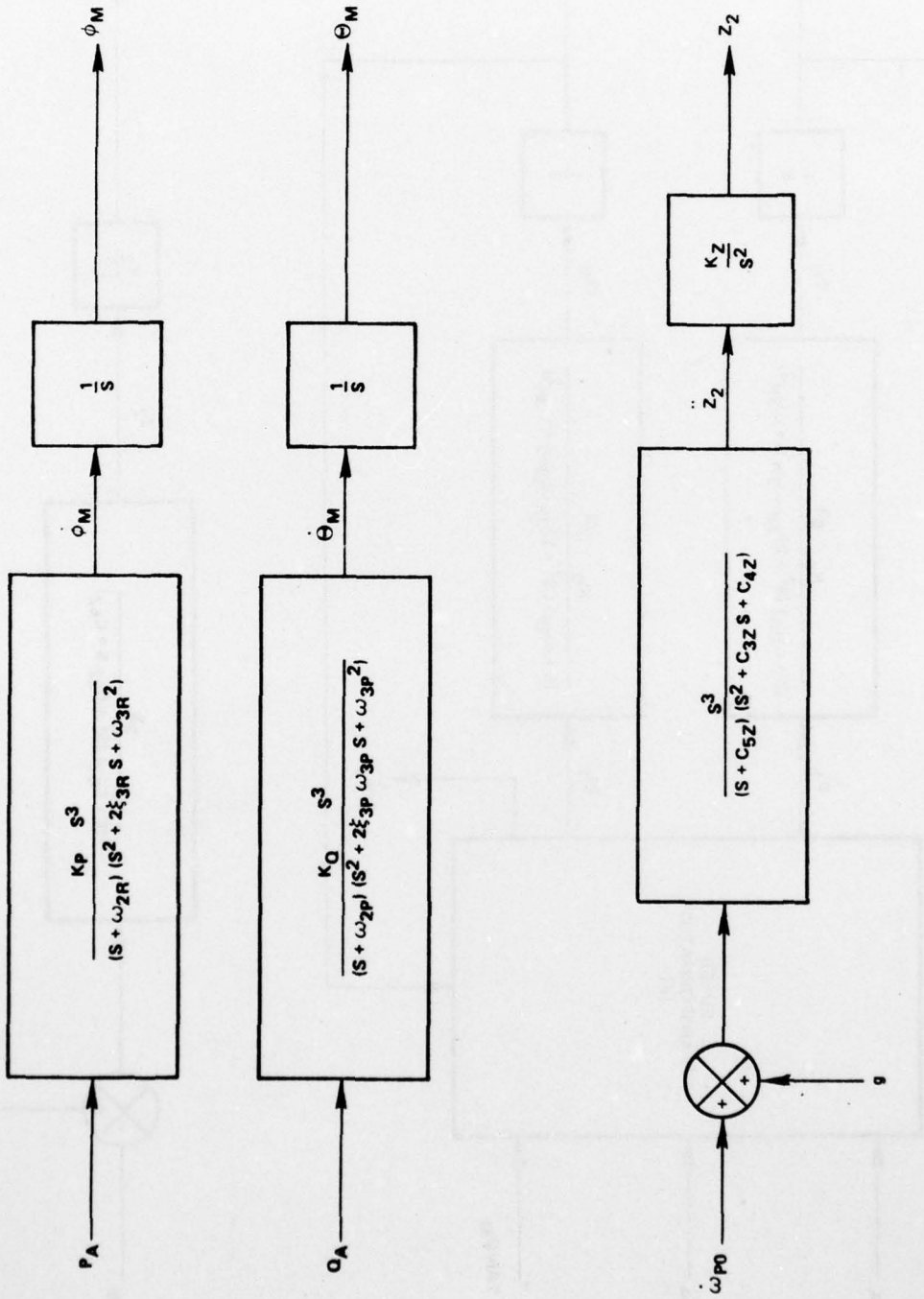

FIGURE C-6 – Linearized Third Order Washout Circuit

HIGH ORDER WASHOUT CIRCUIT WITH TILT (BODY AXIS)

Figure C-7 is a block diagram of a high order body axis washout circuit with tilt. P_A and Q_A are passed through first order washout filters with characteristics $K_P = K_Q = .3028$ and $W_P = W_Q = .4$ to produce P_1 and Q_1, the contribution from the aircraft rotational degrees of freedom. These rotation rates are summed with P_2 and Q_2, the lateral and longitudinal tilt rates to produce P and Q, the total body axis roll and pitch rates for the simulator. R is calculated to insure a $\dot{\Psi}_M$ of zero and P, Q and R are transformed to $\dot{\phi}_M$ and $\dot{\Theta}_M$. The integrations then yield simulator roll and pitch commands, ϕ_M and Θ_M.

The aircraft body axis longitudinal, lateral and vertical accelerations ($\dot{U}_{Po}$, $\dot{V}_{Po}$ and $\dot{W}_{Po}$) represent the desired accelerations and are used to generate the tilt rates. $\dot{U}_{Po}$ and $\dot{V}_{Po}$ are limited to ±.1G's before processing to insure that simulator tilt angles remain at reasonable levels. The vertical acceleration for the high order tilt algorithms is the same as for the first and third order washout circuits. After the deviations from one G have been washed out, -G is added back in and the three modified accelerations, limited $\dot{U}_{Po}$ and $\dot{V}_{Po}$ and washed out $\dot{W}_{Po}$, are transformed to inertial axes based on the current simulator attitude. The inertial Z component, $\ddot{Z}_{Mo}$, is discarded, and the longitudinal and lateral components, $\ddot{X}_{Mo}$ and $\ddot{Y}_{Mo}$, represent the difference between the actual simulator accelerations and the desired simulator accelerations. The cross product and transformation back to body axes yields the desired longitudinal and lateral tilt rates, P_T and Q_T, and R_T is discarded. P_T and Q_T are passed through a shaping network designed to minimize rotational anomalies and the outputs, body axis tilt rates P_2 and Q_2, are summed with the rotational channel rates, P_1 and Q_2. Characteristics of the shaping filter are as follows:

$$W_{1P} = W_{1R} = .004$$

$$Z_{8P} = Z_{8R} = .707$$

$$W_{3P} = W_{3R} = .2$$

$$W_{2R} = W_{2R} = .02$$

The tilt rates rotate the cockpit to null out $\ddot{X}_{Mo}$ and $\ddot{Y}_{Mo}$. When these two inertial components are zero, then the simulator longitudinal and lateral body axis accelerations are equal to the limited $\ddot{U}_{Po}$ and $\ddot{V}_{Po}$.

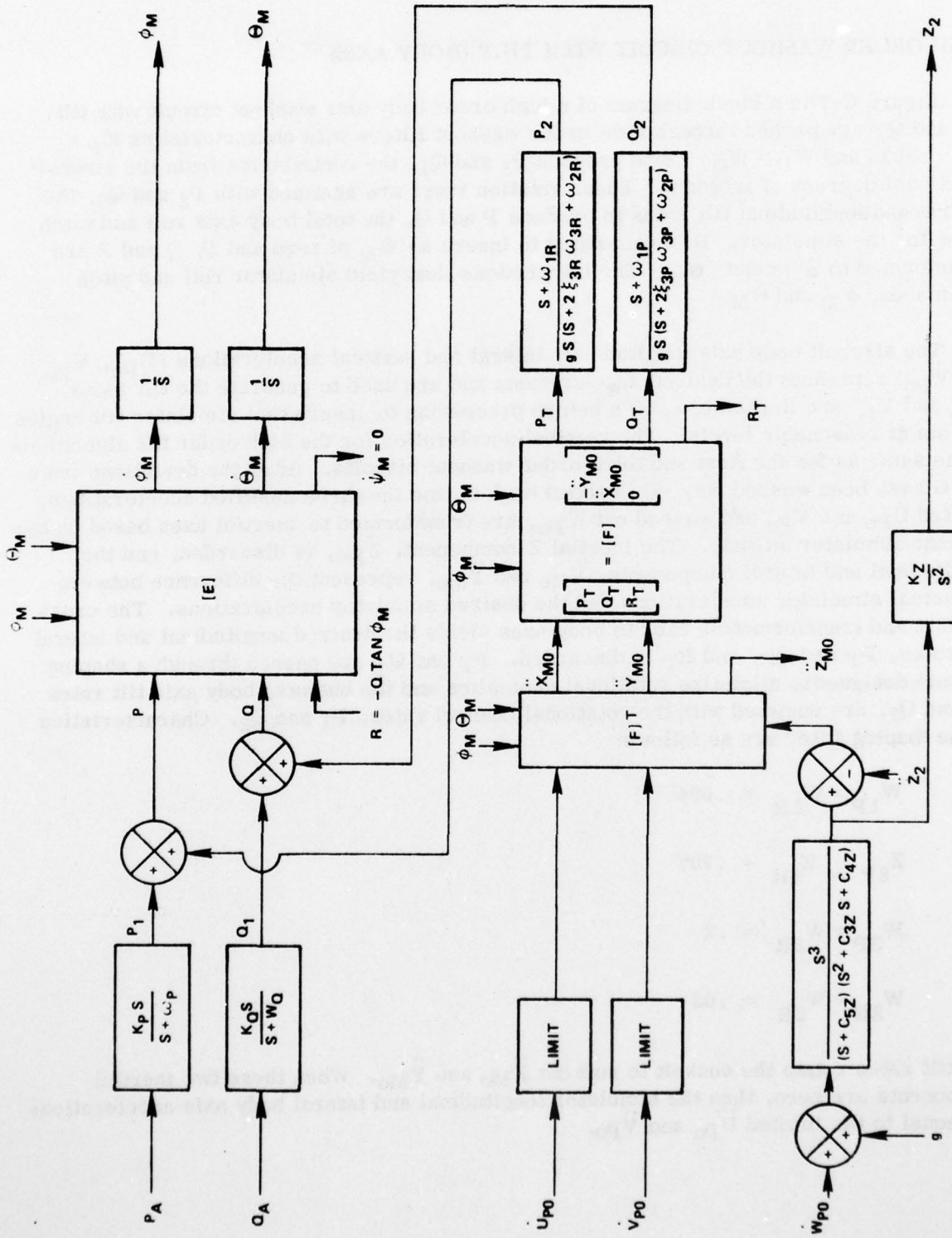

FIGURE C-7 - High Order Body Axis Washout Circuit With Tilt

HIGH ORDER WASHOUT CIRCUIT WITH TILT (INERTIAL AXIS)

A block diagram of a high order inertial axes washout circuit with tilt is shown in figure C-8. P_A, Q_A and R_A (calculated to insure $\dot{\Psi}_1 = 0$), are transferred to Euler angular rates and passed through first order filters to yield $\dot{\phi}_1$ and $\dot{\theta}_1$. These rates represent the achievable rotational motion derived from the aircraft rotational degrees of freedom. The Euler tilt rates, $\dot{\phi}_2$ and $\dot{\theta}_2$, are summed with $\dot{\phi}_1$ and $\dot{\theta}_1$ to form $\dot{\phi}_M$ and $\dot{\theta}_M$ the total rotational motion of the simulator. $\dot{\phi}_M$ and $\dot{\theta}_M$ are then integrated to yield the simulator roll and pitch command, ϕ_M and θ_M.

For the tilt channel, the error signals, $\ddot{X}_{Mo}$ and $\ddot{Y}_{Mo}$, are derived as for the body axis tilt algorithm: limited $\dot{U}_{Po}$ and $\dot{V}_{Po}$ and washed out $\dot{W}_{Po}$ are transformed to inertial axes. A desired tilt rate vector resolved in inertial axes is generated by taking the cross product of the vector

$$\begin{bmatrix} \ddot{X}_{Mo} \\ \ddot{Y}_{Mo} \\ \ddot{Z}_{Mo} \end{bmatrix} \quad \text{and} \quad \begin{bmatrix} 0 \\ 0 \\ -1 \end{bmatrix} \quad g.$$

The desired x and y body axis tilt rates, P_T and Q_T, are obtained by transforming the desired inertial tilt rates to body axes. P_T and Q_T are passed through shaping filters to produce P_2 and Q_2, the body axis tilt rates, and then transformed to the Euler tilt rates, $\dot{\phi}_2$ and $\dot{\theta}_2$, which are summed with the rates from the rotational channel.

HIGH ORDER WASHOUT CIRCUIT WITH TILT (LINEAR TRANSFORMATIONS)

A block diagram of a linearized high order washout circuit with tilt is shown in figure C-9. It is similar to the other tilt algorithms except that rotational transformations are ignored and the transformation of body axis accelerations to inertial axes is linearized using the small angle approximation.

NONLINEAR ADAPTIVE WASHOUT CIRCUIT (BODY AXIS)

The block diagram in figure C-10 shows the computational flow for a non-linear adaptive body axis washout circuit. Adaptive parameters P_ϕ, P_θ and P_Z are generated to minimize the cost functions:

$$J_\phi = 1/2\,(P_A - P)^2 + B_Y/2\,(\int P dt)^2 + C_Y/2(P)^2 + W_Y\,(\ddot{Y}_M)^2$$

$$J_\theta = 1/2\,(Q_A - Q)^2 + B_X/2\,(\int Q dt)^2 + C_X/2\,(Q)^2 + W_X\,(\ddot{X}_M)^2$$

$$J_Z = 1/2\,(\dot{W}_A + g - \ddot{Z}_2)^2 + (C_Z/2(Z_2)^2 + D_Z/2\,(\dot{Z}_2)^2$$

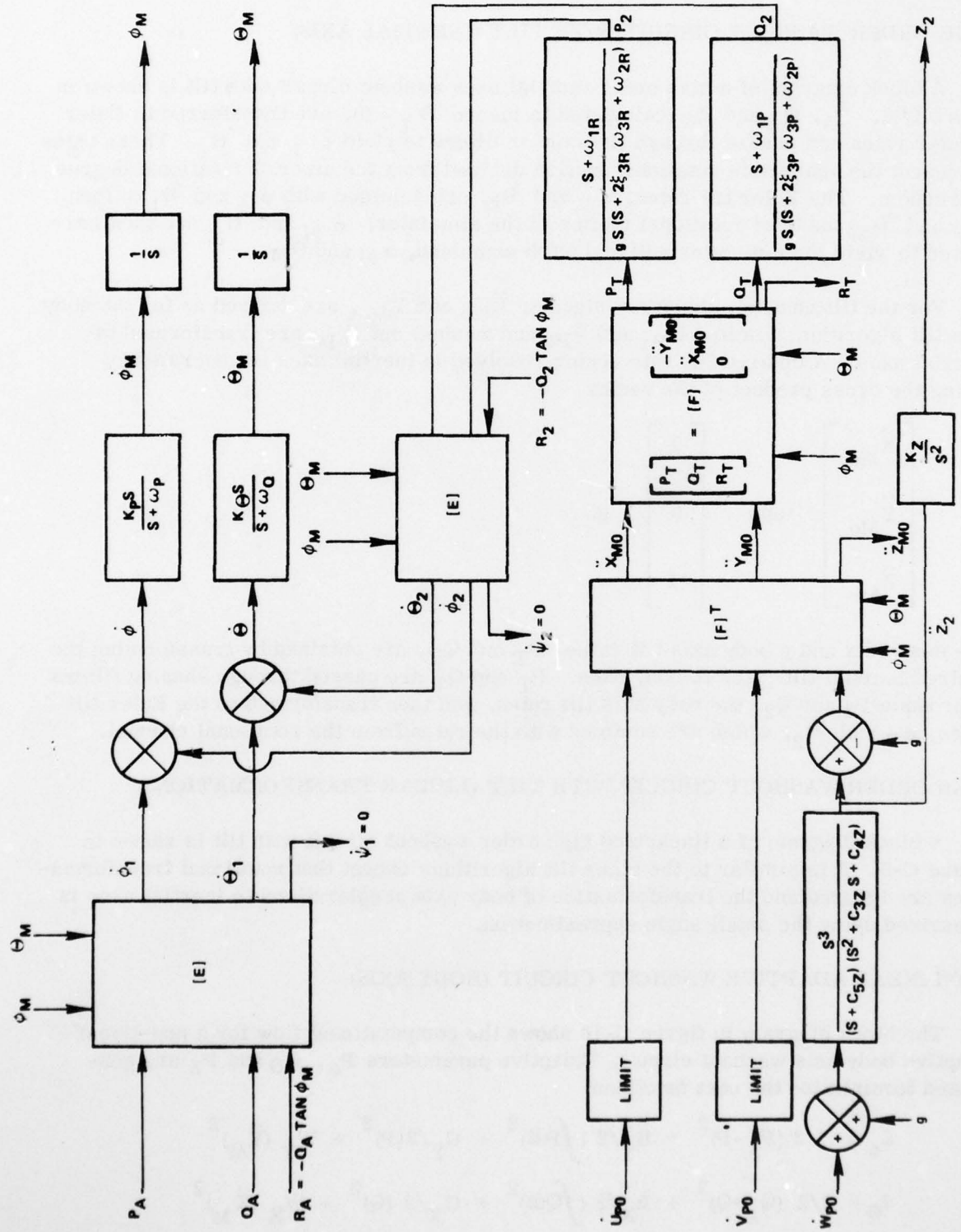

FIGURE C-8 - High Order Inertial Axis Washout Circuit With Tilt

AD-A053 830 NAVAL AIR DEVELOPMENT CENTER WARMINSTER PA SYSTEMS D--ETC F/G 5/9
INVESTIGATION OF MOTION BASE DRIVE TECHNIQUES,(U)
MAR 78 M E BITNER
UNCLASSIFIED NADC-77306-20 NL

2 OF 2
AD
A053830

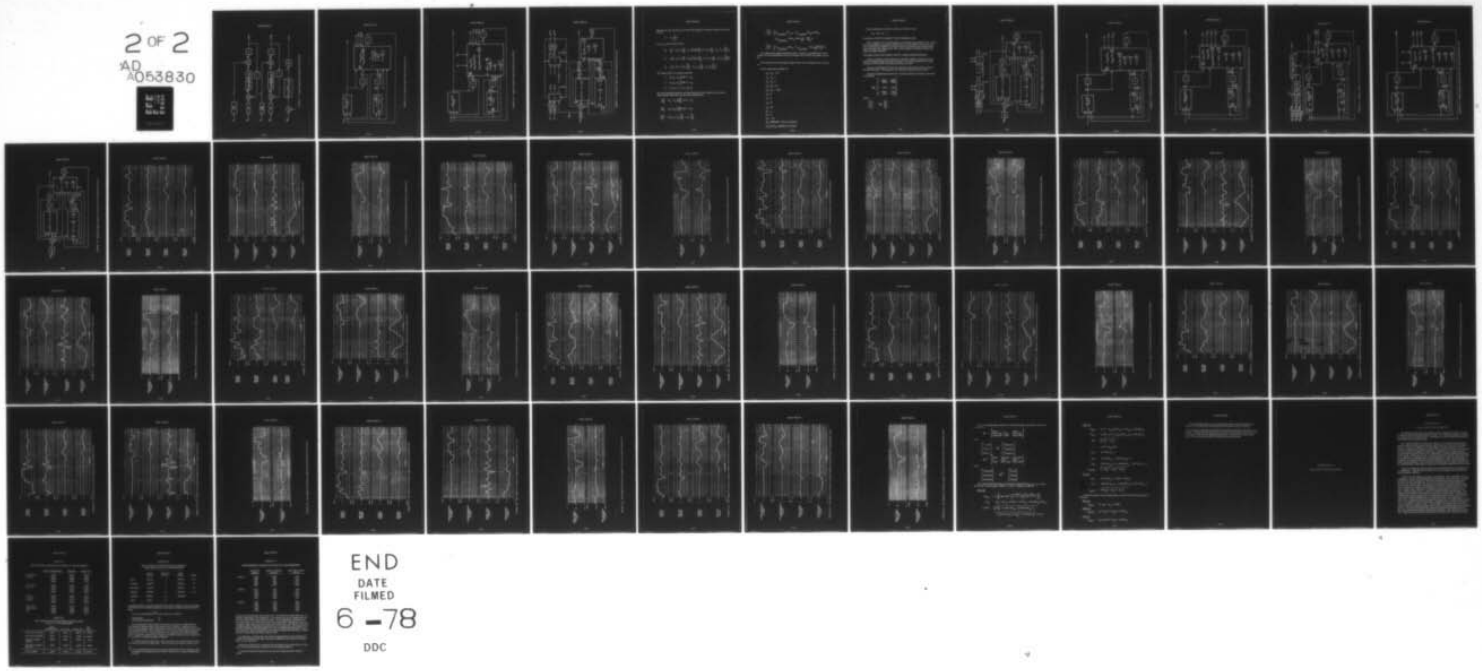

END
DATE
FILMED
6 -78
DDC

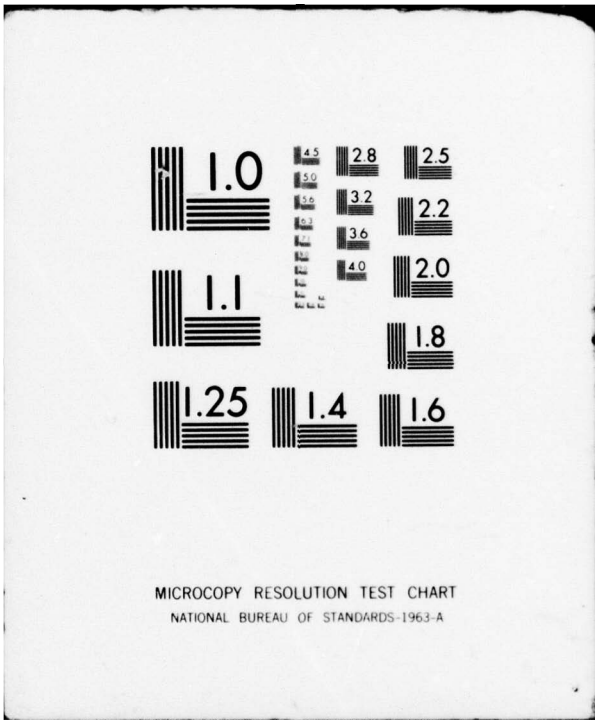
1.0
1.1
1.25
1.4
1.6
1.8
2.0
2.2
2.5
2.8
3.2
3.6
4.0
4.5
5.0
5.6
MICROCOPY RESOLUTION TEST CHART
NATIONAL BUREAU OF STANDARDS-1963-A

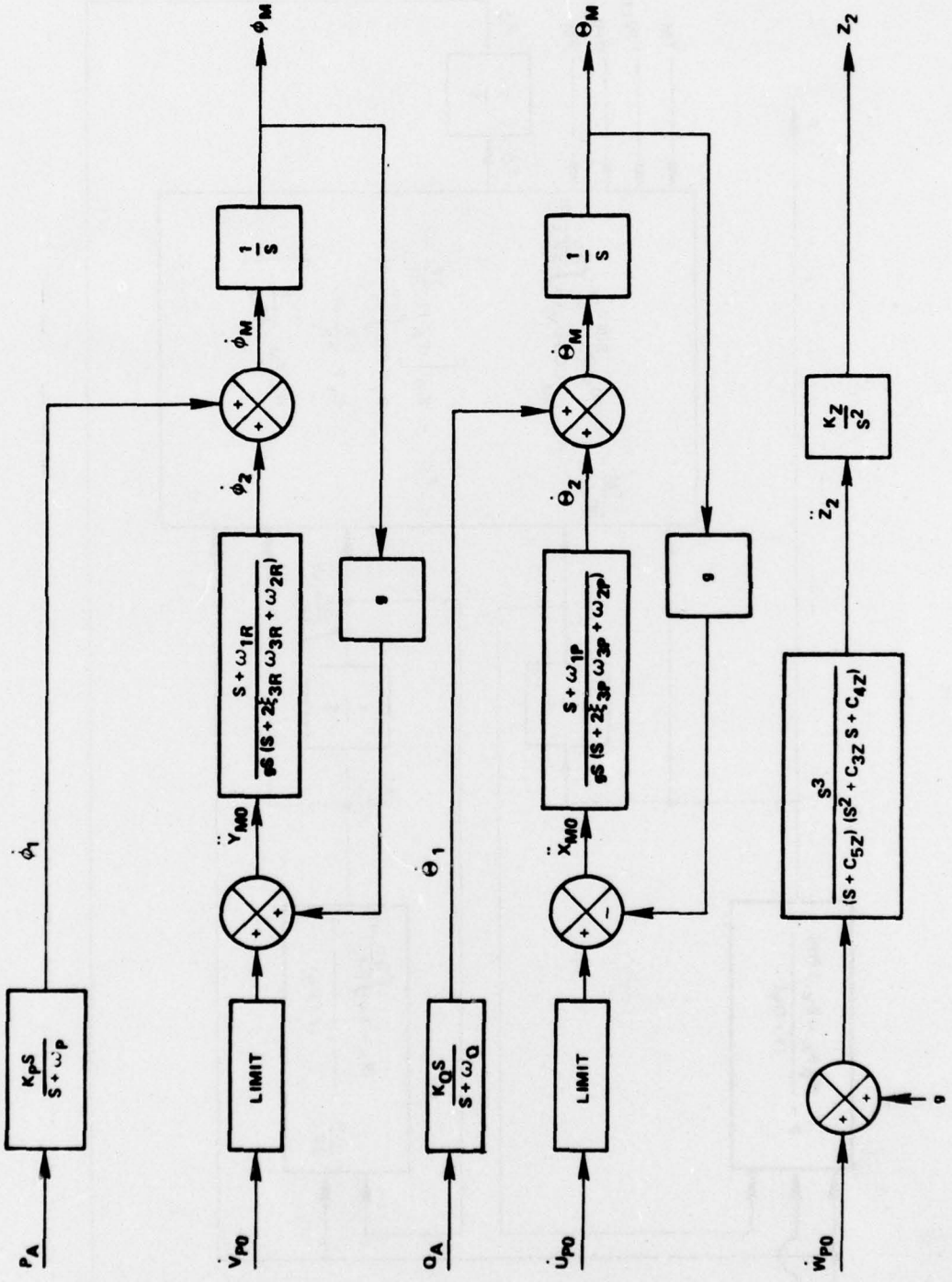

FIGURE C-9 - Linearized High Order Washout Circuit With Tilt

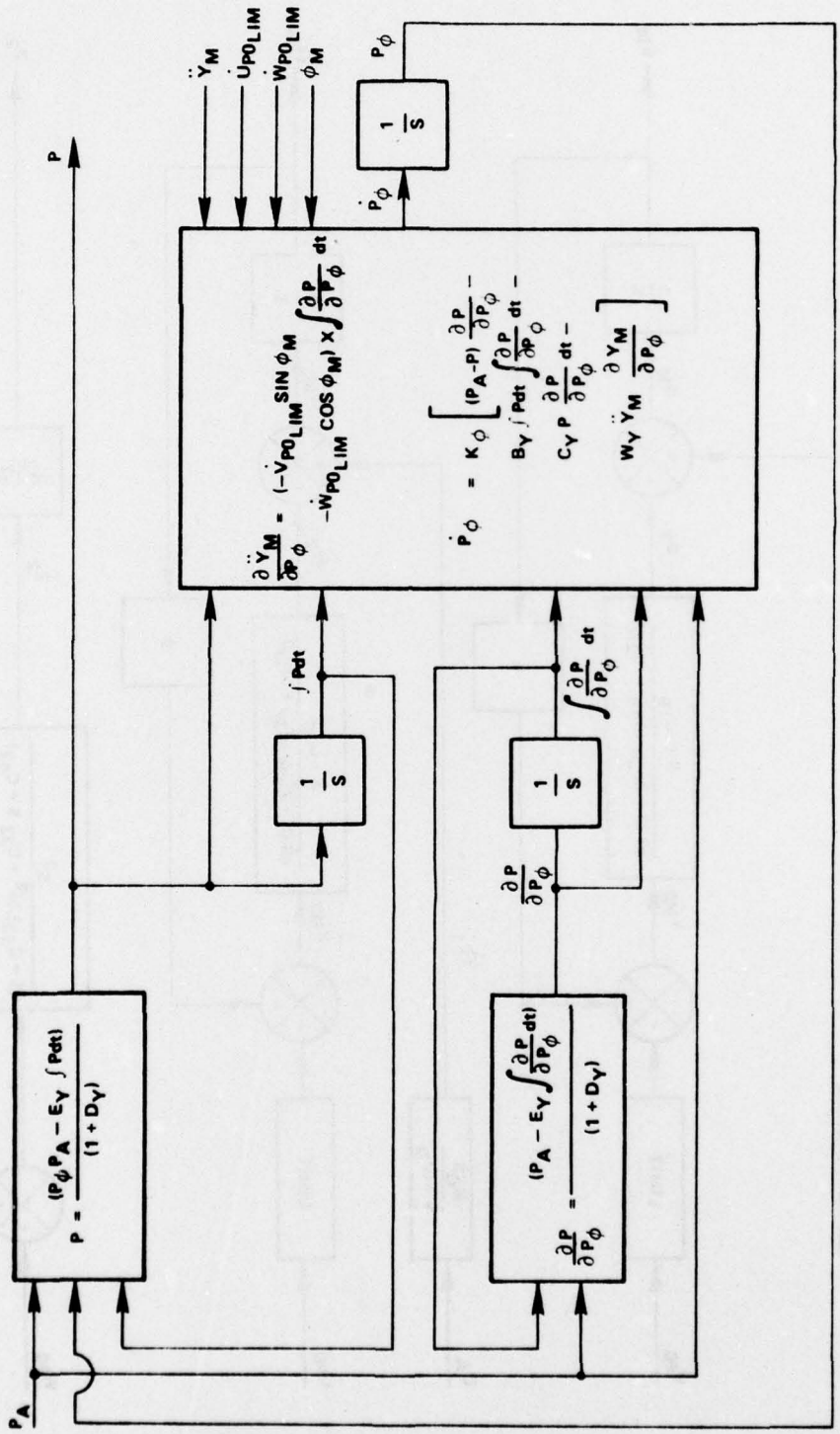

FIGURE C-10 - Nonlinear Adaptive Body Axis Washout Circuit

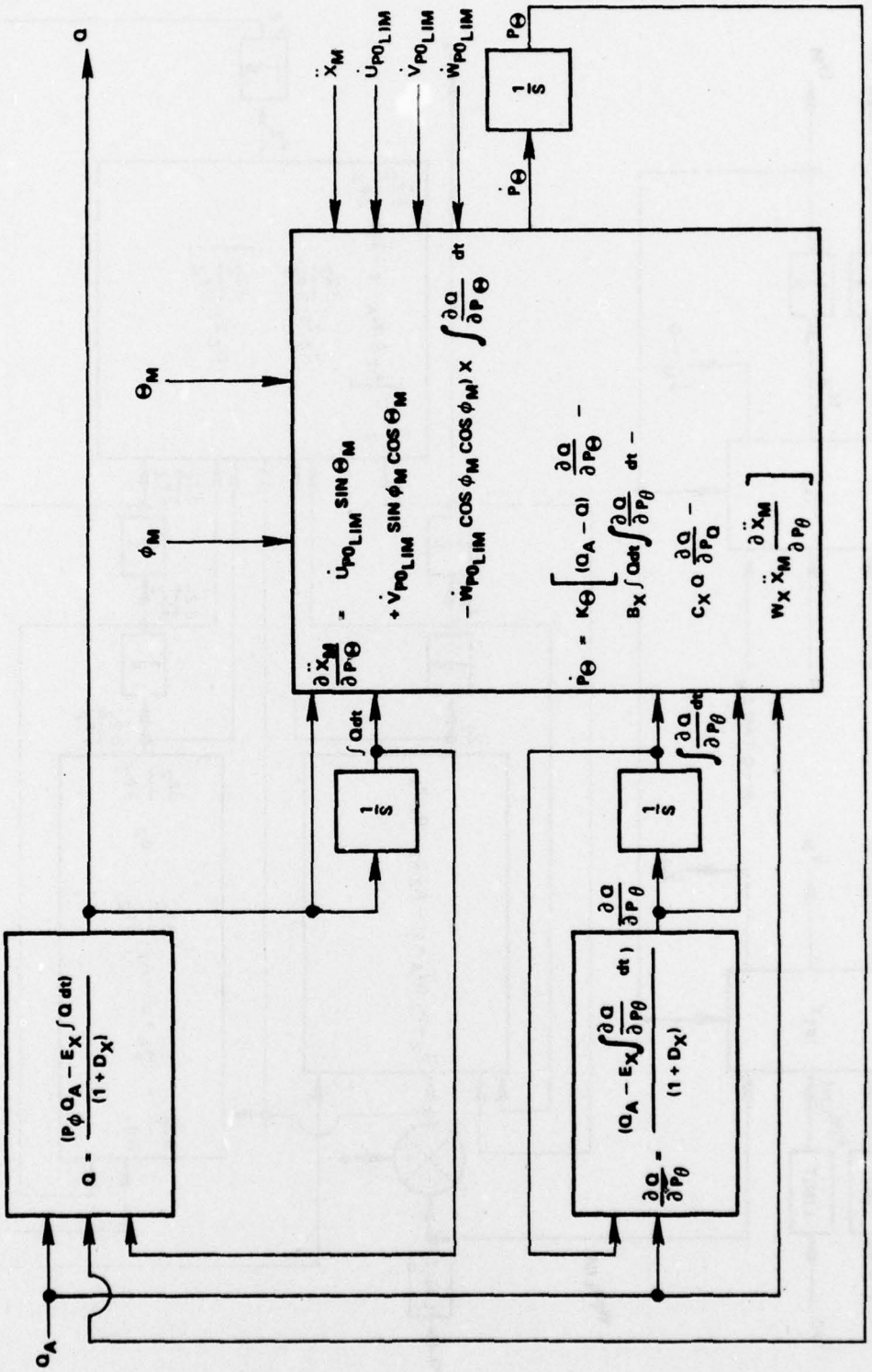

FIGURE C-10 - Nonlinear Adaptive Body Axis Washout Circuit (Con't)

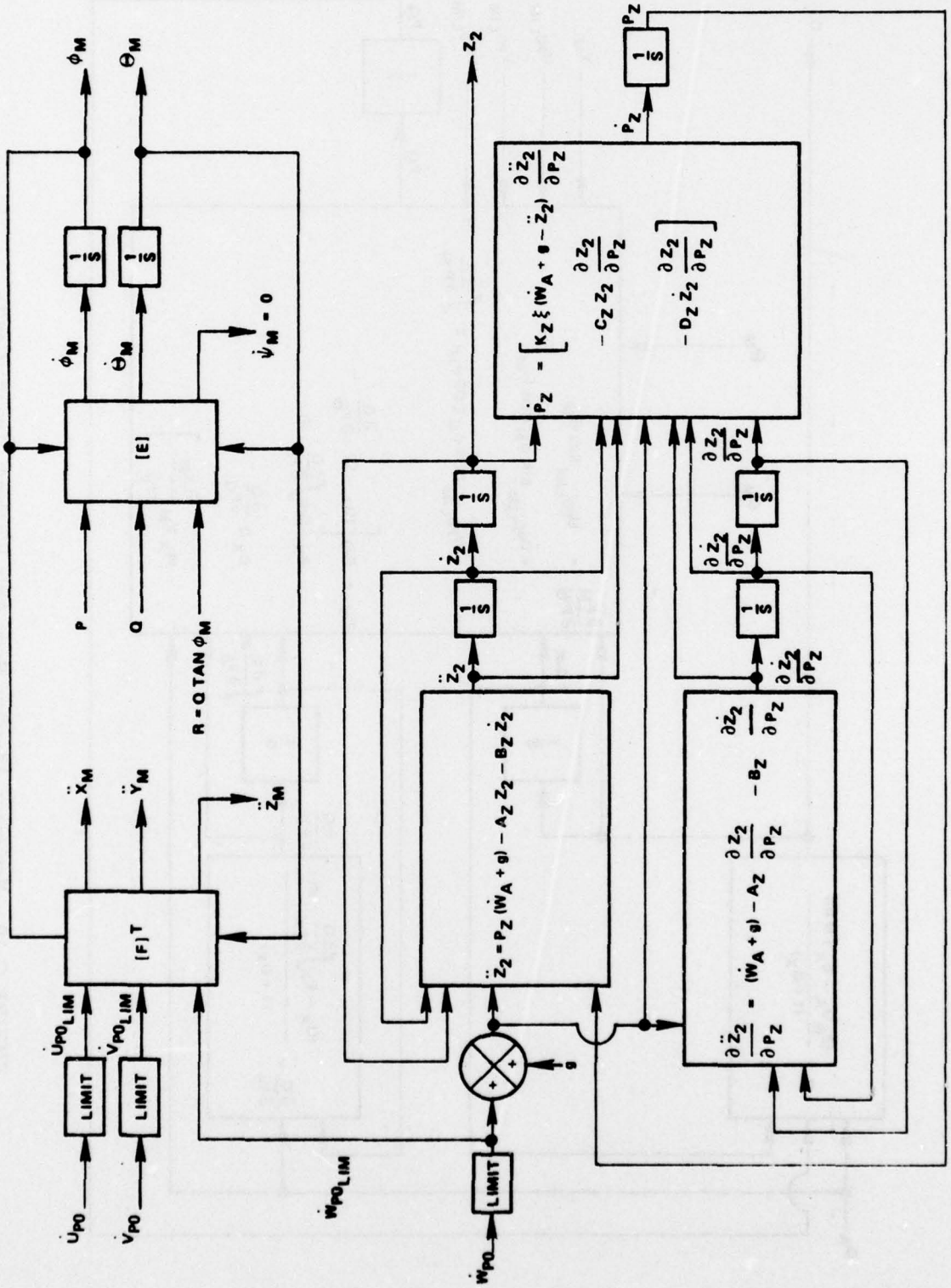

FIGURE C-10 - Nonlinear Adaptive Body Axis Washout Circuit (Con't)

Equations for $\dot{P}_\phi$, $\dot{P}_\theta$ and $\dot{P}_Z$ are derived by applying the method of continuous steepest descent:

$$P_i = -K_i \frac{\partial J_i}{\partial P_i}.$$

For J_ϕ, J_θ and J_Z this becomes:

$$\dot{P}_\phi = K_\phi \left\{ (P_A - P) \frac{\partial P}{\partial P_\phi} - B_Y \int P dt \int \frac{\partial P}{\partial P_\phi} dt - C_Y P \frac{\partial P}{\partial P_\phi} - W_Y \dot{Y}_M \frac{\partial \dot{Y}_M}{\partial P_Y} \right\}$$

$$\dot{P}_\theta = K_\theta \left\{ (Q_A - Q) \frac{\partial Q}{\partial P} - B_X \int Q dt \int \frac{\partial Q}{\partial P_\theta} dt - C_X Q \frac{\partial Q}{\partial P_\theta} - W_X \ddot{X}_M \frac{\partial \ddot{X}_M}{\partial P_X} \right\}$$

$$\dot{P}_Z = X_Z \left\{ (\dot{W}_A + g - \ddot{Z}_2) \frac{\partial \ddot{Z}_2}{\partial P_Z} - C_Z Z_2 \frac{\partial Z_2}{\partial P_Z} - D_Z \dot{Z}_2 \frac{\partial \dot{Z}_2}{\partial P_Z} \right\}$$

The adaptive filters are defined as follows:

$$P = (P_\phi P_A - E_Y \int P dt)/(1 + D_Y)$$

$$Q = (P_\theta Q_A - E_X \int Q dt)/(1 + D_X)$$

$$\ddot{Z}_2 = P_Z (\dot{W}_A + g) - A_Z Z_2 - B_Z \dot{Z}_2.$$

The state sensitivity equations are then derived from the definition of the adaptive filters and the body axis to inertial axis transformation:

$$\frac{\alpha P}{\alpha P_\phi} = (P_A - E_Y \int \frac{\partial P}{\partial P_\phi} dt)/(1 + D_Y)$$

$$\frac{\alpha Q}{\alpha P_\theta} = (Q_A - E_X \int \frac{\partial Q}{\partial P_\theta} dt)/(1 + D_X)$$

$$\frac{\alpha Z_2}{\alpha P_Z} = (\dot{W}_A + g) - A_Z \frac{\partial Z_2}{\partial P_Z} - B_Z \frac{\partial \dot{Z}_2}{\partial P_Z}$$

$$\frac{\partial \ddot{X}_M}{\partial P_\Theta} = \left(\dot{U}_{Po_{LIMITED}} \sin \Theta_M + \dot{V}_{Po_{LIMITED}} \sin \phi_M \cos \Theta_M - \dot{W}_{Po_{LIMITED}} \cos \phi_M \cos \Theta_M \right) X \frac{\partial Q}{\partial P_\Theta} \, dt$$

$$\frac{\partial \ddot{X}_M}{\partial P_\phi} = \left(-\dot{V}_{Po_{LIMITED}} \sin \phi_M - \dot{W}_{Po_{LIMITED}} \cos \phi_M \right) X \int \frac{\partial P}{\partial P_\phi} \, dt$$

The output of the rotational adaptive filters, P and Q, are transformed to Euler angular rates and integrated to form the simulator roll and pitch commands, ϕ_M and Θ_M.

The output of the vertical channel adaptive filter is the simulator heave command, Z_2.

Washout parameter settings are:

$B_X = B_Y = 6.25$

$C_X = C_Y = 0.$

$D_X = D_Y = 0.$

$E_X = E_Y = 2.5$

$W_X = W_Y = .0001$

$A_Z = 3.$

$B_Z = 6.$

$C_Z = 9.$

$D_Z = 36.$

$K_\phi = 1.$

$K_\Theta = 1.$

$K_Z = .09$

$\dot{W}_{Po}$ LIMITED to -29 and -35 ft/sec^2

$\dot{U}_{Po}$ and $\dot{V}_{Po}$ LIMITED to ±5 ft/sec^2

Initial conditions for the state variables are all zero except:

$$P_{\phi} = P_{\theta} = P_Z = 1.$$

NONLINEAR ADAPTIVE WASHOUT CIRCUIT (INERTIAL AXIS)

Shown in figure C-11 is a block diagram of an inertial axis washout circuit. Derivation of the equations is analogous to that for the body axis adaptive washout equations. For the inertial axis washout, the adaptive filters are applied to Euler angular rates rather than body axis angular rates. The vertical channel is identical to that for the body axis adaptive washout.

NONLINEAR ADAPTIVE WASHOUT CIRCUIT (LINEAR TRANSFORMATION)

Figure C-12 shows a block diagram for a nonlinear adaptive washout circuit for which the transformations have been linearized. The vertical channel is once again the same as for the body and inertial axis washout circuits.

Figures C-13 through C-24 show the response of each of the washout circuits to the same maneuver. The maneuver was a turn to the left followed by a climb.

The Euler transformation matrix for a link three-degree-of-freedom motion base is as follows:

$$[E] = \begin{bmatrix} 1 & \frac{\text{SIN}\phi}{\text{TAN}\theta} & \frac{\text{COS}\phi}{\text{TAN}\theta} \\ 0 & \text{COS}\phi & -\text{SIN}\theta \\ 0 & \frac{\text{SIN}\phi}{\text{COS}\theta} & \frac{\text{COS}\phi}{\text{COS}\theta} \end{bmatrix}$$

where

$$\begin{bmatrix} \phi \\ \dot{\theta} \\ \dot{\psi} \end{bmatrix} = [E] \begin{bmatrix} P \\ Q \\ R \end{bmatrix}$$

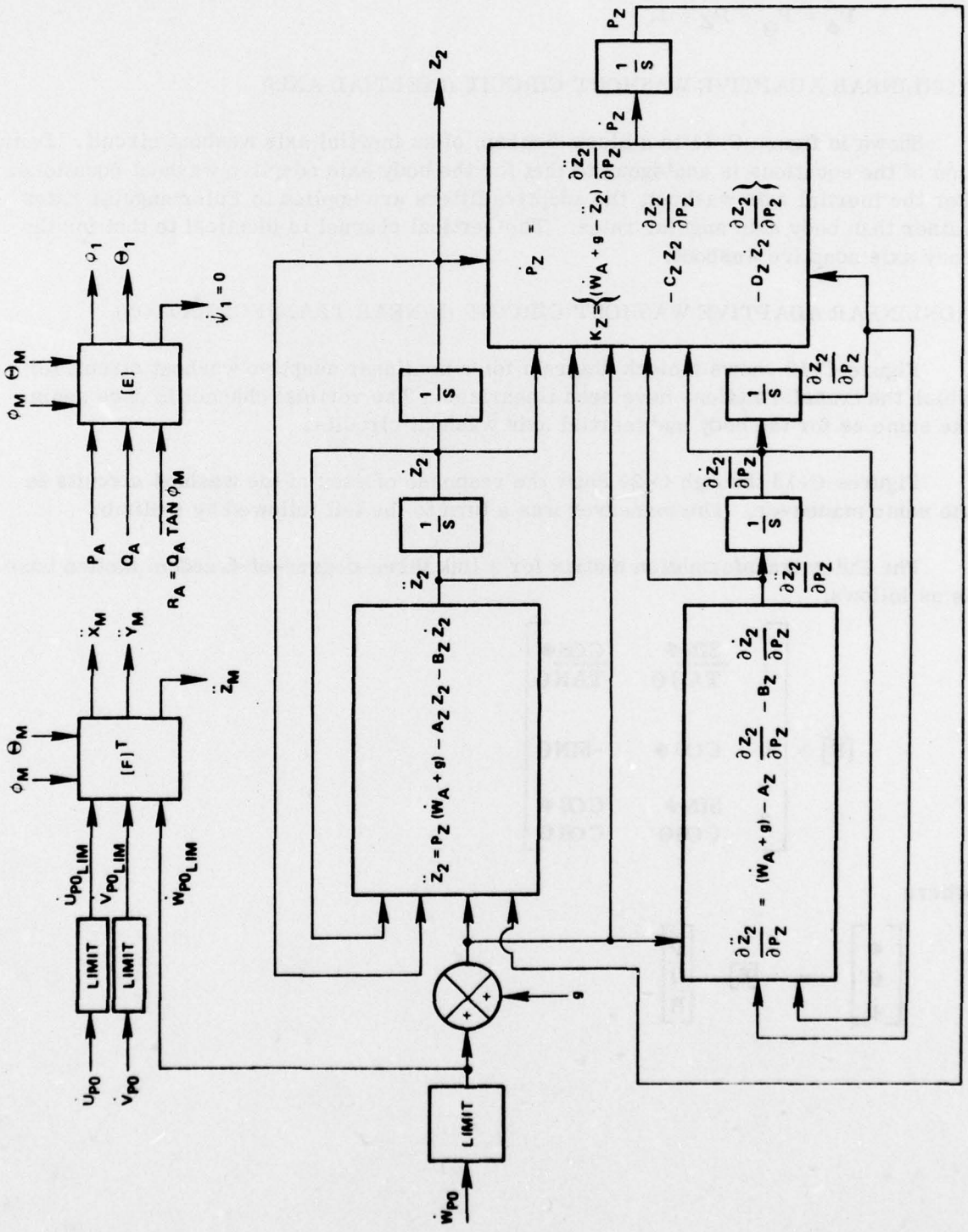

FIGURE C-11 - Nonlinear Adaptive Inertial Axis Washout Circuit

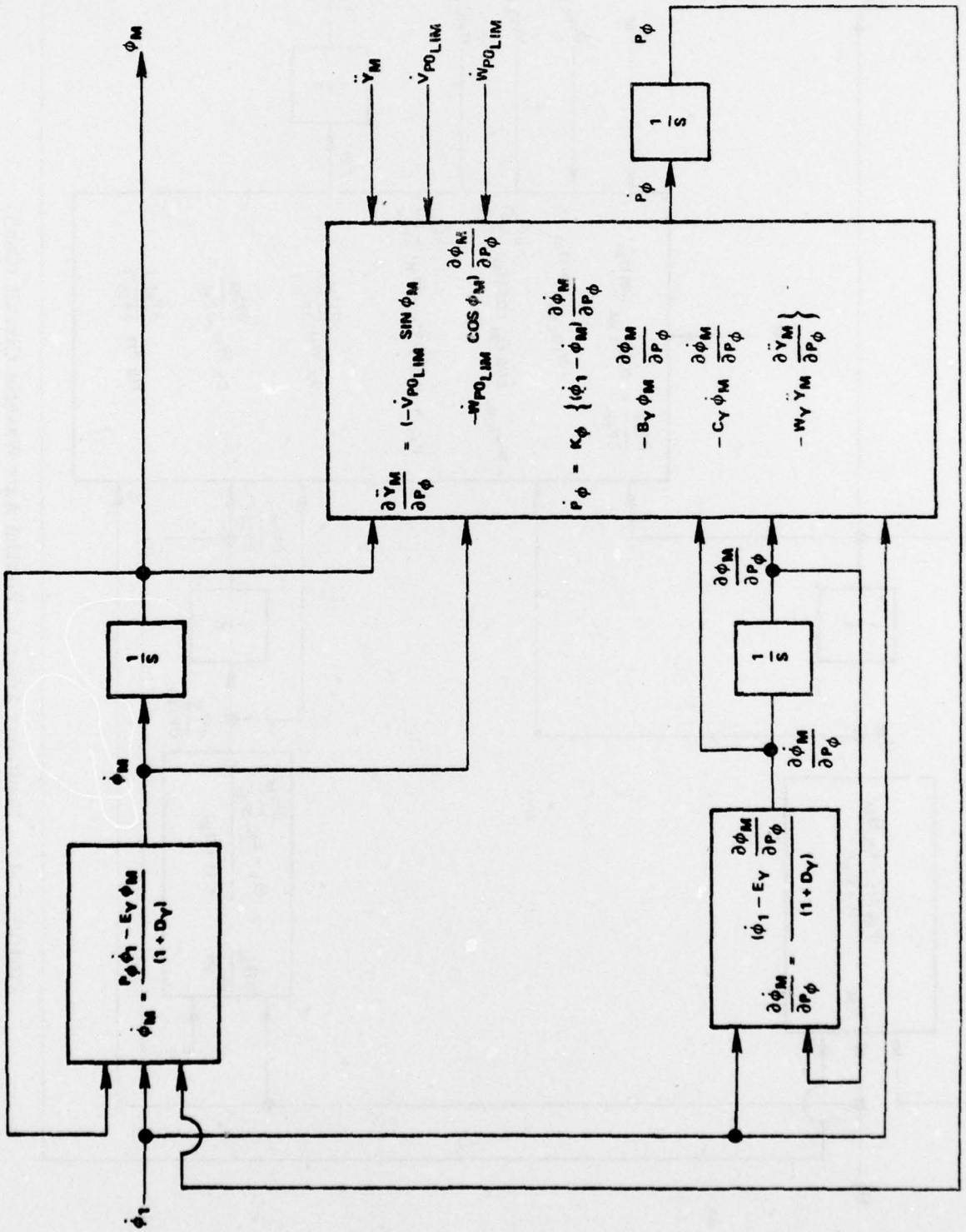

FIGURE C-11 - Nonlinear Adaptive Inertial Axis Washout Circuit (Con't)

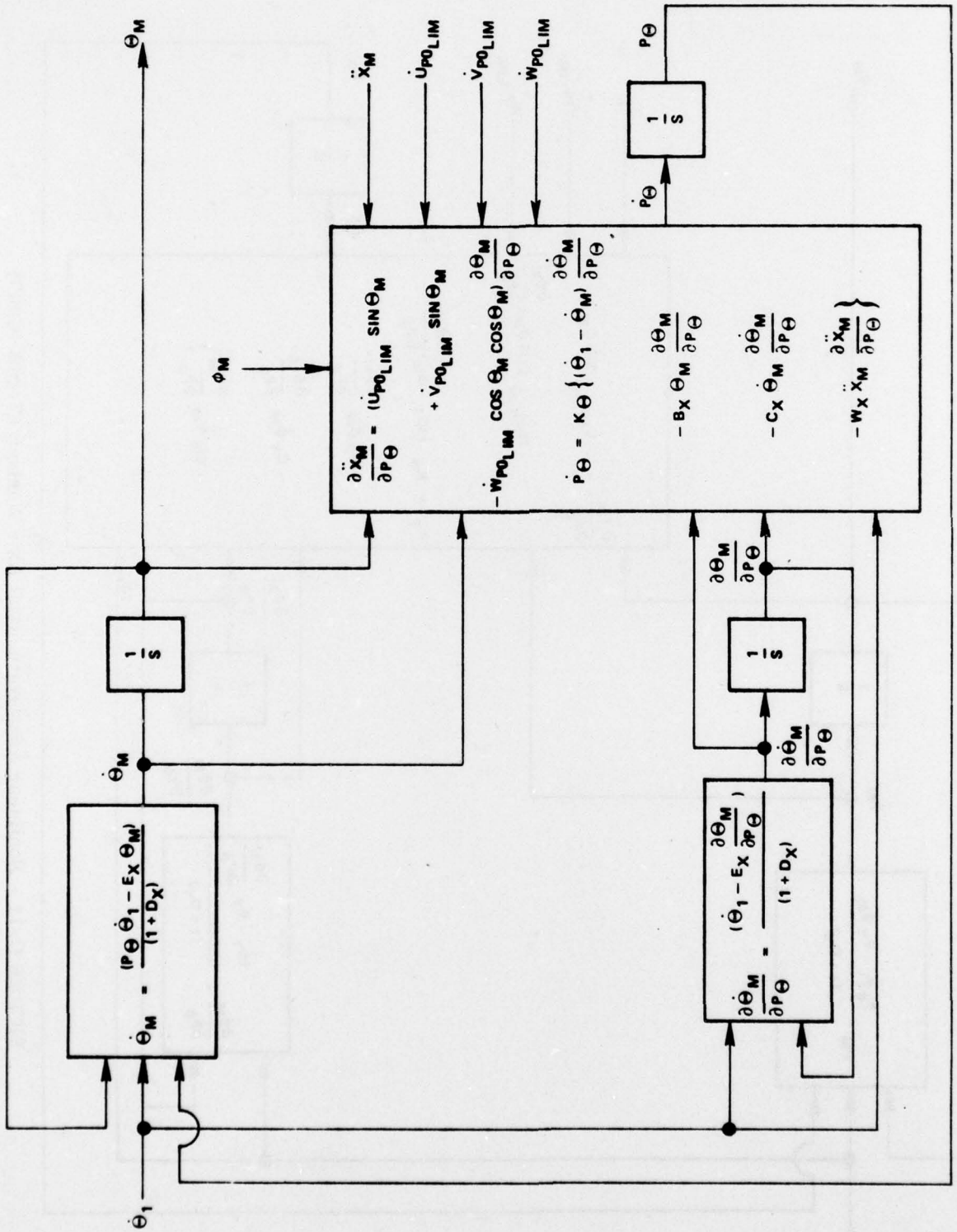

FIGURE C-11 - Nonlinear Adaptive Inertial Axis Washout Circuit (Con't)

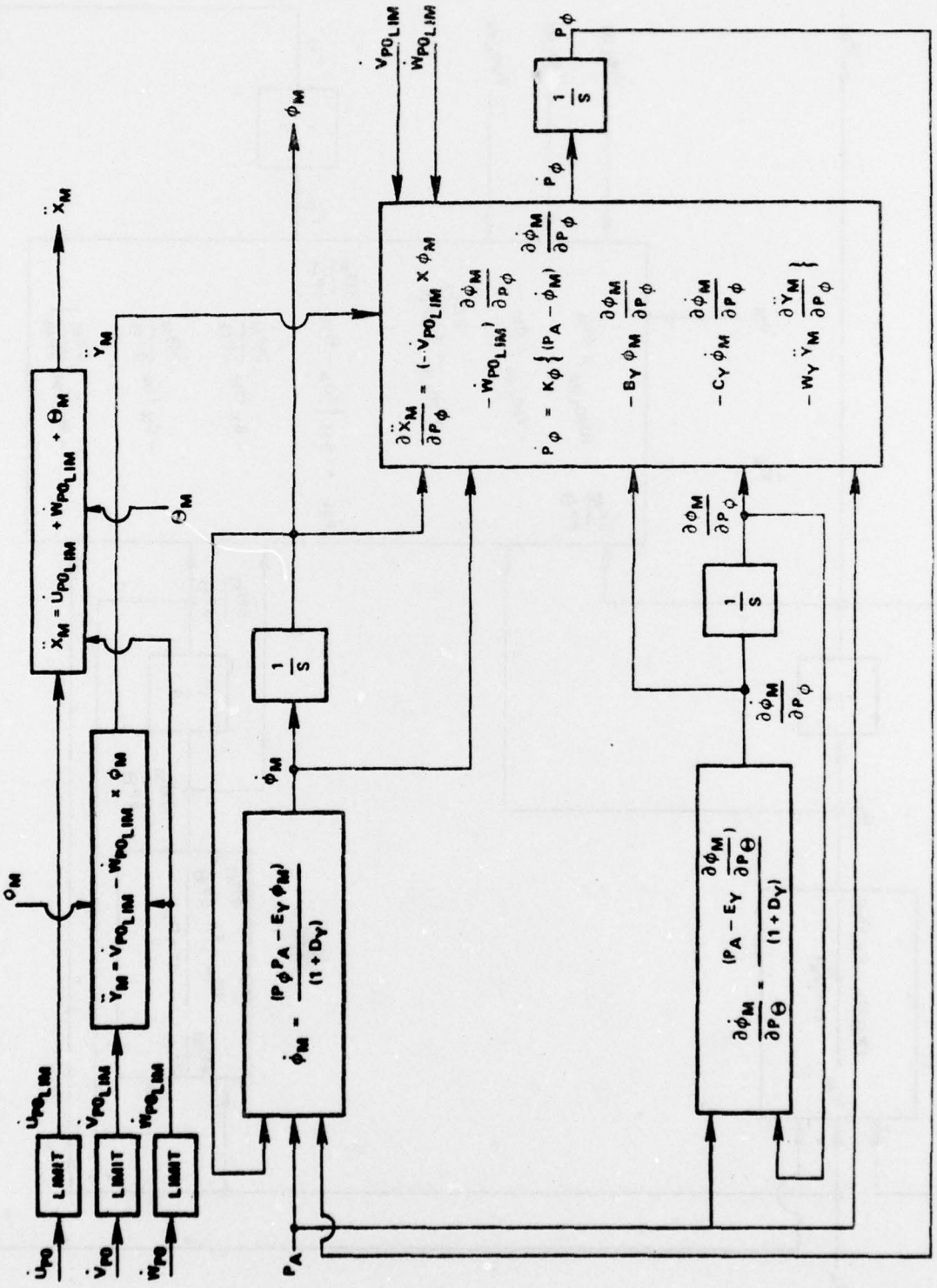

FIGURE C-12 - Nonlinear Adaptive Washout Circuit With Linear Transformations

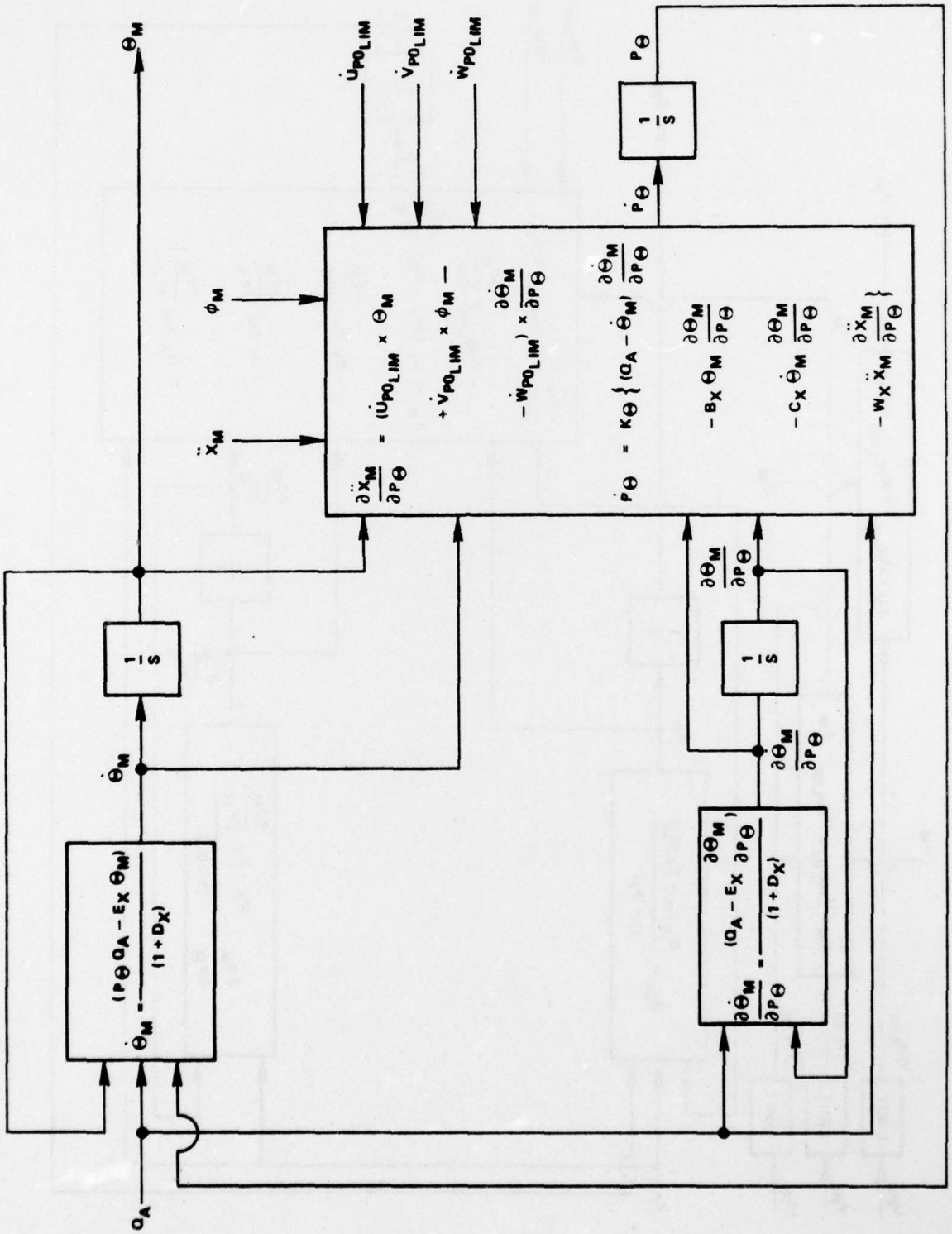

FIGURE C-12 - Nonlinear Adaptive Washout Circuit With Linear Transformations (Con't)

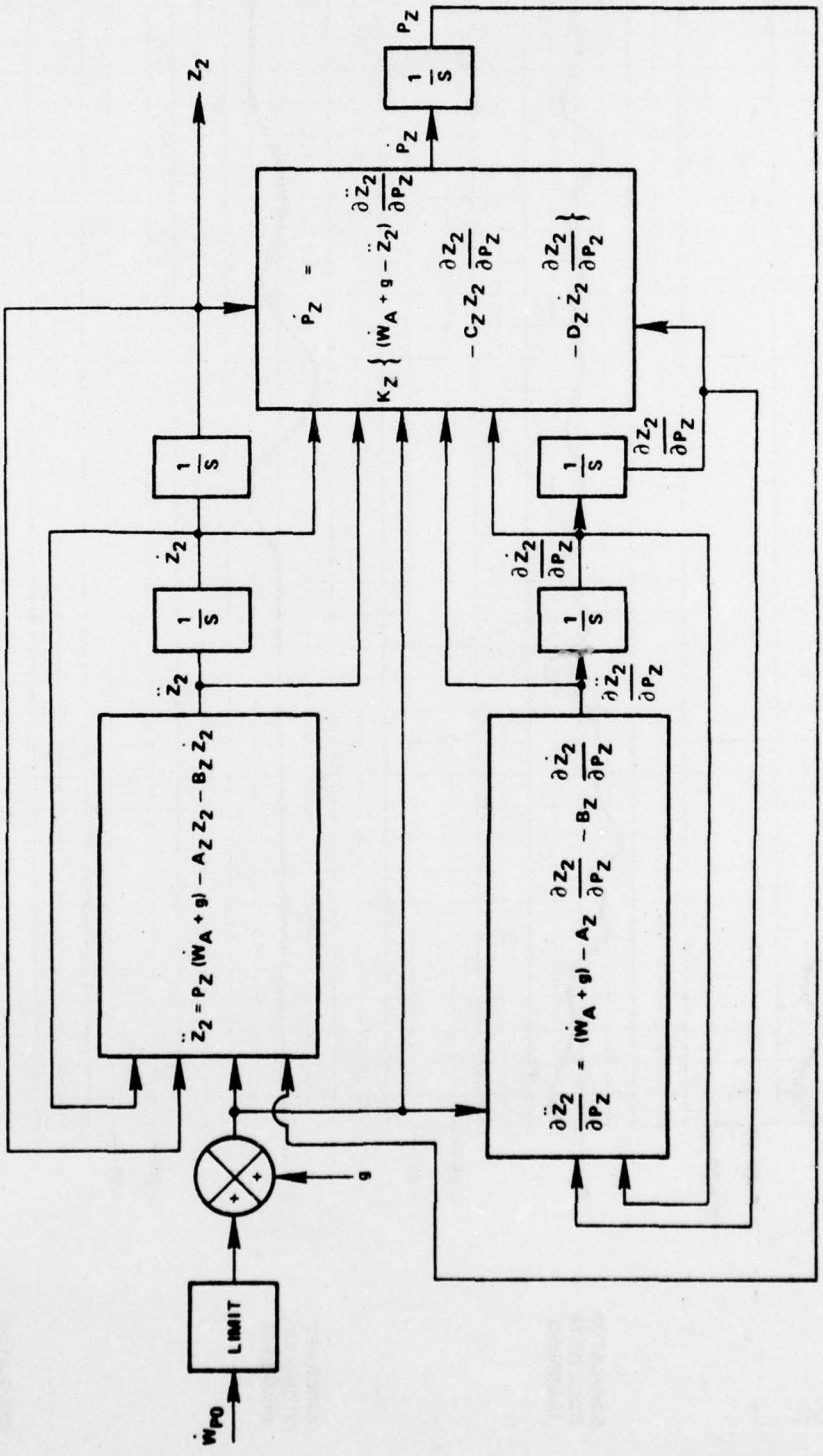

FIGURE C-12 - Nonlinear Adaptive Washout Circuit With Linear Transformations (Con't)

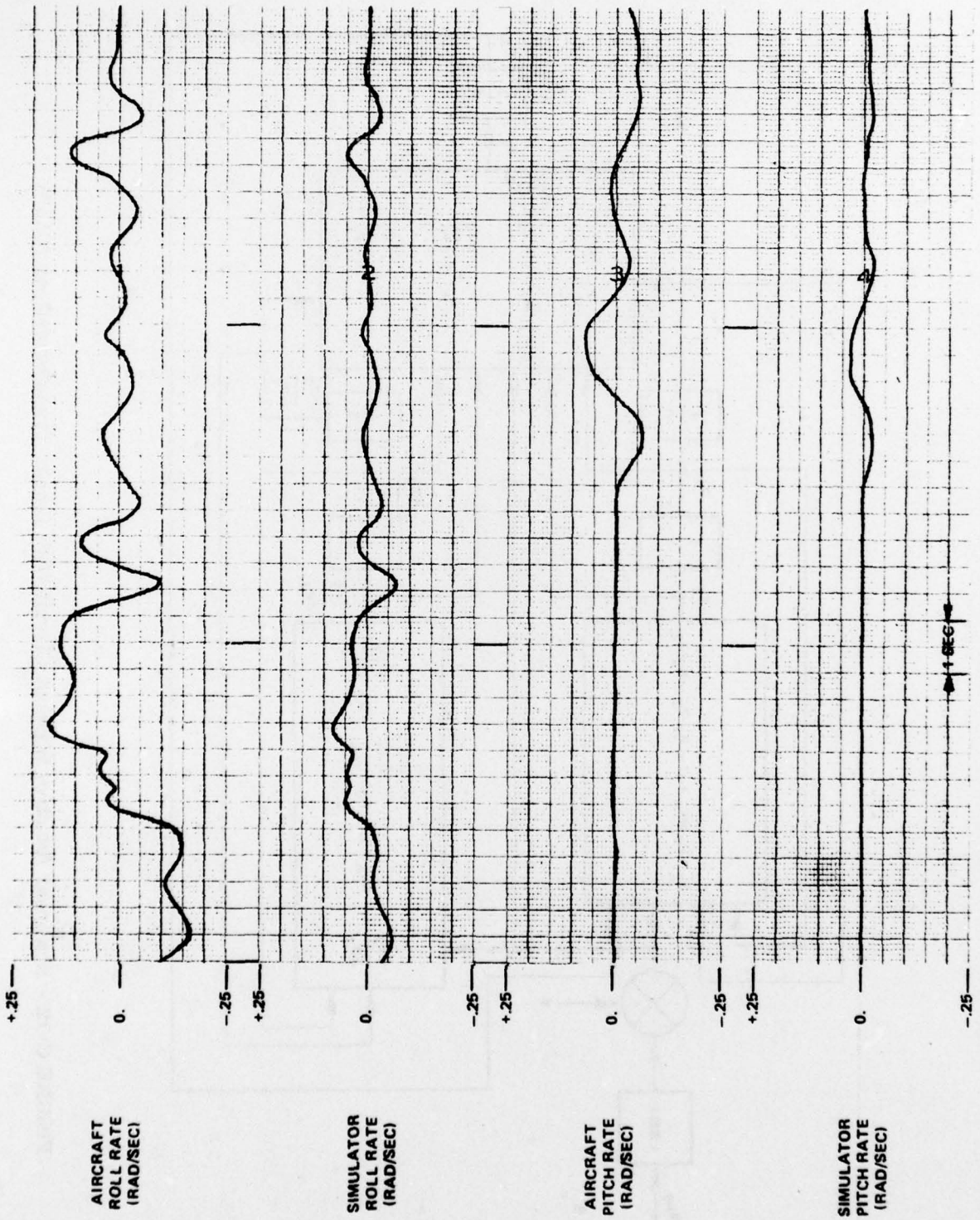

FIGURE C-13 - First Order Body Axis Washout Circuit Time History

FIGURE C-13 - First Order Body Axis Washout Circuit Time History (Con't)

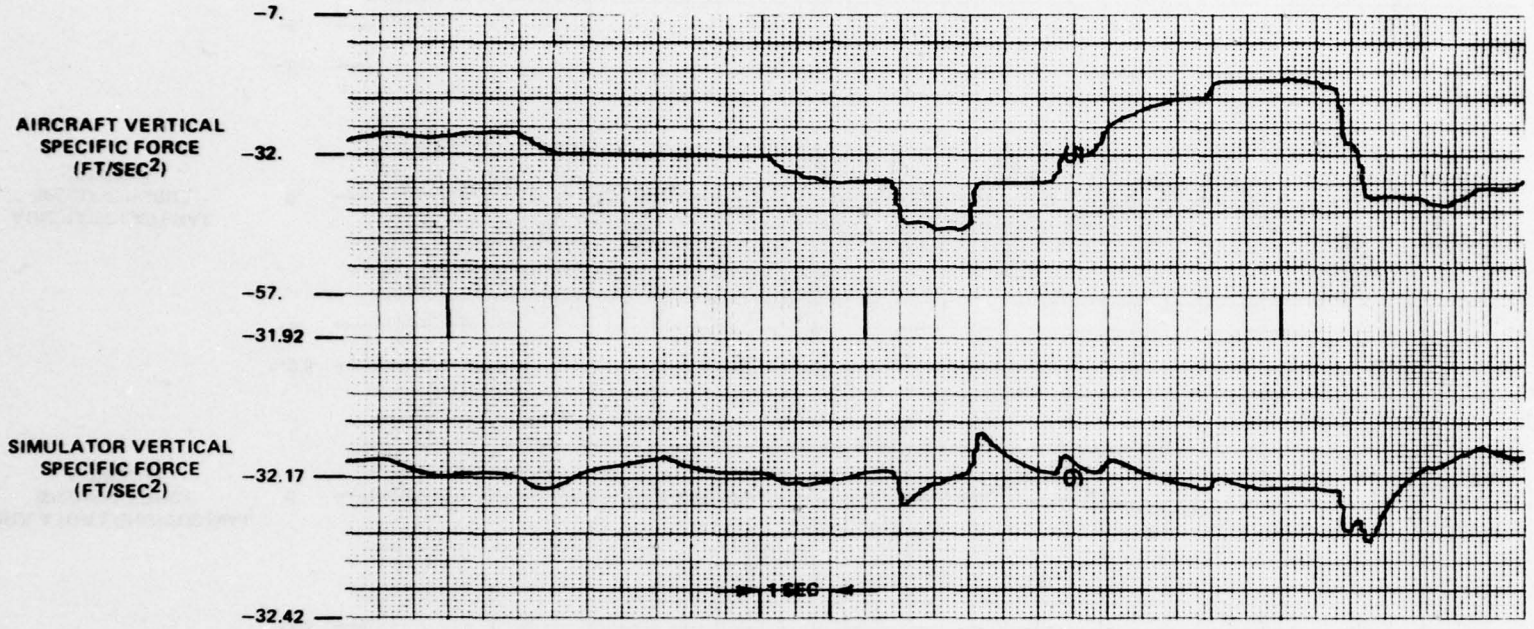

FIGURE C-13 - First Order Body Axis Washout Circuit Time History (Con't)

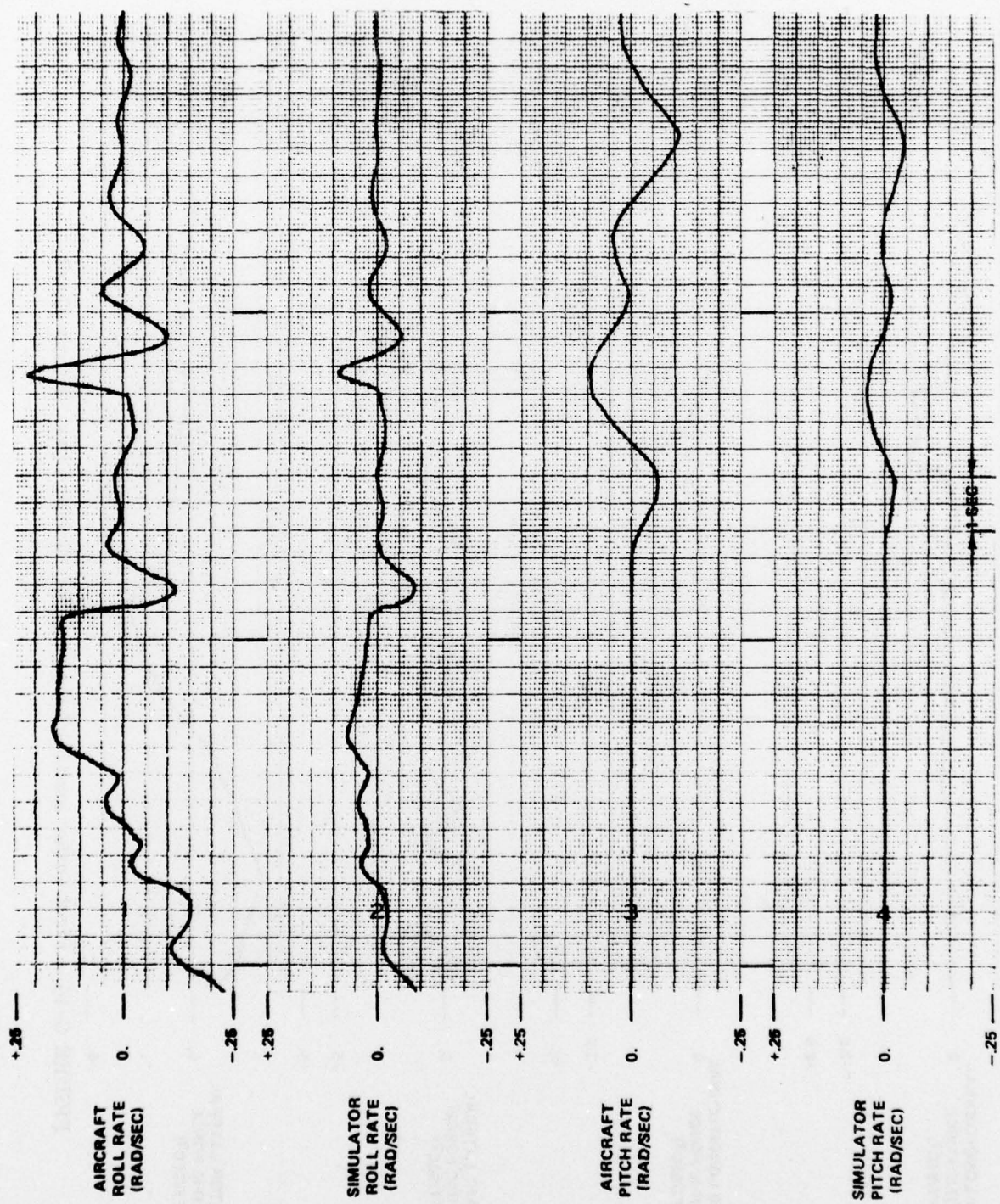

FIGURE C-14 - First Order Inertial Axis Washout Circuit Time History

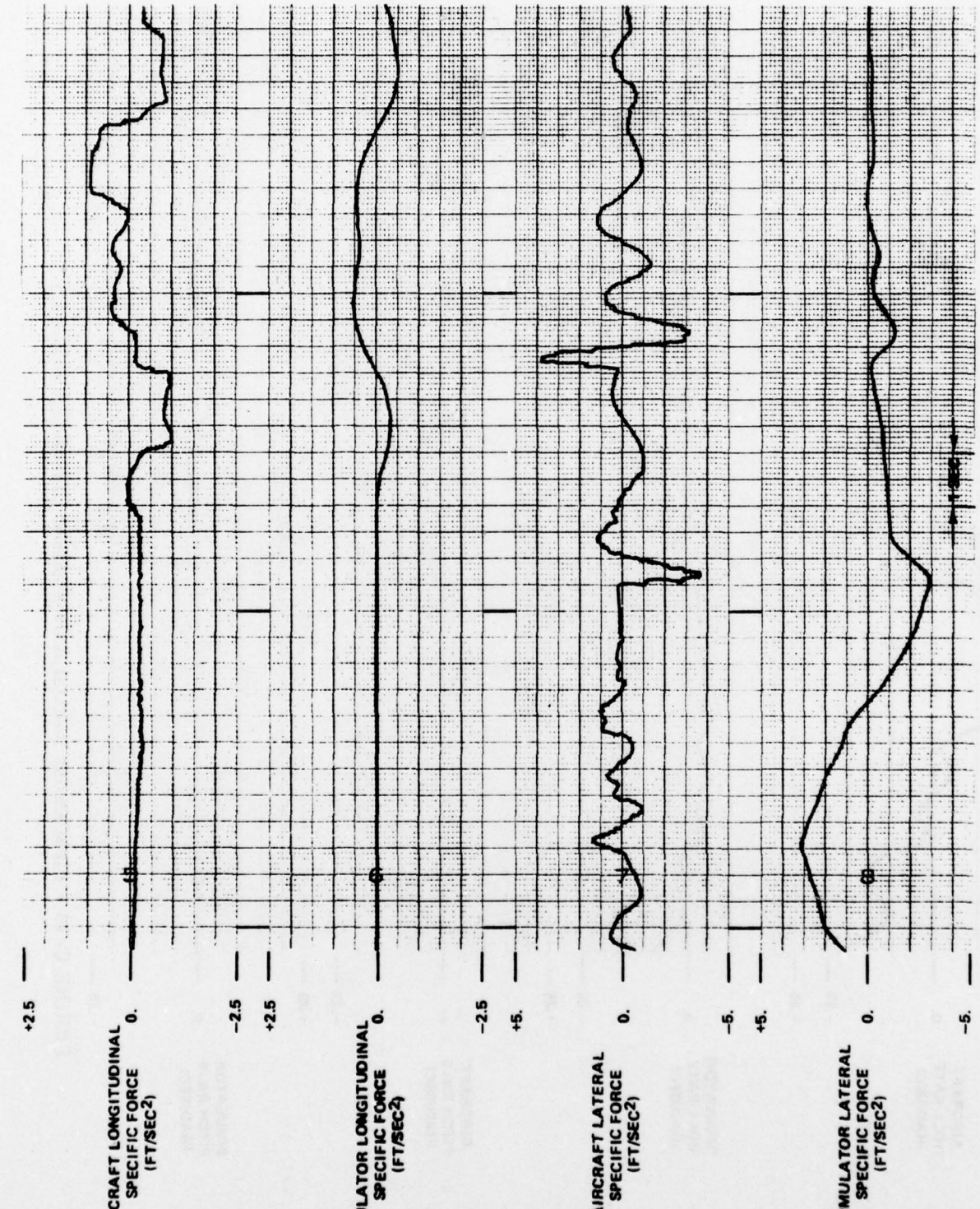

FIGURE C-14 - First Order Inertial Axis Washout Circuit Time History (Con't)

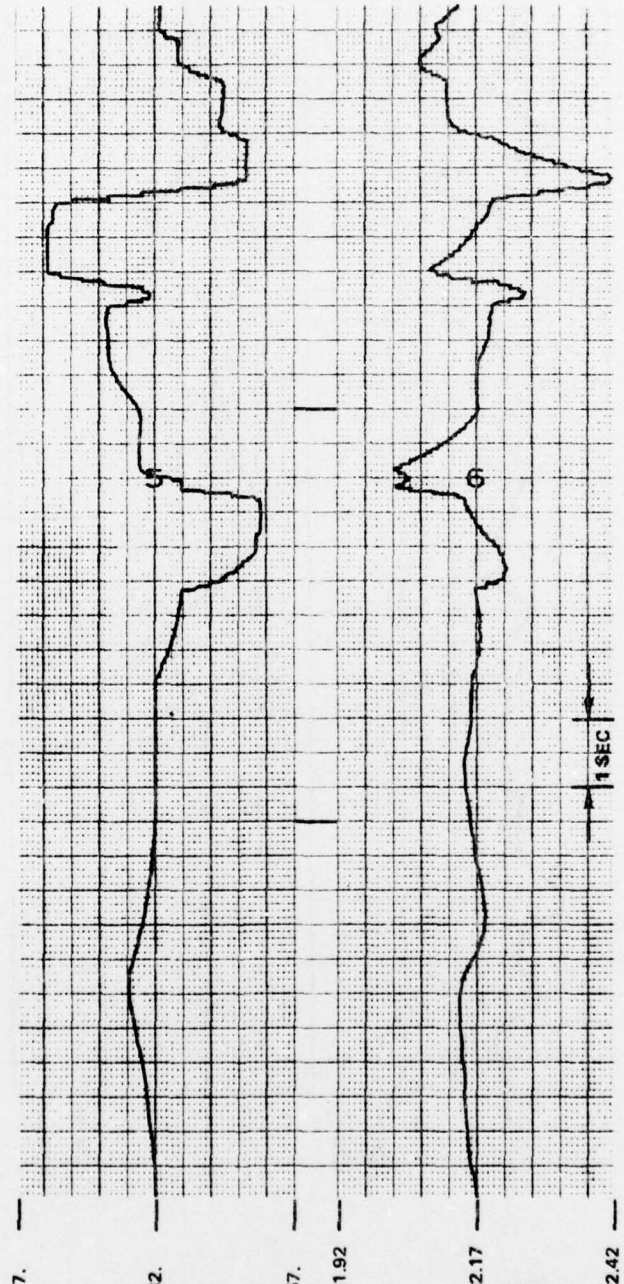

FIGURE C-14 - First Order Inertial Axis Washout Circuit Time History (Con't)

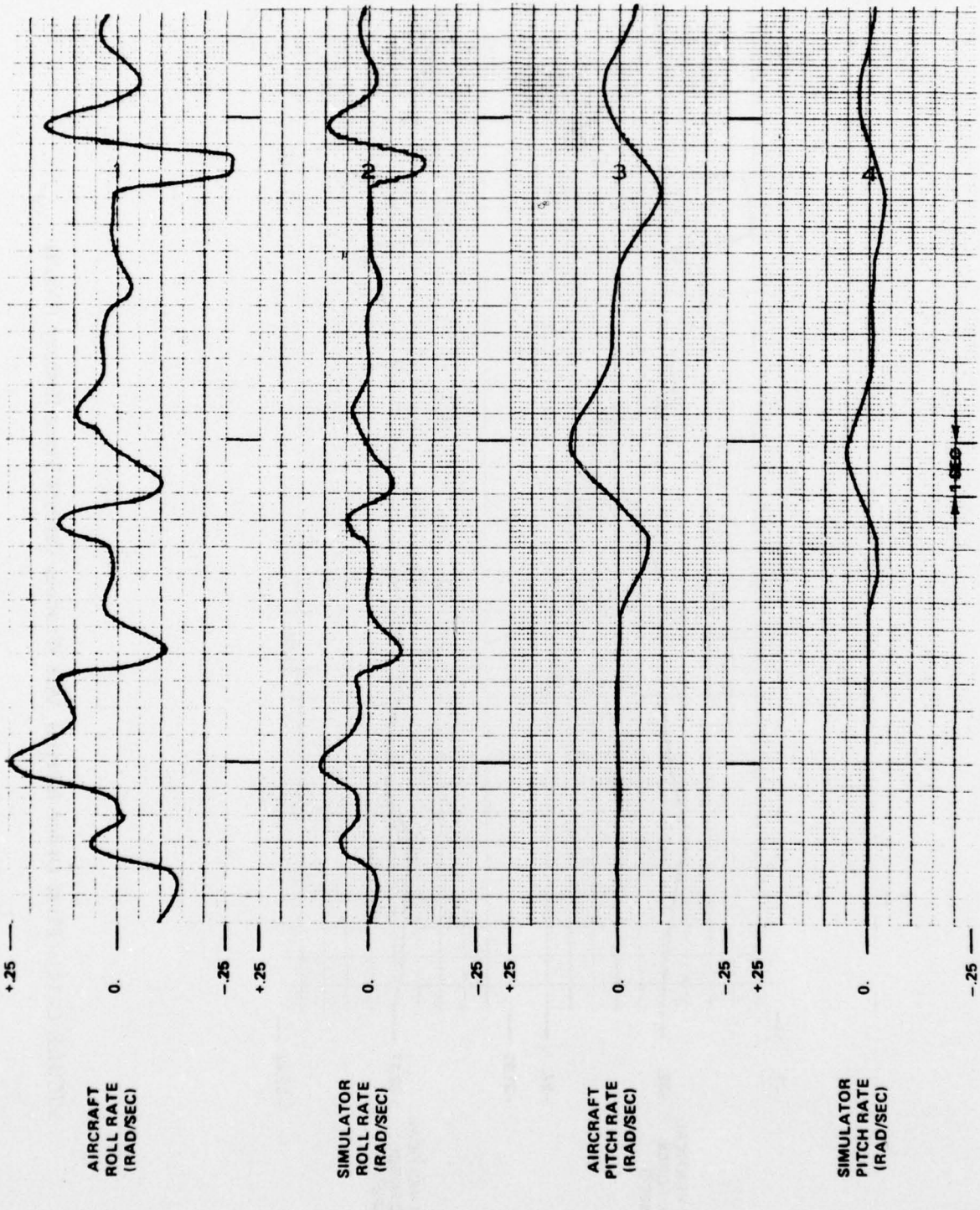

FIGURE C-15 - Lincarized First Order Washout Circuit Time History

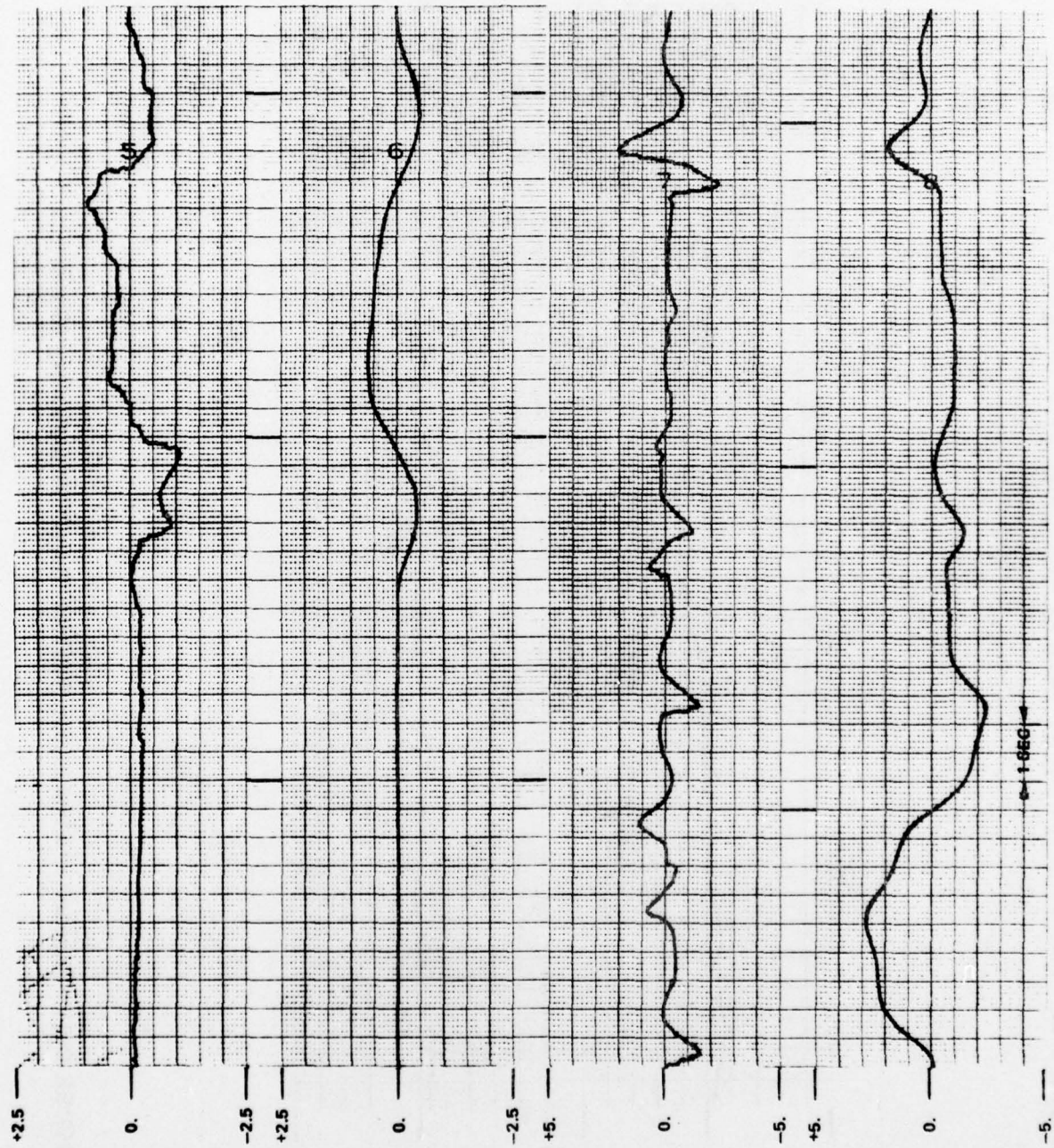

FIGURE C-15 - Linearized First Order Washout Circuit Time History (Con't)

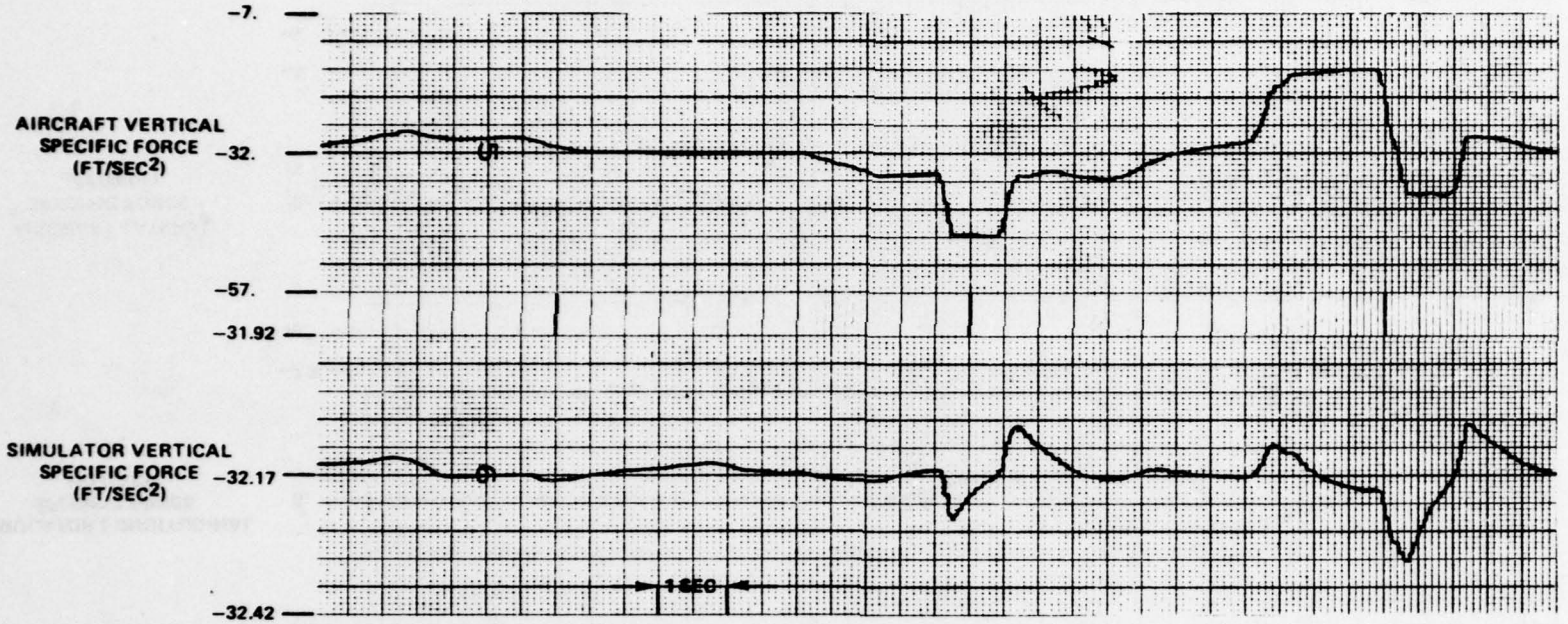

FIGURE C-15 - Linearized First Order Washout Circuit Time History (Con't)

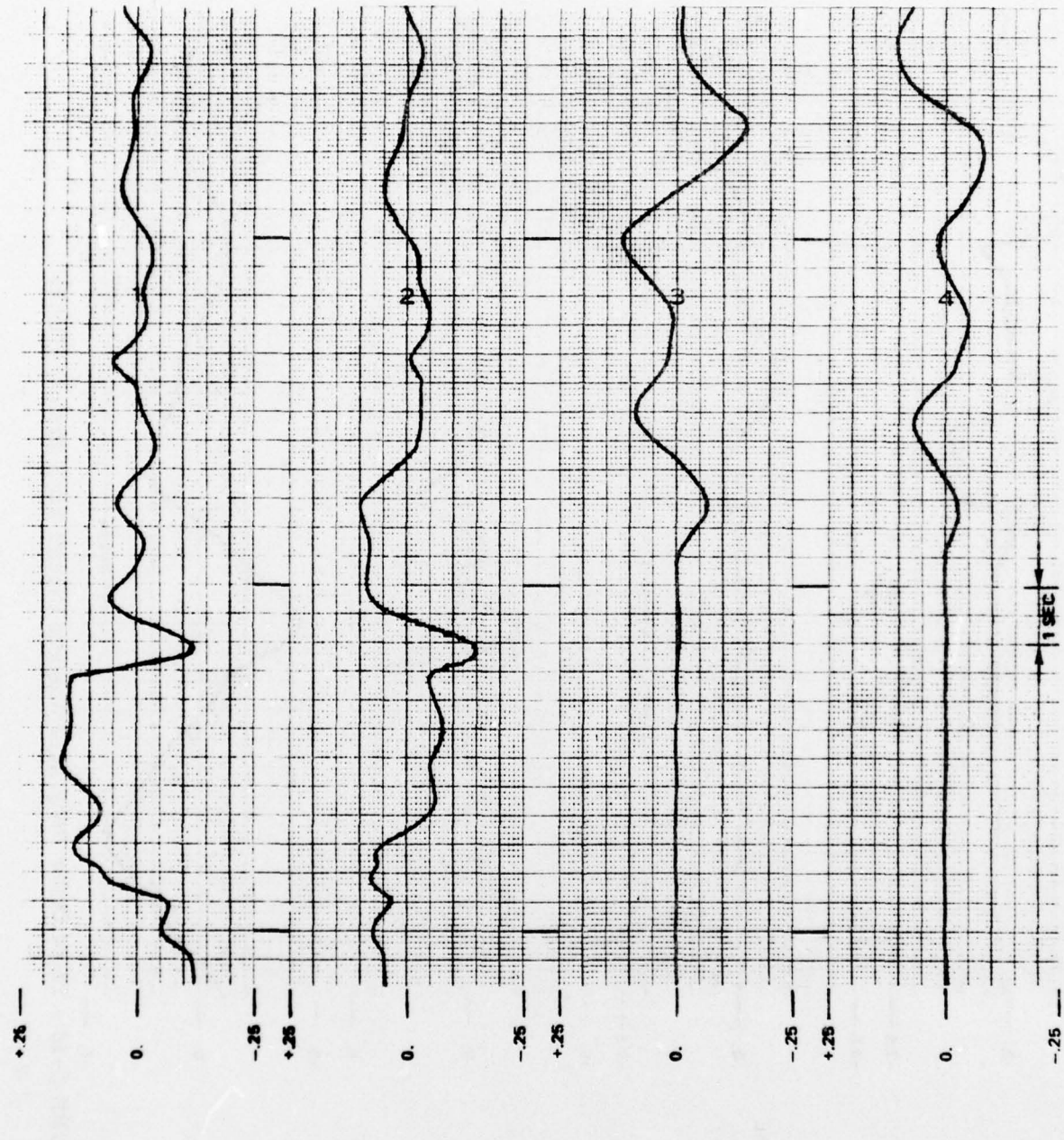

FIGURE C-16 - Third Order Body Axis Washout Circuit Time History

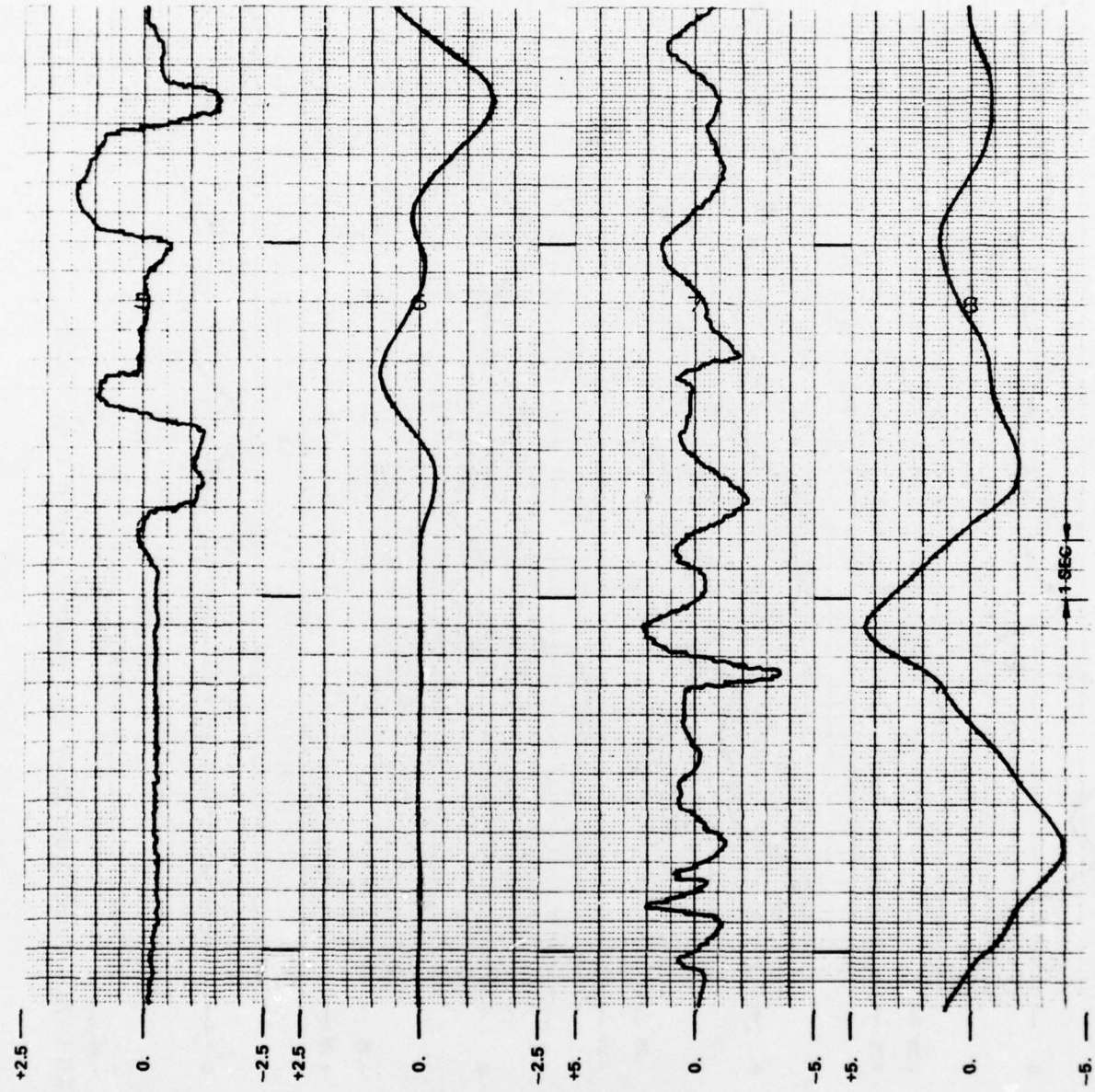

FIGURE C-16 - Third Order Body Axis Washout Circuit Time History (Con't)

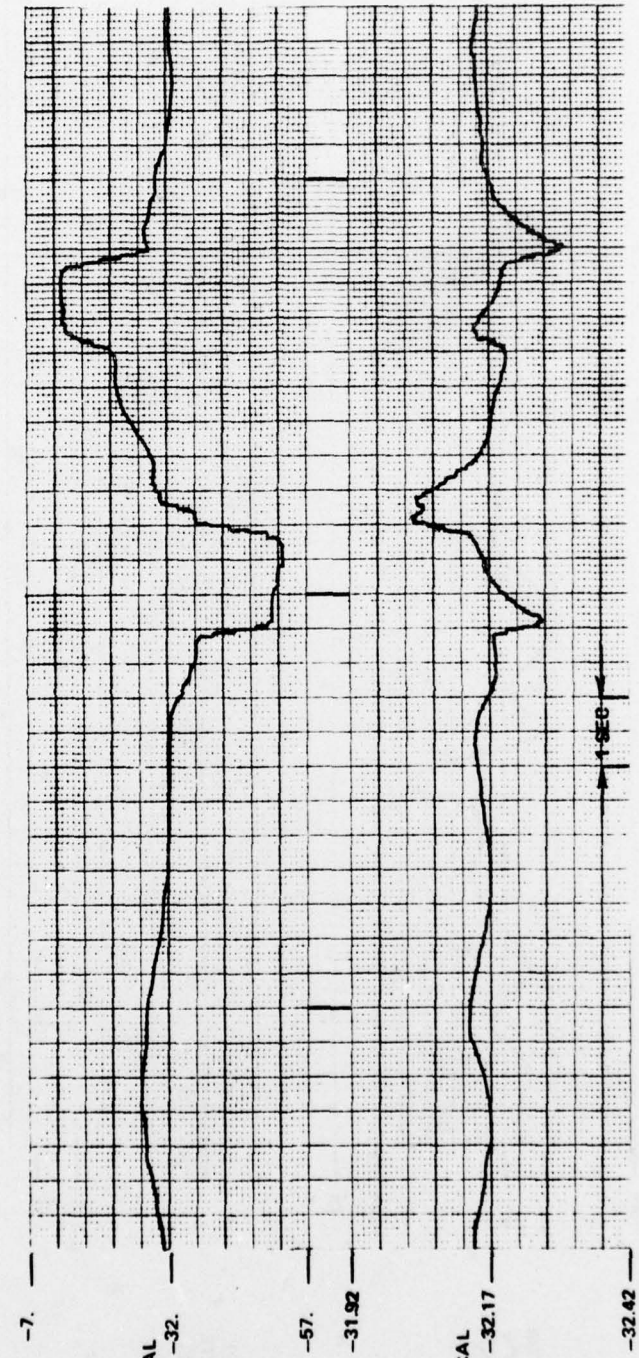

FIGURE C-16 - Third Order Body Axis Washout Circuit Time History (Con't)

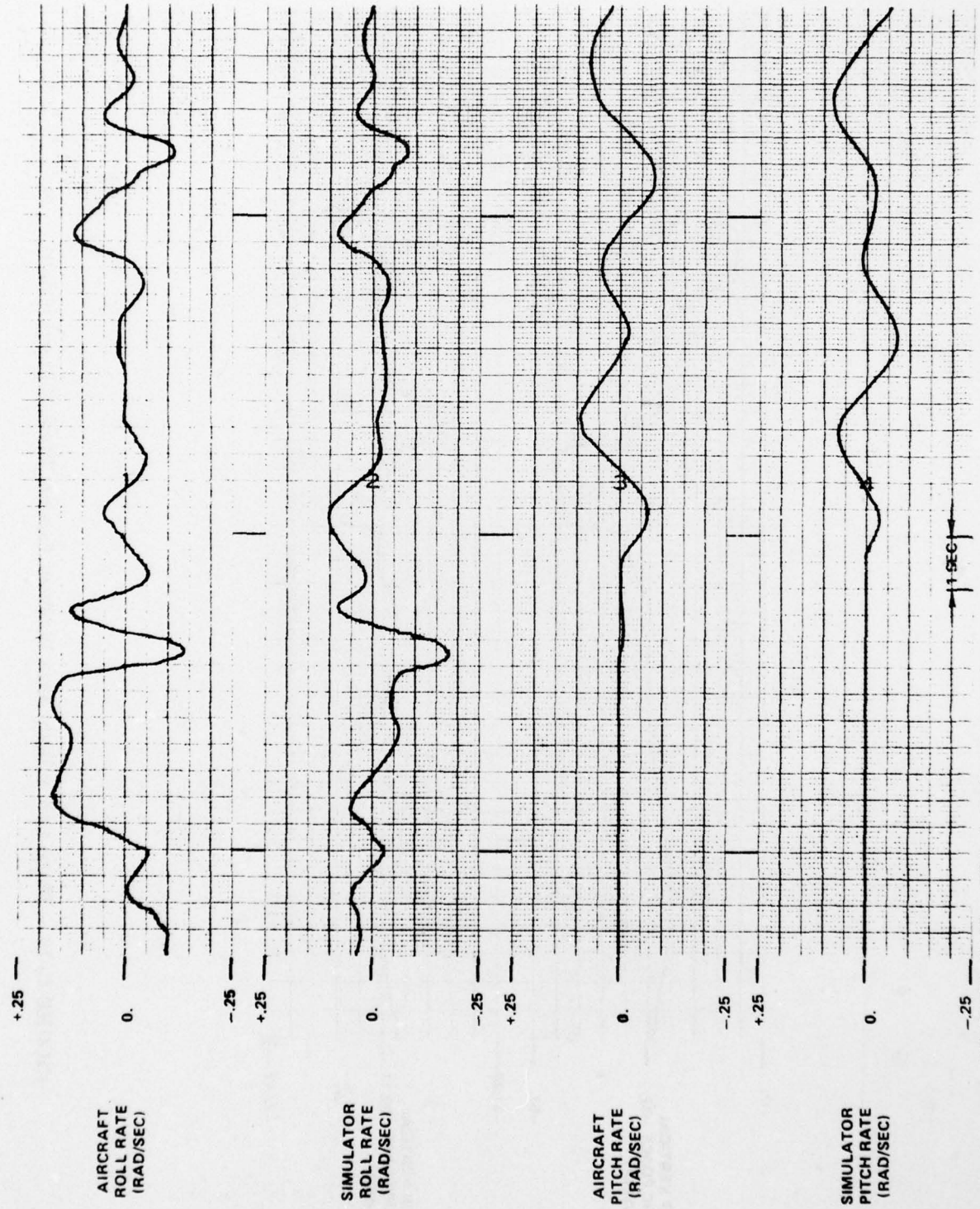

FIGURE C-17 - Third Order Inertial Axis Washout Circuit Time History

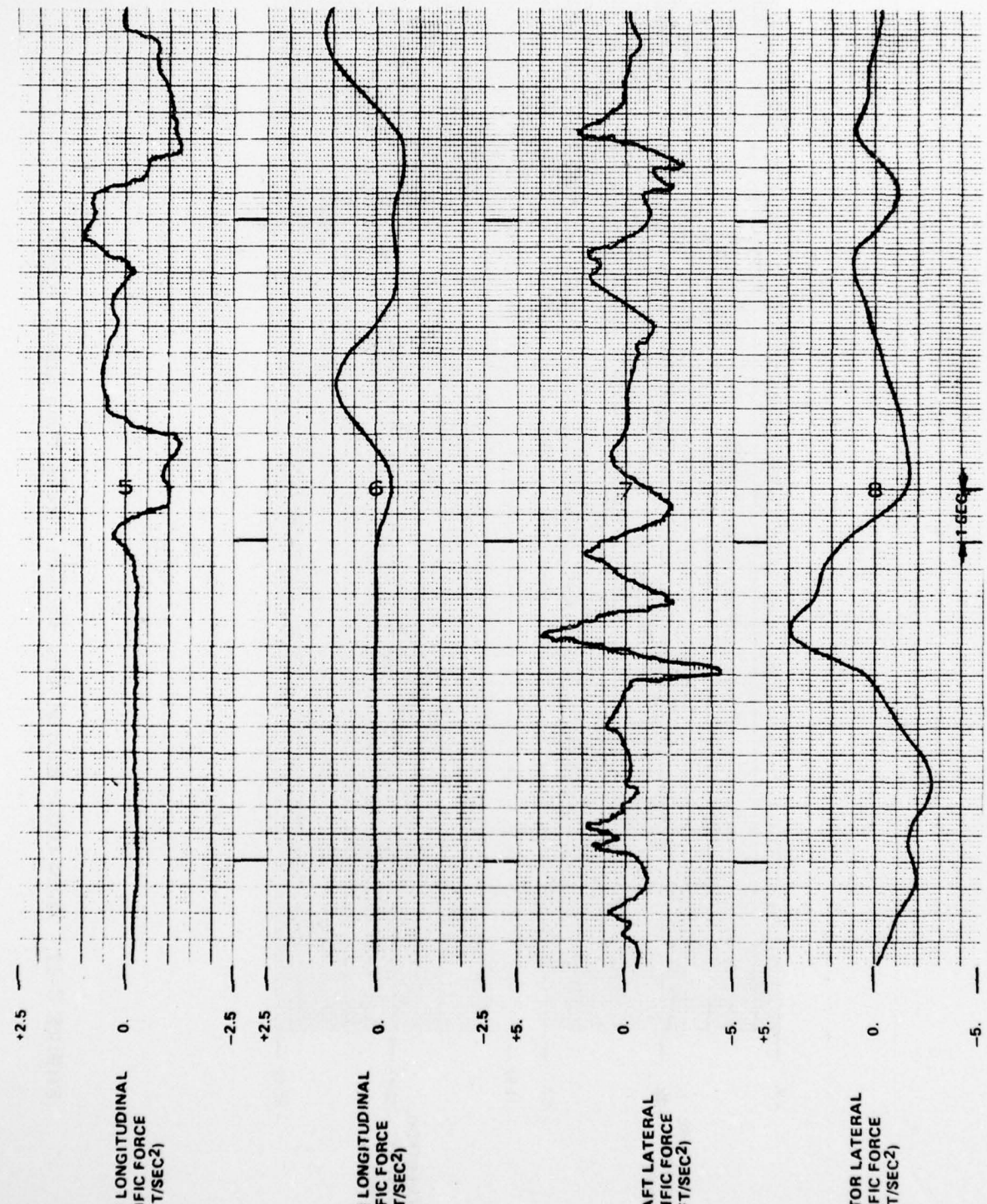

FIGURE C-17 - Third Order Inertial Axis Washout Circuit Time History (Con't)

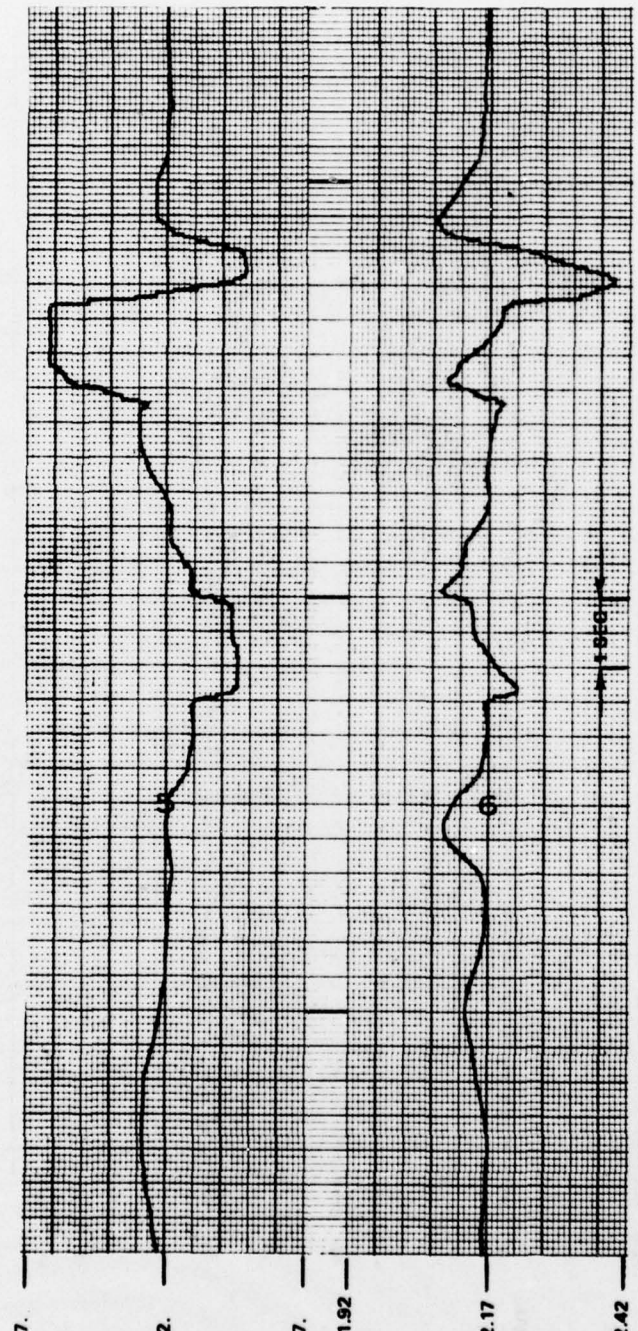

FIGURE C-17 - Third Order Inertial Axis Washout Circuit Time History (Con't)

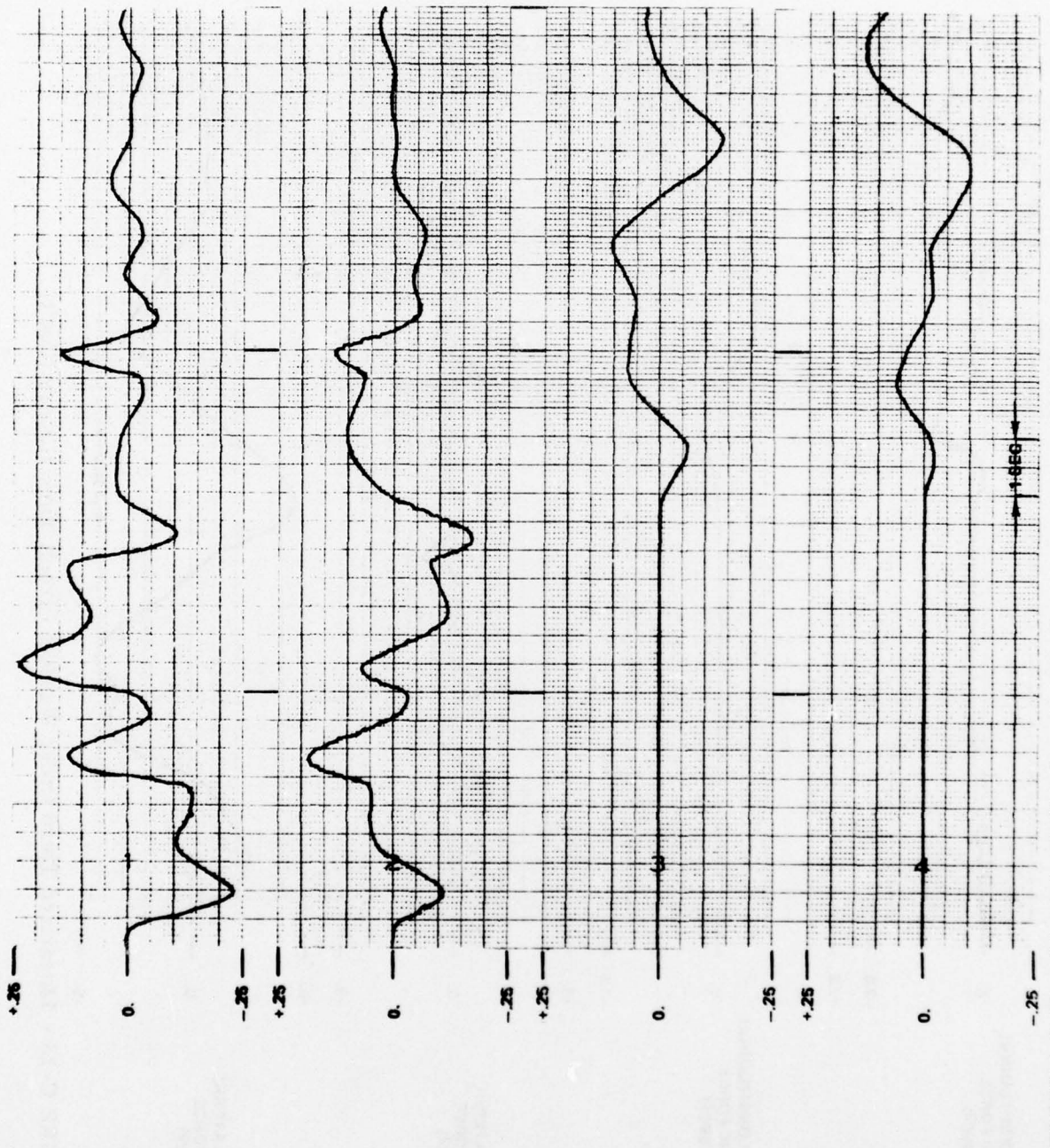

FIGURE C-18 - Linearized Third Order Washout Circuit Time History

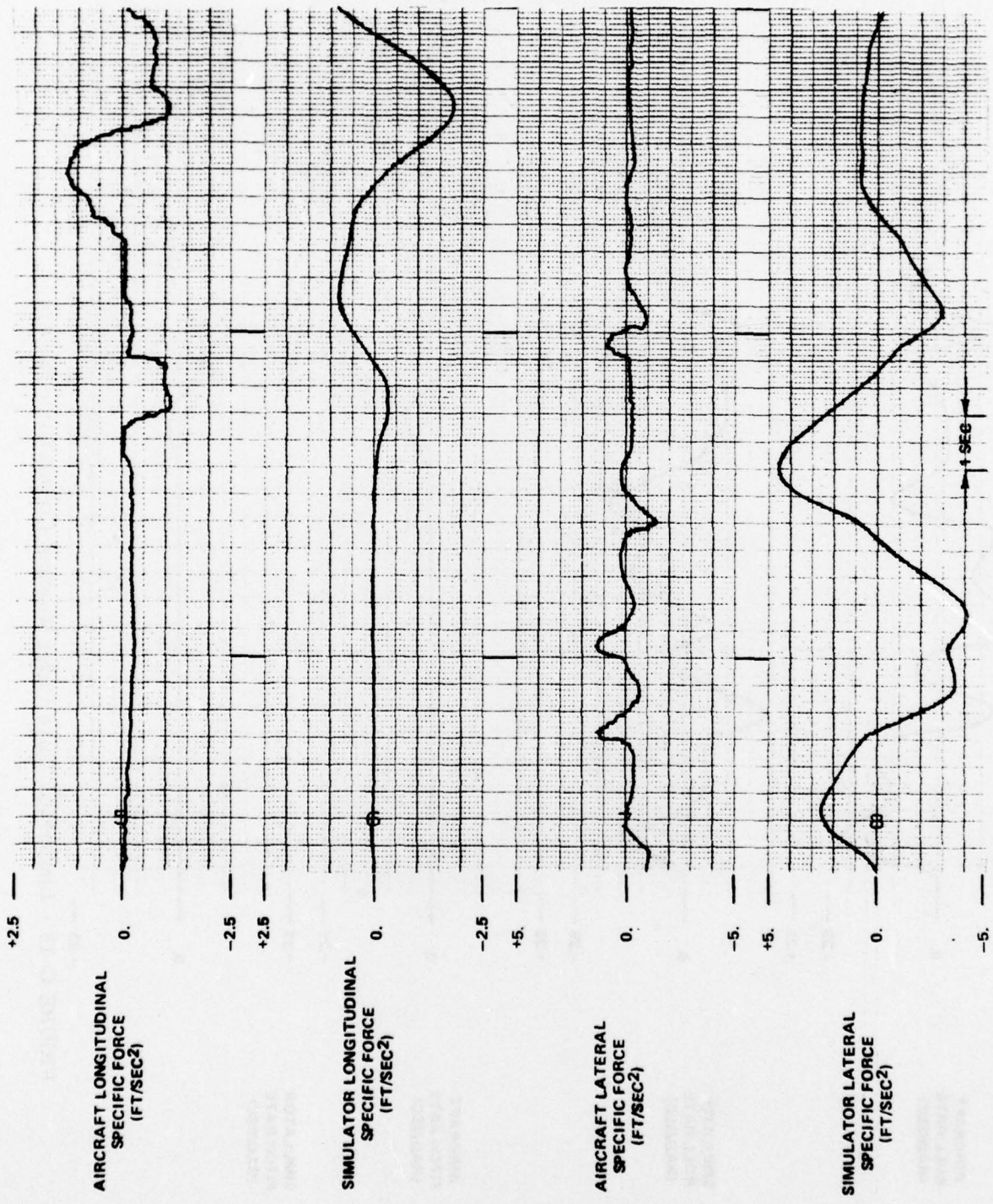

FIGURE C-18 - Linearized Third Order Washout Circuit Time History (Con't)

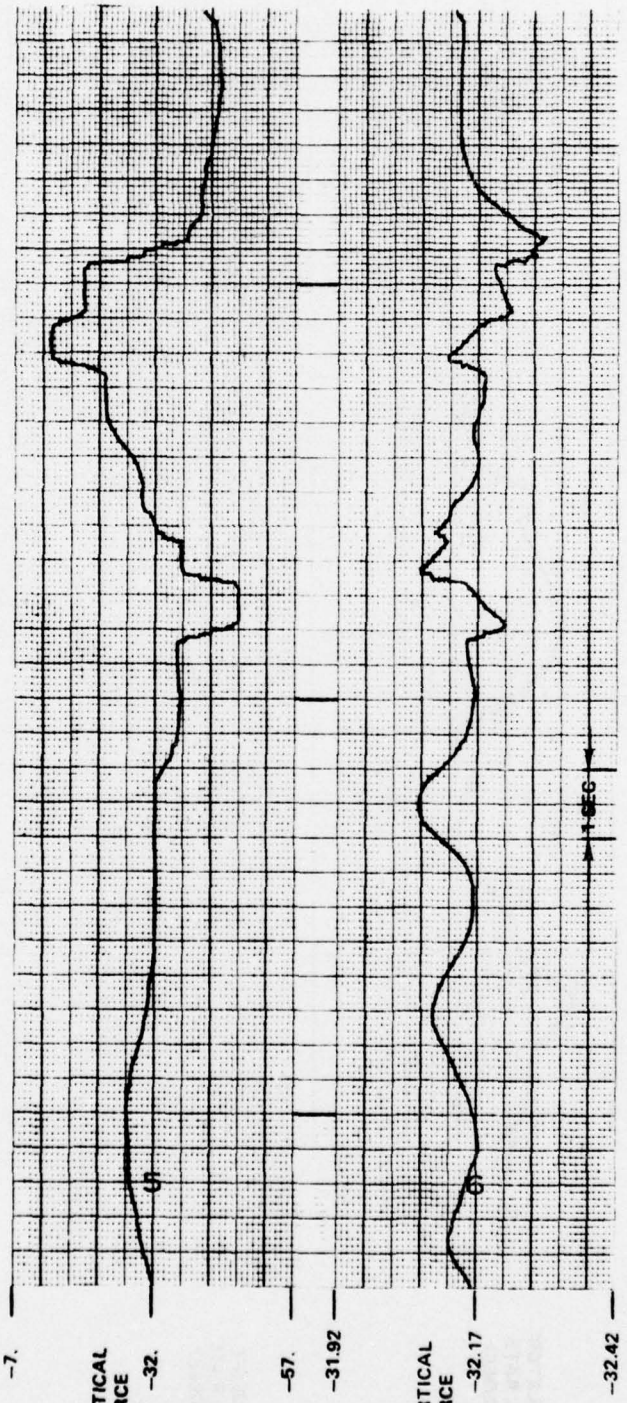

FIGURE C-18 - Linearized Third Order Washout Circuit Time History (Con't)

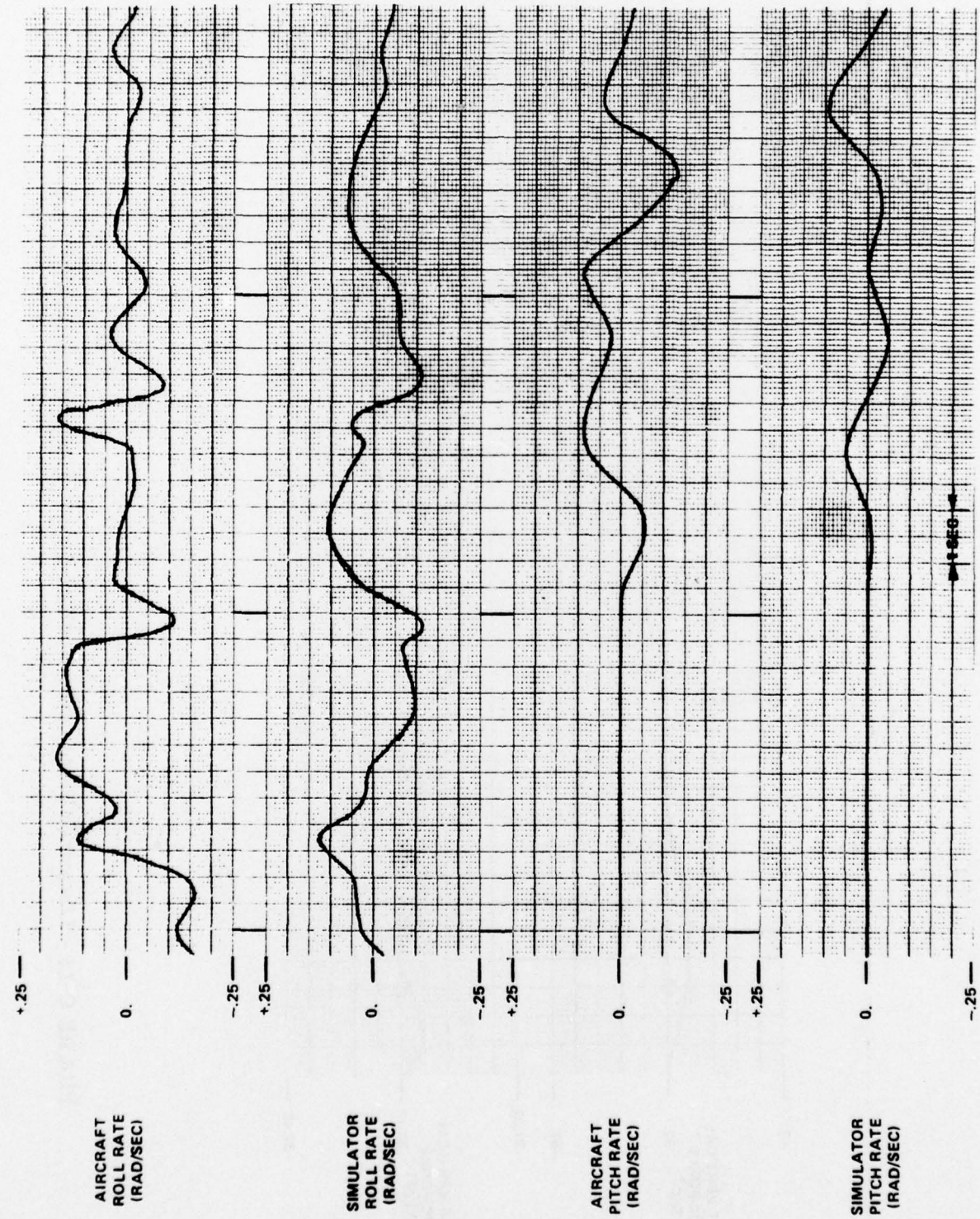

FIGURE C-19 - Time History For High Order Body Axis Washout Circuit With Tilt

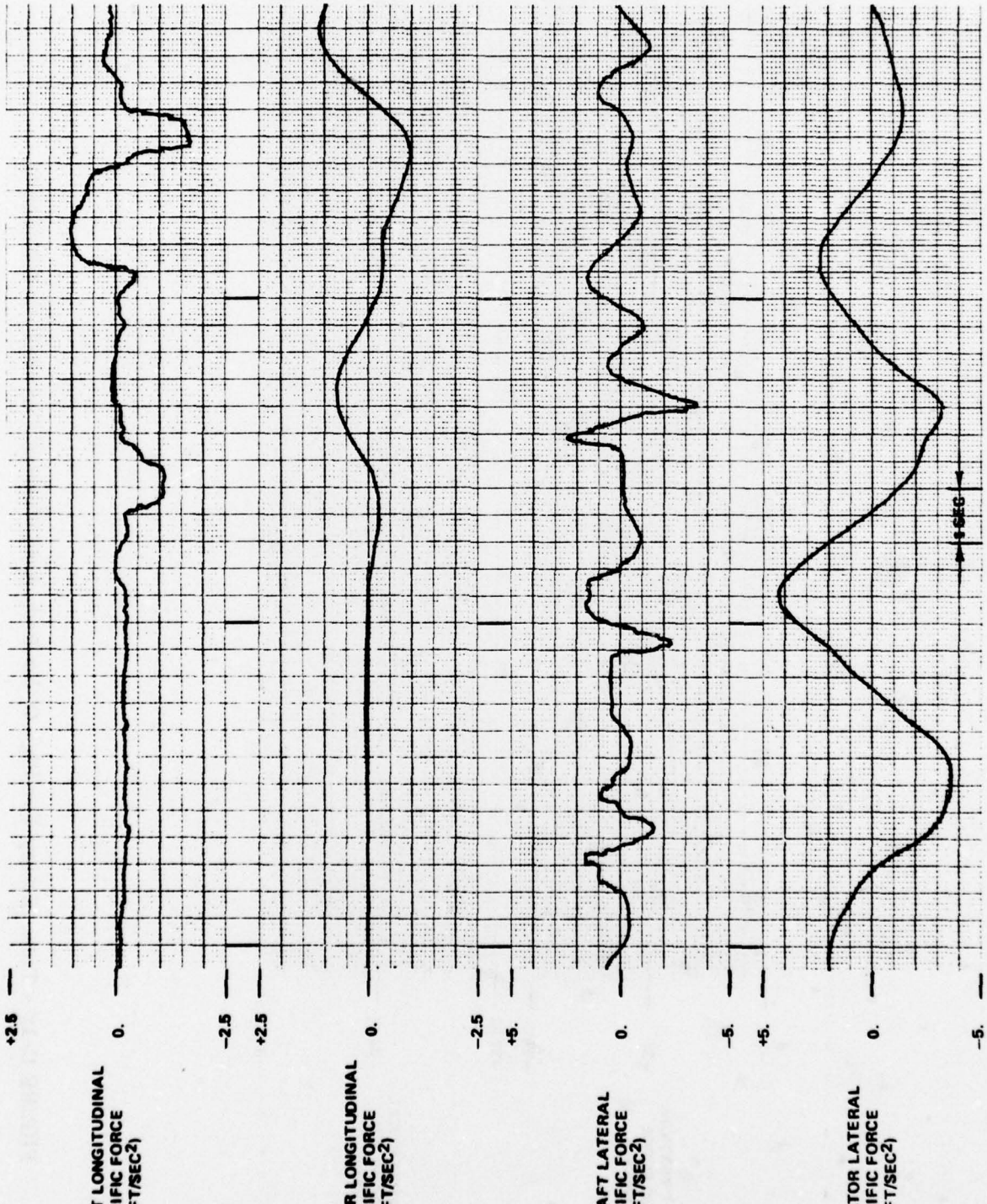

FIGURE C-19 - Time History For High Order Body Axis Washout Circuit With Tilt (Con't)

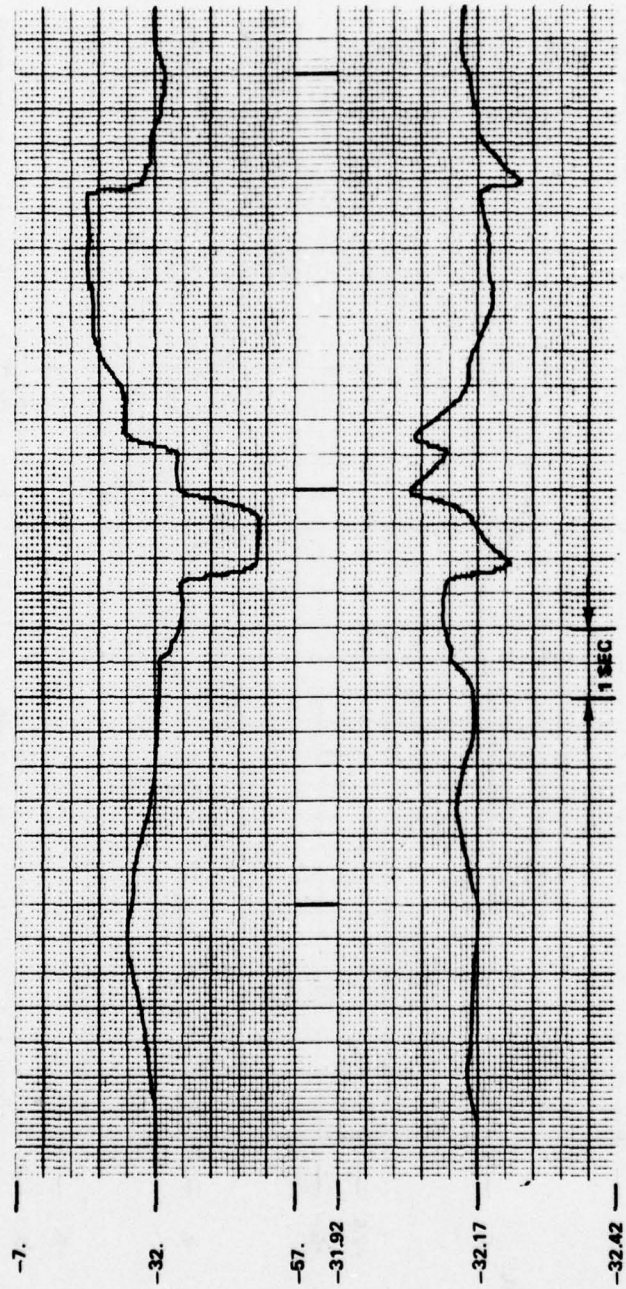

FIGURE C-19 - Time History For High Order Body Axis Washout Circuit With Tilt (Con't)

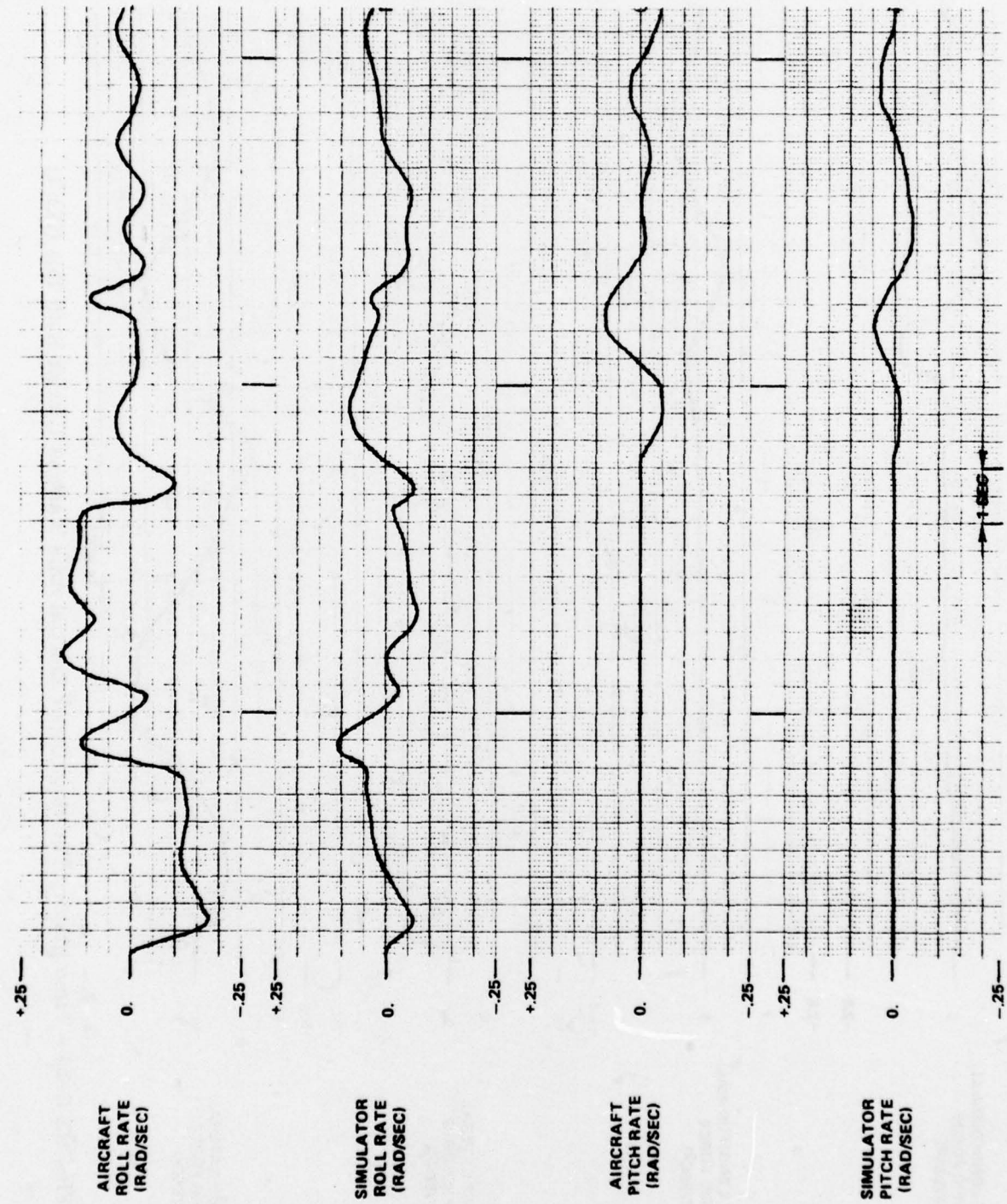

FIGURE C-20 - Time History For High Order Inertial Axis Washout Circuit With Tilt

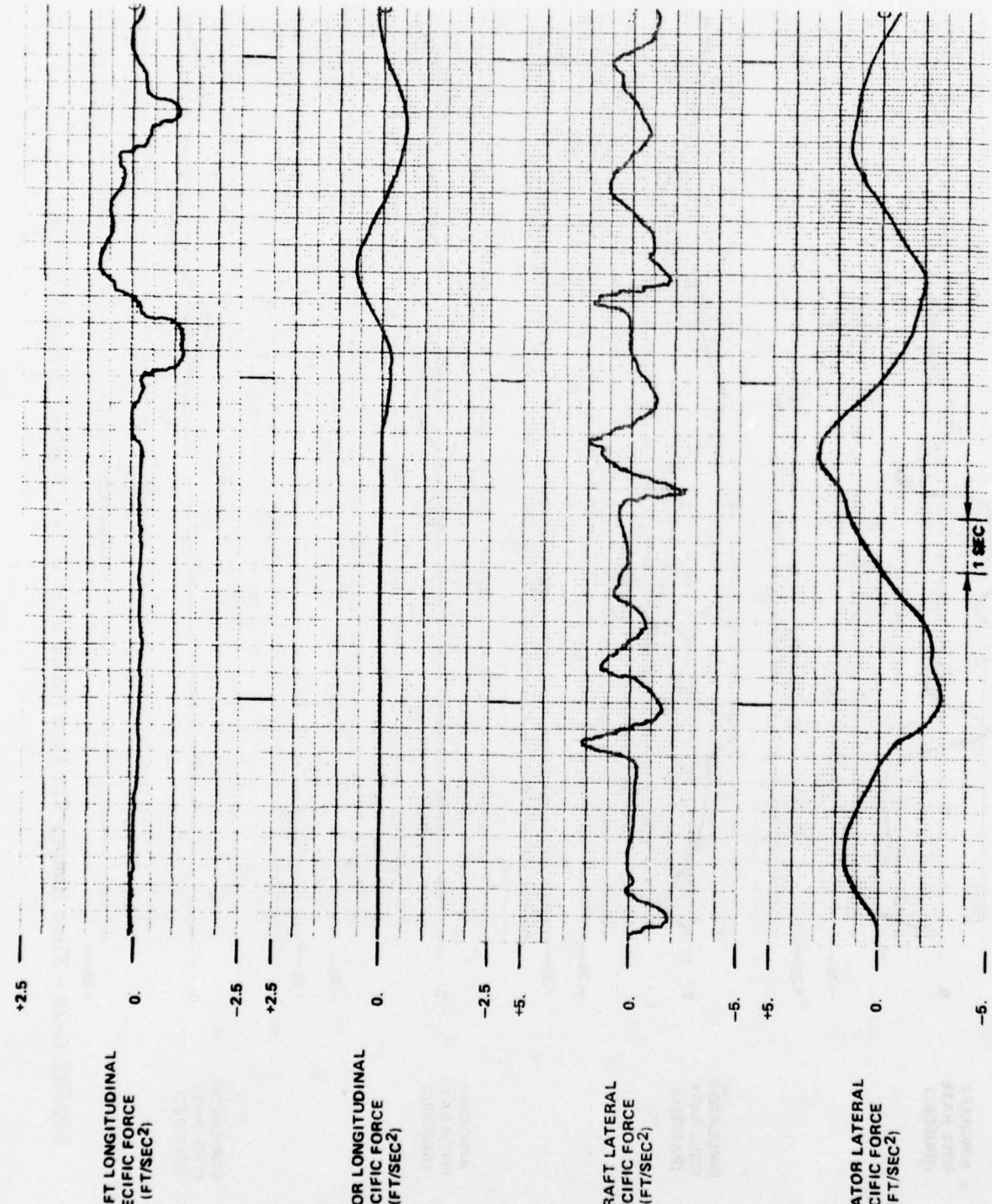

FIGURE C-20 - Time History For High Order Inertial Axis Washout Circuit With Tilt (Con't)

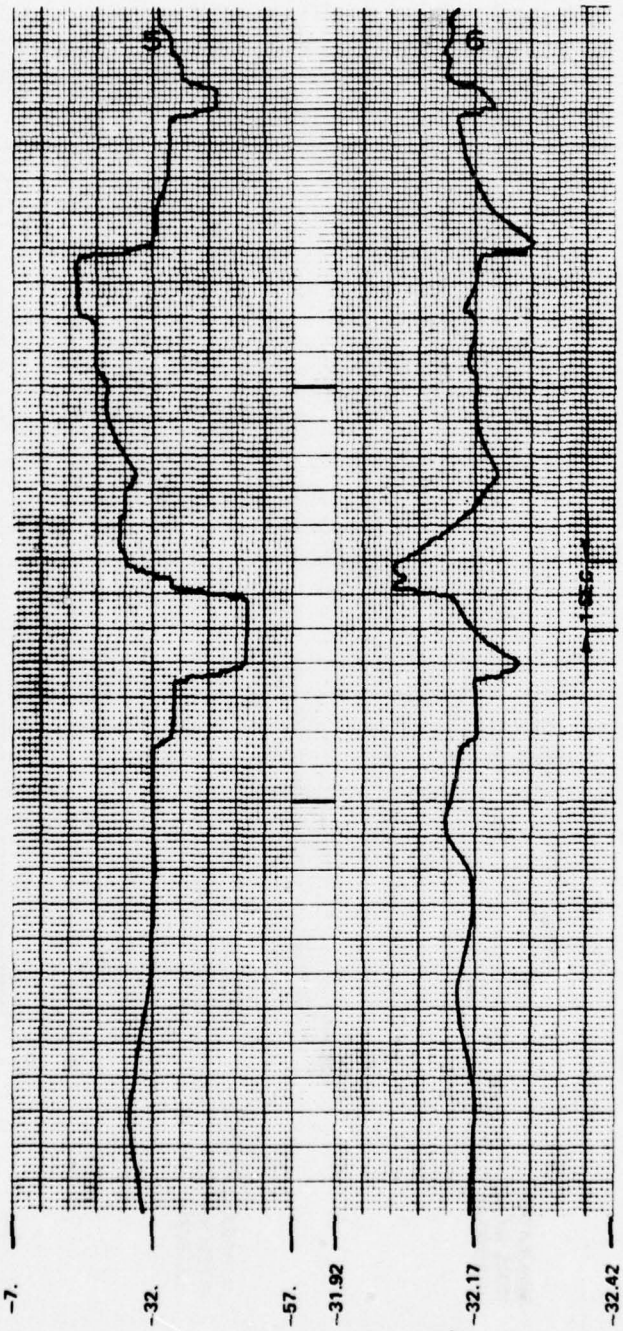

FIGURE C-20 - Time History For High Order Inertial Axis Washout Circuit With Tilt (Con't)

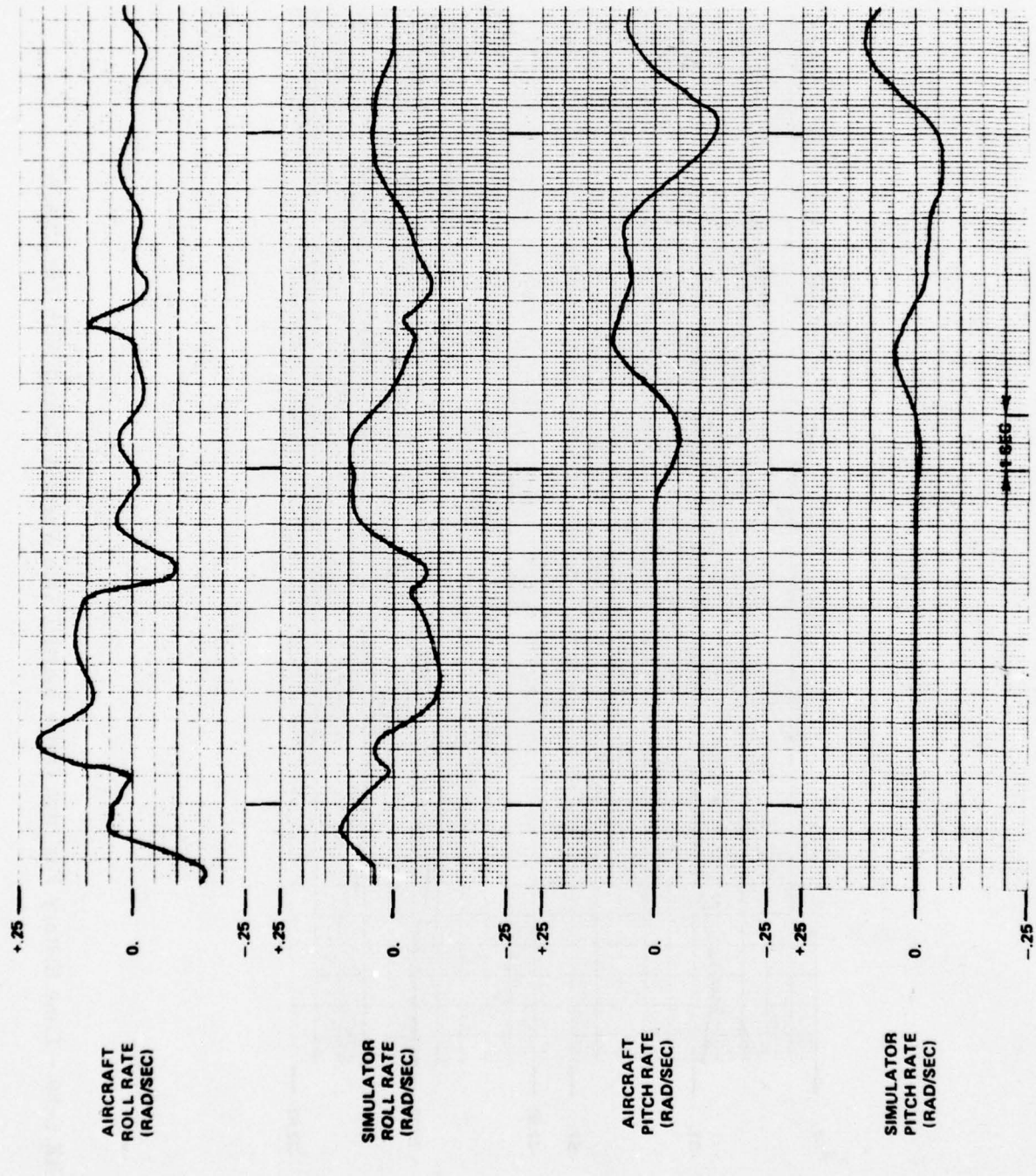

FIGURE C-21 - Time History For Linearized High Order Washout Circuit With Tilt

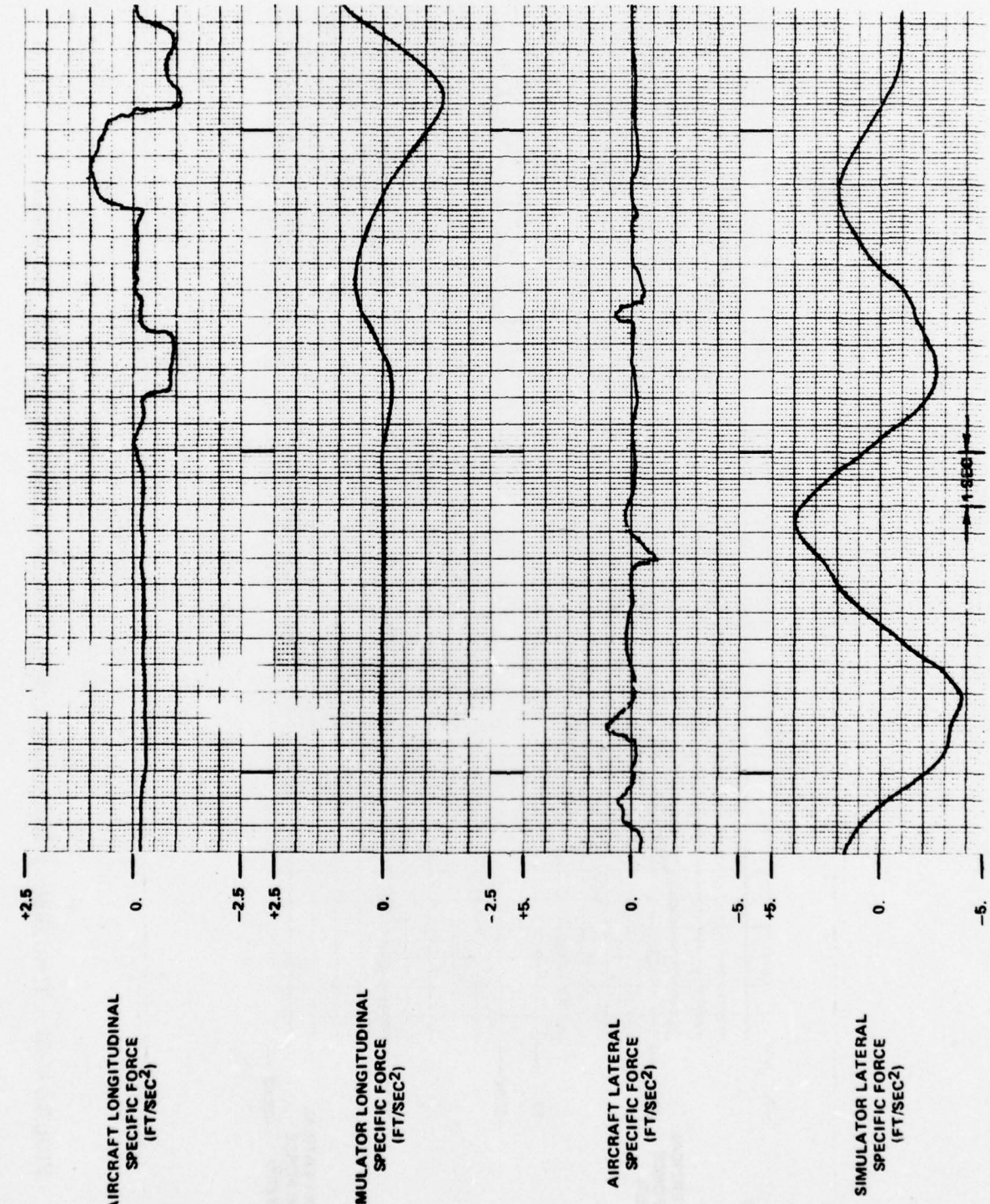

FIGURE C-21 - Time History For Linearized High Order Washout Circuit With Tilt (Con't)

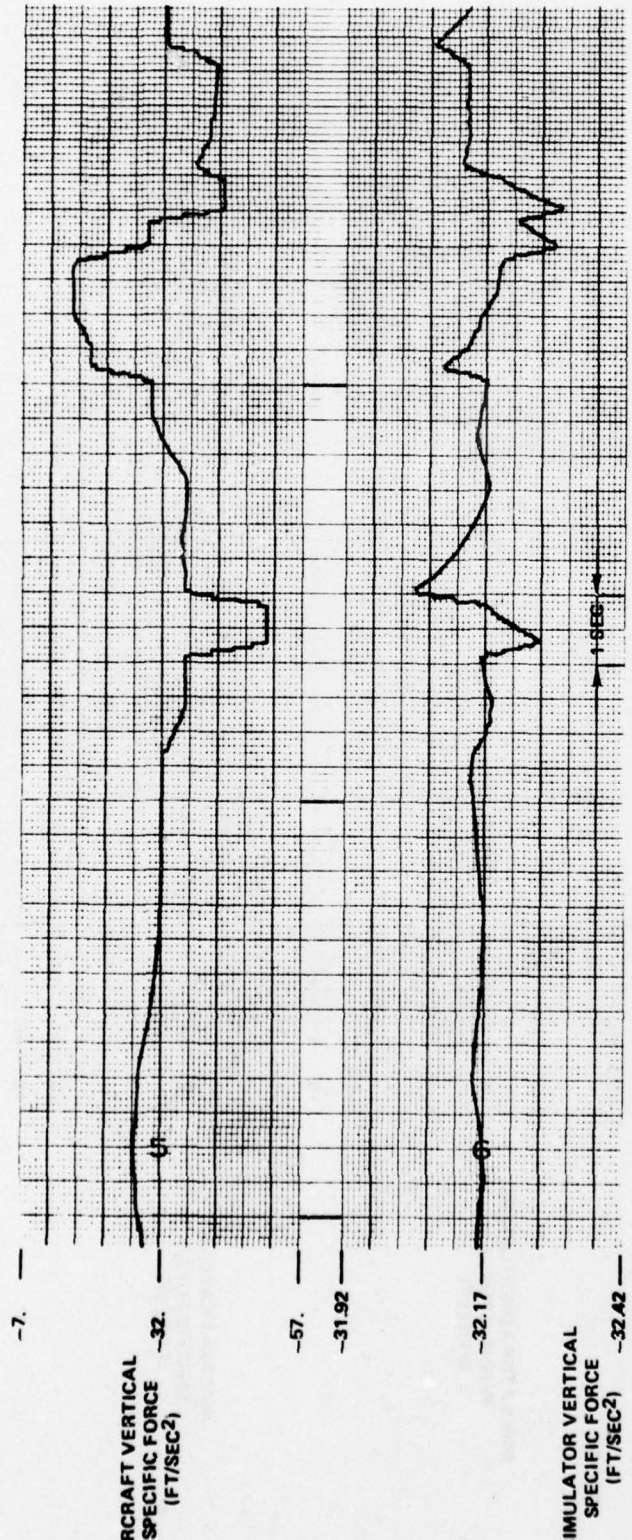

FIGURE C-21 - Time History For Linearized High Order Washout Circuit With Tilt (Con't)

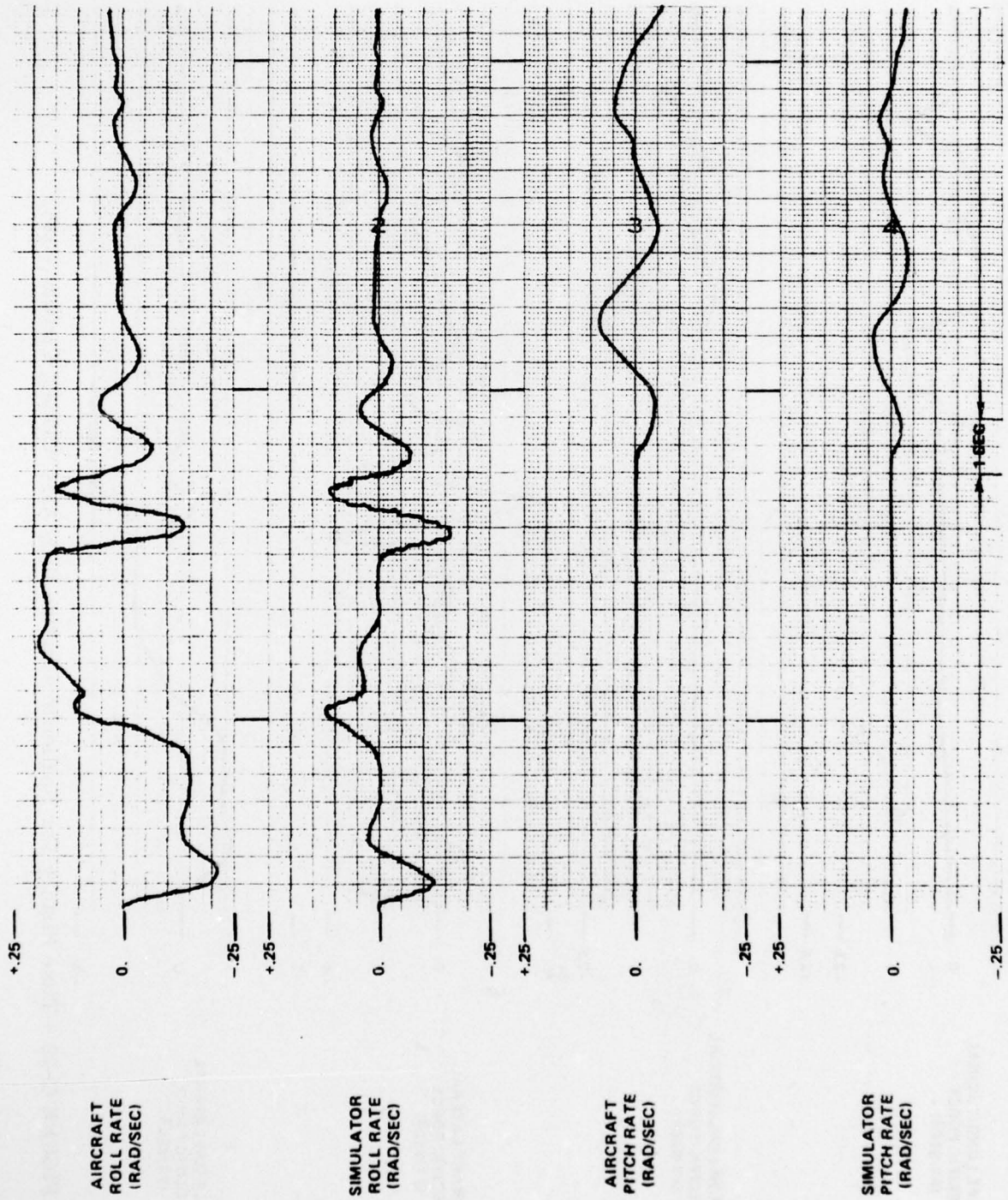

FIGURE C-22 - Time History For Nonlinear Adaptive Body Axis Washout Circuit

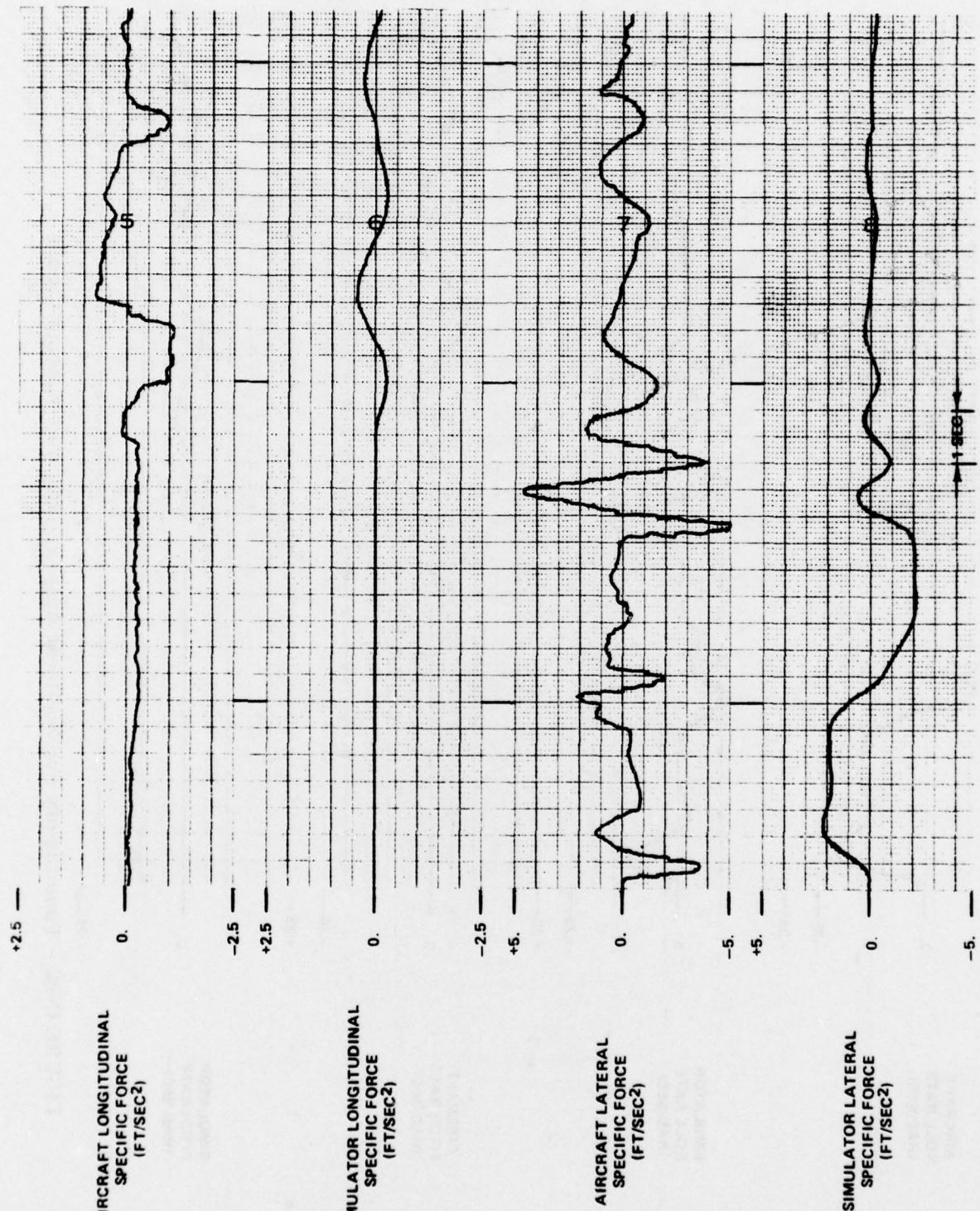

FIGURE C-22 - Time History For Nonlinear Adaptive Body Axis Washout Circuit (Con't)

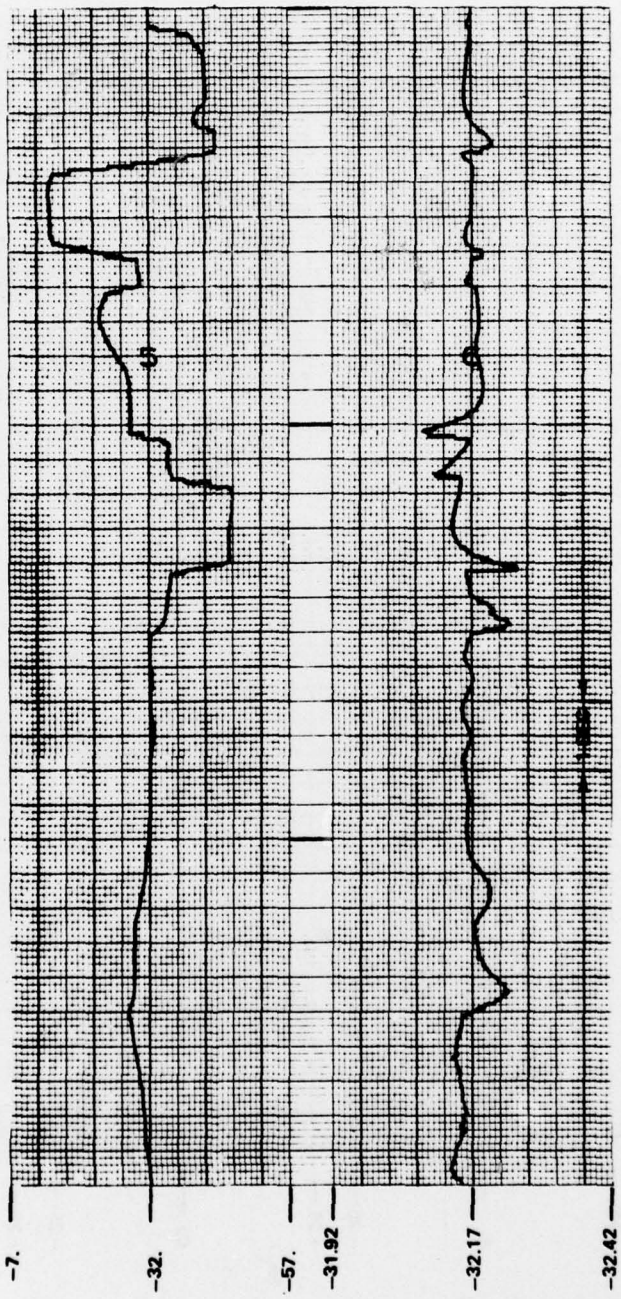

FIGURE C-22 - Time History For Nonlinear Adaptive Body Axis Washout Circuit (Con't)

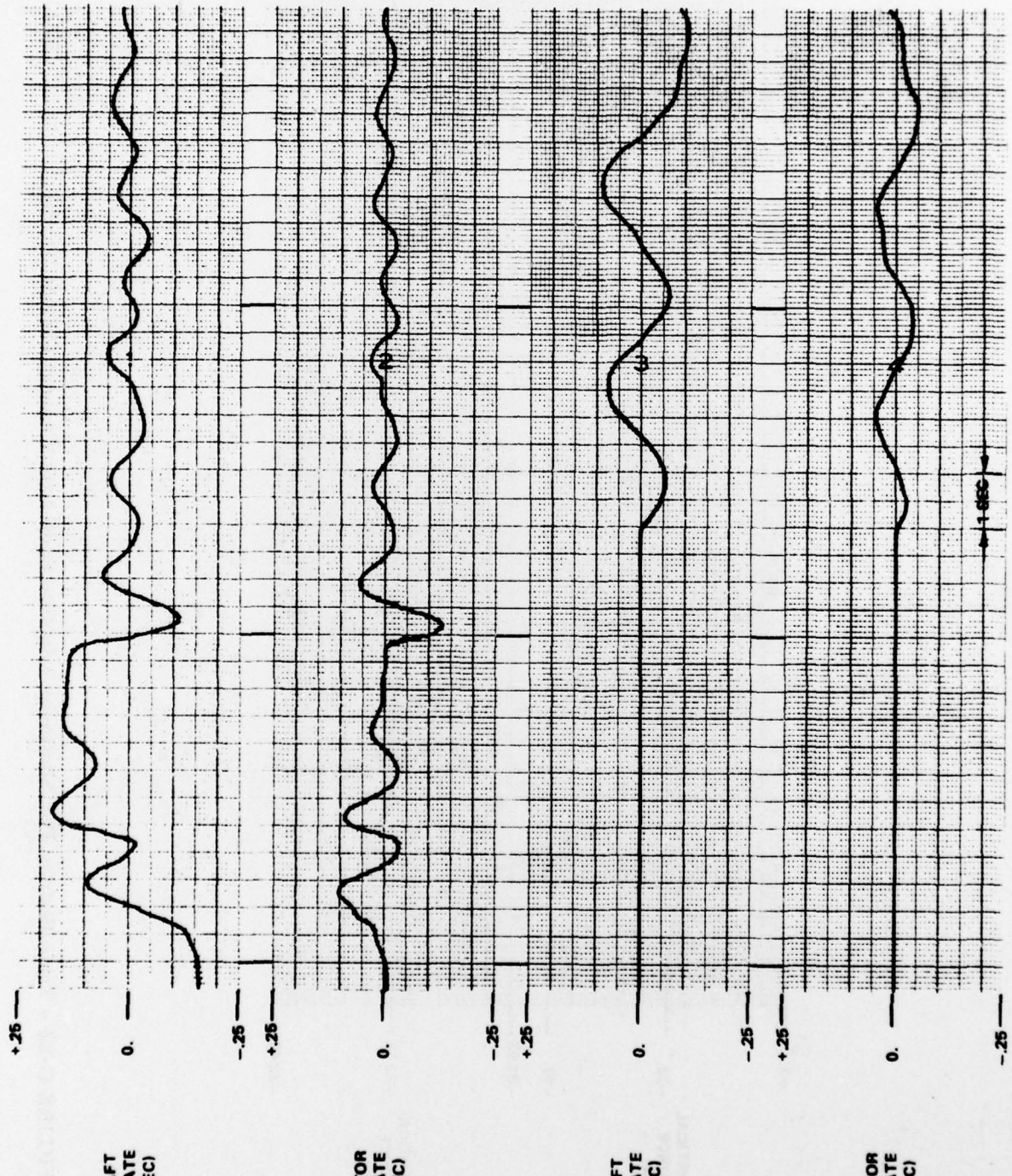

FIGURE C-23 - Time History For Nonlinear Adaptive Inertial Axis Washout Circuit

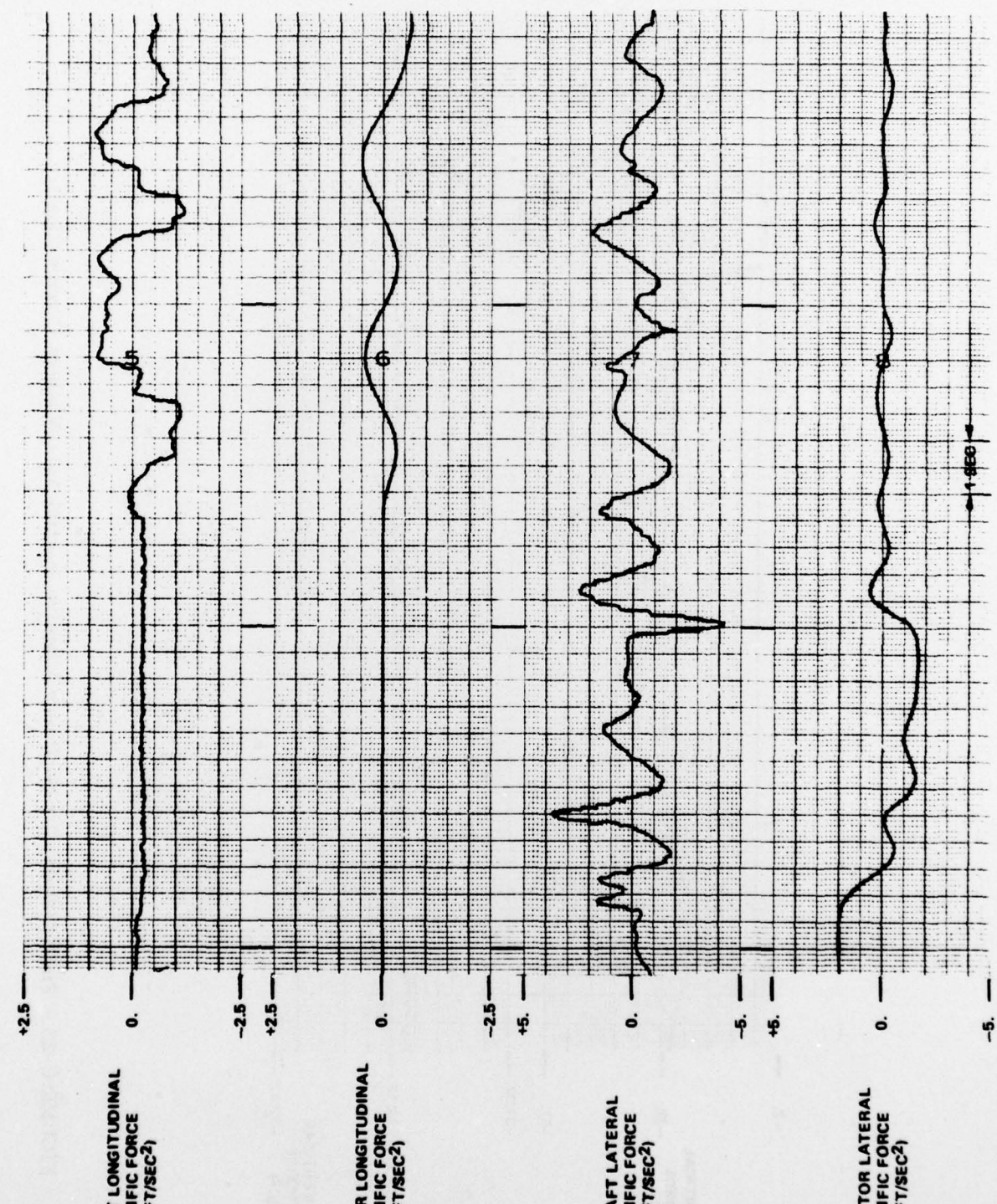

FIGURE C-23 - Time History For Nonlinear Adaptive Inertial Axis Washout Circuit (Con't)

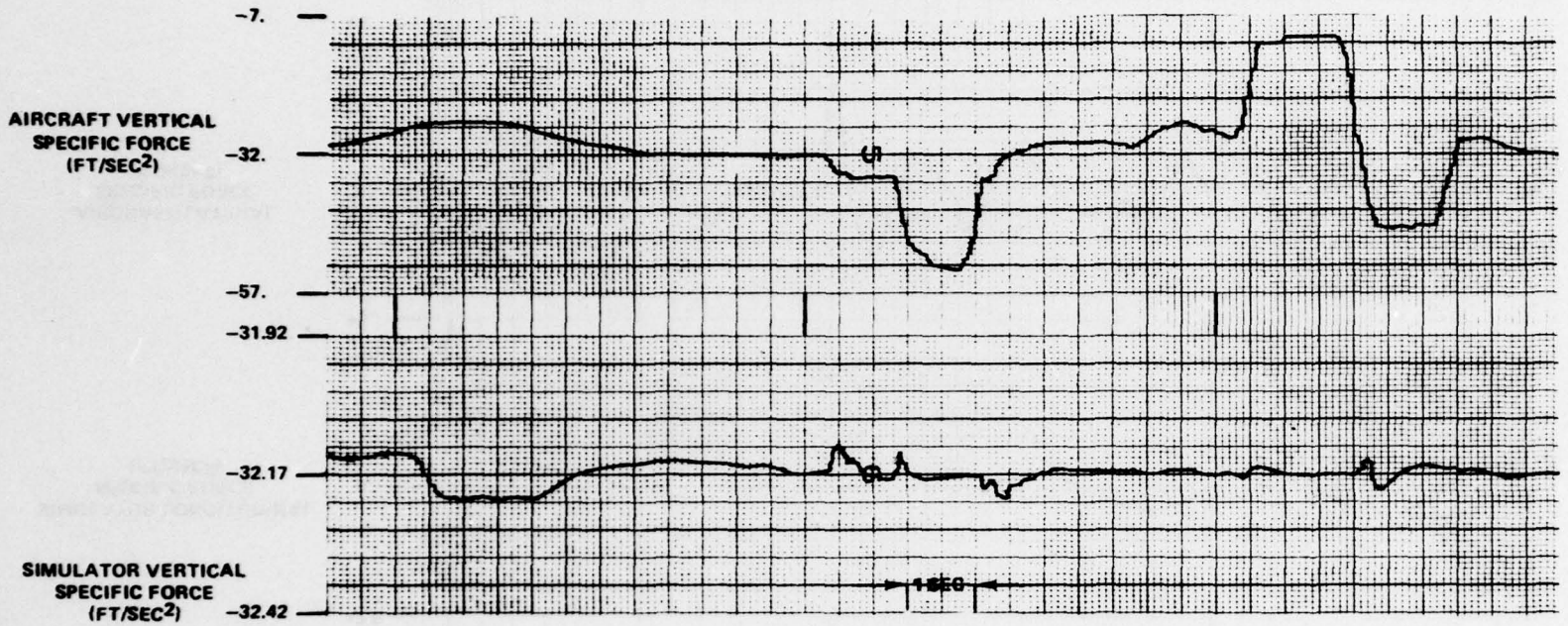

FIGURE C-23 - Time History For Nonlinear Adaptive Inertial Axis Washout Circuit (Con't)

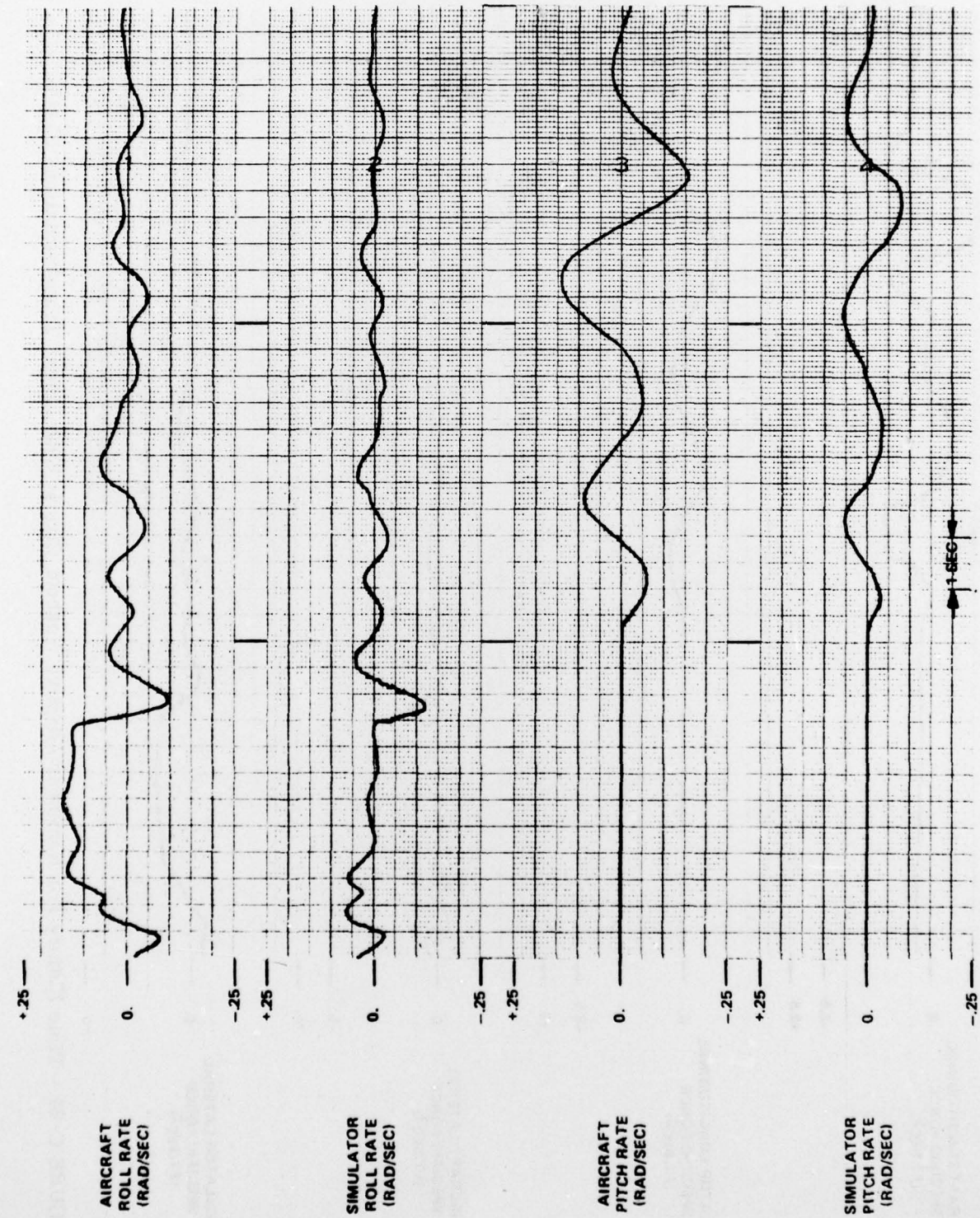

FIGURE C-24 - Time History For Nonlinear Adaptive Washout Circuit With Linear Transformations

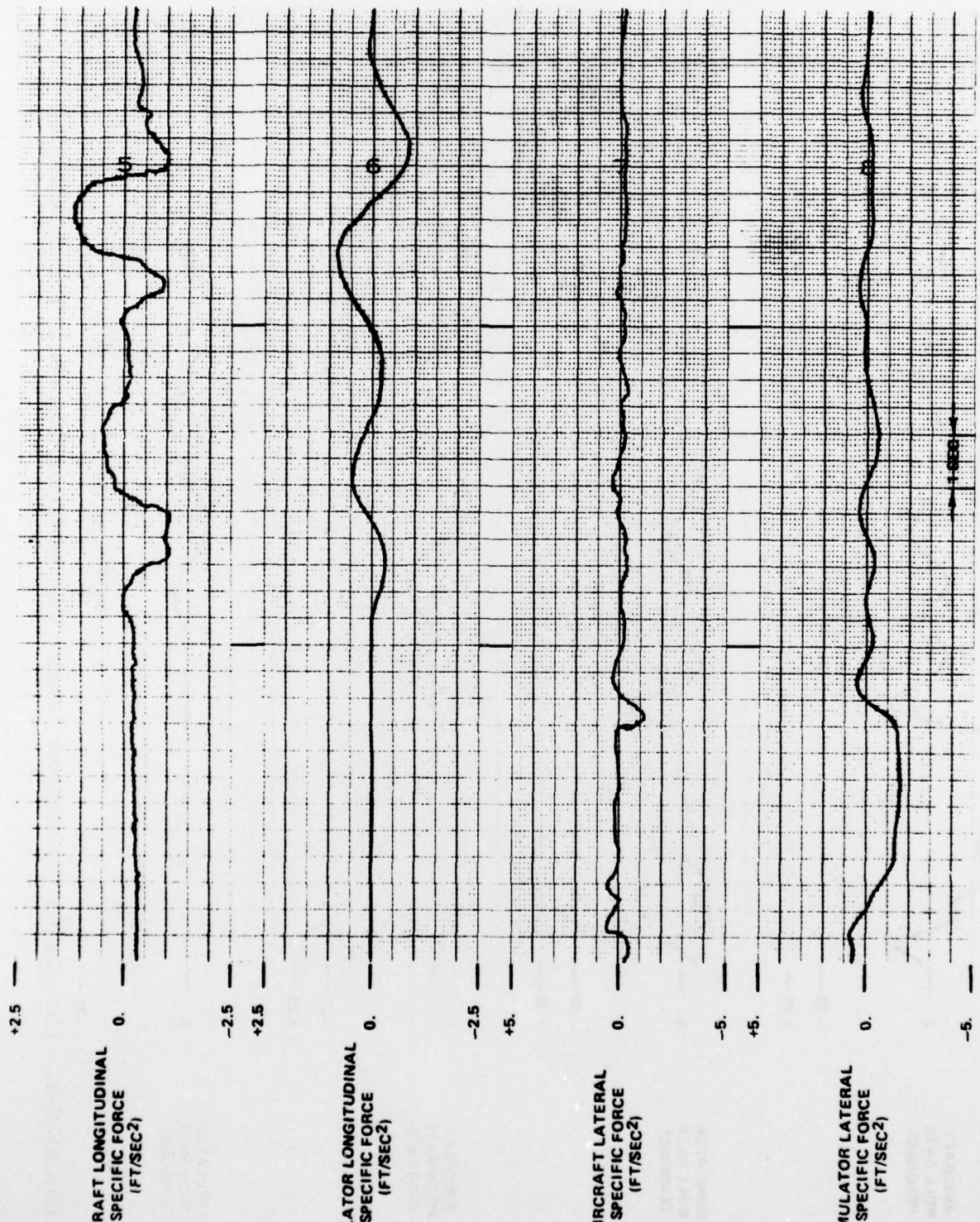

FIGURE C-24 - Time History For Nonlinear Adaptive Washout Circuit With Linear Transformations (Con't)

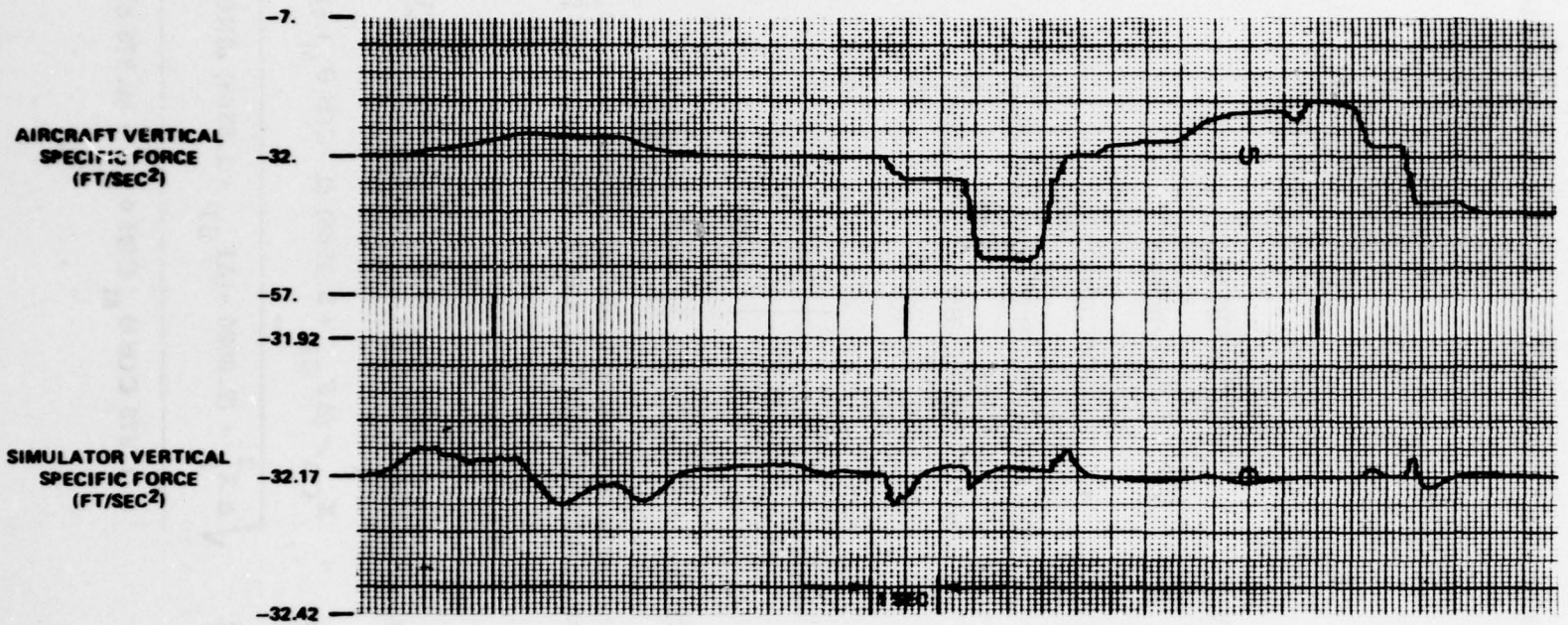

FIGURE C-24 - Time History For Nonlinear Adaptive Washout Circuit With Linear Transformations (Con't)

The axis transformation matrices for a link three-degree-of-freedom motion base are given as:

$$[F] = \begin{bmatrix} \cos\theta & 0 & -\sin\theta \\ \sin\phi \sin\theta & \cos\phi & \sin\phi \cos\theta \\ \cos\phi \sin\theta & -\sin\phi & \cos\phi \cos\theta \end{bmatrix}$$

where

$$\begin{bmatrix} X_{BODY} \\ Y_{BODY} \\ Z_{BODY} \end{bmatrix} = [F] \begin{bmatrix} X_{INERTIAL} \\ Y_{INERTIAL} \\ Z_{INERTIAL} \end{bmatrix}$$

$$[F]^T = \begin{bmatrix} \cos\theta & \sin\phi \sin\theta & \cos\phi \sin\theta \\ 0 & \cos\phi & -\sin\phi \\ -\sin\theta & \sin\phi \cos\theta & \cos\phi \cos\theta \end{bmatrix}$$

where

$$\begin{bmatrix} X_{INERTIAL} \\ Y_{INERTIAL} \\ Z_{INERTIAL} \end{bmatrix} = [F]^T \begin{bmatrix} X_{BODY} \\ Y_{BODY} \\ Z_{BODY} \end{bmatrix}$$

The transformation from pitch, roll and heave commands (ϕ_M, θ_M, Z_2) to right, left and rear leg commands (L RIGHT, L LEFT, L REAR) is as follows:

Rear Leg

$$\Delta X_{CG} = 7.5 \left(0.3547 - \sin^{-1} \left(\frac{2.6025 - Z_2 - \Delta F_{CP} \sin\theta_M}{7.5} \right) \right)$$

$$\Delta X_R = X_{CG} + (\Delta F_{CP} + 2.3568)(1 - \cos\theta_M) - 1.875 \sin\theta_M \cos\phi_M$$

$$L\ REAR = \sqrt{\Delta X_R^2 + (2.6025 - (\Delta F_{CP} + 2.3568) \sin\theta_M - Z_2 + (1.875 \cos\theta_M \cos\phi_M)^2 + (1.875 \sin\phi_M)^2} - 4.4775$$

Right Leg

$$\Delta X_{SP} = (4.81 - X_{CP})(\cos\Theta_M - 1) + \Delta X_{CG} - 3.075 \sin\Theta_M$$

$$\Delta Z_{SP} = 2.6025 + (4.81 - \Delta F_{CP}) \sin\Theta_M - Z_2 + 3.075 \cos\Theta_M$$

$$TSP = \sqrt{\Delta X_{SP}^2 + \Delta Z_{SP}^2}$$

$$\xi = \cos^{-1}(\Delta Z_{SP}/TSP)$$

$$\Delta X_R = TSP \sin(\Theta_M - \xi)$$

$$\Delta Y_R = 3.075 \sin\phi_M + 4.7344(\cos\Theta_M - 1)$$

$$\Delta Z_R = TSP \cos(\Theta_M - \xi) - 4.7344 \sin\phi_M + 3.075(\cos\phi_M - 1)$$

$$L_{RIGHT} = \sqrt{(\Delta X_R)^2 + (\Delta Y_R)^2 + (\Delta Z_R)^2}$$

Left Leg

$$\Delta Y_L = 3.075 \sin\phi_M + 4.7344(1 - \cos\phi_M)$$

$$\Delta Z_L = TSP \cos(\Theta_M - \xi) + 4.7344 \sin\phi_M + 3.075(\cos\phi_M - 1)$$

$$L_{LEFT} = \sqrt{(\Delta X_R)^2 + (\Delta Y_L)^2 + (\Delta Z_L)^2}$$

A linearized version of this transformation, accurate to better than 5 percent is as follows:

Rear Leg

$$L_{REAR} = Z_2 + \Theta_M (F_{CP} + 2.3568)$$

Right Leg

$$L_{RIGHT} = Z_2 - \Theta_M (4.81 - \Delta F_{CP}) + 4.7344\phi_M$$

Left Leg

$$L_{LEFT} = Z_2 = \Theta_M (4.81 - \Delta F_{CP}) - 4.7344\phi_M$$

In these transformations, ΔF_{CP} represents the distance in feet forward to the desired center of pitch from the pivot point attaching the simulator to the floor.

These equations represent the leg position commands in feet from the simulator level position. An input of 65.844 volts will move the legs one linear foot. The rear leg zero volt position is also the zero displacement position. A bias of 30.864 volts must be applied to the front legs to bring the simulator to its level position.

APPENDIX D

ANALYSIS TECHNIQUES

APPENDIX D

ANALYSIS TECHNIQUES

The statistical tests used in this study are of the "sampled permutation" variety, an extension of the Fisher Randomization method. The sampled permutation technique was chosen because it requires that no assumptions be made concerning the underlying distribution of the experimental data.

For comparing different washout types and the use of washouts in different axis systems, (Phase II of the experiment) the statistic used was an F ratio. Computation of the F ratios for row differences (washout types) and column differences (use of washouts in different axis systems) was carried out exactly as it would be for a standard two-way analysis of variance with replication. Ordinarily these F ratios would be compared with tabulated values for the F distribution to test for statistical significance of the results. Such action, however, implies an assumption that the experimental data is a sample from a population with a normal distribution. Rather than make this assumption, the sampled permutation technique generates its own F distribution from the actual experimental data. The F ratios for rows and columns are then compared with the newly generated F distribution to determine the statistical significance of the results.

Table D-I contains the data for attitude error variances from the second phase of the experiment. Analysis of this data will serve as an example of the use of the sampled permutation technique.

There are twelve washout/axis system combinations. Each combination has four replications - one for each pilot taking part in this phase of the experiment. Averages are taken over the four pilots for each of the washout/axis system combinations to form the cell means of table D-II. From the row and column totals in table D-II (washout type and axis system of application respectively) it appears that the attitude error variances are roughly equal regardless of the axis system used while the variances for third order washouts are substantially larger than for the other washout types. These results, however, need to be tested for statistical significance. The standard two-way ANOVA table for this data is shown in table D-III. At this point the F distribution must be generated by the sampled permutation method. The data from each pilot is randomly shuffled and a new table formed from the shuffled data. F ratios are recalculated and checked against the F ratios from the original data arrangement. Once again the data from each pilot is shuffled and new F ratios calculated and compared with the original F ratios. This procedure is repeated many times and a count is made of how many times the actual F ratios exceed those generated by shuffling the data. The size of the data sample prohibits examining all permutations of the data - thus the origin of the term "sampled permutations". The implications are that the F ratios for the actual experimental results will exceed the F ratios generated by

TABLE D-I

ATTITUDE ERROR VARIANCES FOR PHASE II OF THE EXPERIMENT

	Linear Transformation	Body Axis	Inertial Axis
First Order Washout	.05869	.03414	.01370
	.02152	.03279	.03053
	.03058	.02223	.05994
	.04536	.07591	.11633
Third Order Washout	.12220	.01938	.01375
	.12968	.07327	.13285
	.06578	.04907	.29300
	.06578	.07655	.04063
Adaptive Nonlinear Washout	.06357	.04340	.01700
	.02664	.11704	.19751
	.07545	.01903	.03588
	.05643	.06711	.04235
High Order Washout with Tilt	.02760	.04384	.01521
	.01438	.08191	.04337
	.02982	.03964	.02213
	.05507	.10487	.04411

TABLE D-II

CELL MEANS FOR ATTITUDE ERROR VARIANCES FROM PHASE II OF THE EXPERIMENT

	Linear Transformation	Body Axis	Inertial Axis	Row Totals
First Order Washout	.15615	.16507	.22050	.54172
Third Order Washout	.38713	.21827	.48023	1.08563
Nonlinear Adaptive Washout	.22209	.24658	.29274	.76141
High Order Washout with Tilt	.12687	.27026	.12482	.52195
Column Totals	.89224	.90018	1.11829	2.91071

TABLE D-III

ANOVA TABLE FOR ATTITUDE ERROR VARIANCES
FROM SECOND PHASE OF THE EXPERIMENT

	Sum of Squares	Degrees of Freedom	Mean Squares	F Ratio
Rows	.0171810	3	.0057270	2.20
Columns	.0020570	2	.0010285	.39
Interaction	.0114877	6	.0019146	.74
Subtotal	.0307257	11	.0027932	1.07
Residual	.093764	36	.00260446	
Total	.12449	47		

permuting the data a large percentage of the time if the results are due to actual physical differences in the washout algorithms rather than just ordinary statistical fluctuations.

The levels of significance(1) for the results are as follows:

Washout Type	.08
Axis System of Application	.76

The implications of these statistics are that the axis system of application for washouts has no physical effect on the attitude error variances. However, there is some indication that the poorer performance of third order washout filters is not merely a statistical fluctuation. While a significance level of .08 is not normally considered convincing (.05 or .01 are common test levels for significance) the author feels that this is a reportable result since the sampled permutation technique is not considered to be as sensitive as standard analysis techniques.

For Phase III of this experiment, a two-way analysis of variance with the sampled permutation technique was again used. Table D-IV shows the data for position error

(1) Level of significance here refers to the percentage of time that F ratios generated by randomly permuting the data exceed the F ratios of the original arrangement of the data.

TABLE D-IV

POSITION ERROR VARIANCE FOR PHASE III OF THE EXPERIMENT

	First Order Washout	Adaptive Nonlinear Washout	High Order Washout with Tilt
Pilot #1	.4683	1.6945	.1655
	.2006	.5818	.2674
	.4857	.3651	.0562
	.3084	.3432	1.4548
	.2011	1.5972	.1902
Pilot #2	1.5214	.6351	.2412
	.4921	.6001	.8324
	.2214	.7274	4.3081
	.2929	.2578	.2193
	.5678	.3053	.3180
Pilot #3	.3279	.6875	.4821
	.3080	.1175	.5671
	.0486	.0684	.2109
	.4269	.1248	.4025
	.2294	.1214	.0784

variance for the third phase of the experiment. The data was arranged differently for analysis of this phase of the experiment. The columns now refer to washout types and the rows contain data from the different pilots. Each washout/pilot combination has five replications. The ANOVA table is set up as before and the sampled permutation technique is applied as in the second phase of the experiment. The data from each pilot is shuffled and an F distribution is generated from the actual data. Once again the implication is that the observed results are not due to statistical fluctuations if it can be shown that the F ratios calculated from the original arrangement of the data are larger than the F ratios generated by permuting the data.

The differences in performance for the three washout filters must be attributed to statistical fluctuations rather than real physical differences since the level of significance is .75 in this case.

Individual comparisons of washouts for the third phase of the experiment were also made with a two-way analysis of variance with sampled permutation.

A sampled permutation student test was used for comparing motion versus no motion.